

Luca F. Cameretti

**Modeling of
Thermodynamic
Properties in
Biological Solutions**

Cuvillier Verlag Göttingen

Modeling of Thermodynamic Properties in Biological Solutions

Dissertation
submitted to
The Faculty of Biochemical and Chemical Engineering
by

Luca F. Cameretti
born in Iserlohn (Germany)

for the Degree of

Dr.-Ing.

Day of oral examination: September 3rd, 2008

Approved by:
Prof. Dr. Gabriele Sadowski
Prof. Dr. Andrzej Górak
Prof. Dr. Rolf Wichmann

Dortmund University of Technology
September 2008

Bibliografische Information der Deutschen Nationalbibliothek

Die Deutsche Nationalbibliothek verzeichnet diese Publikation in der Deutschen Nationalbibliografie; detaillierte bibliografische Daten sind im Internet über <http://dnb.ddb.de> abrufbar.

1. Aufl. - Göttingen : Cuvillier, 2009

Zugl.: (TU) Dortmund, Univ., Diss., 2008

978-3-86727-848-5

© CUVILLIER VERLAG, Göttingen 2009

Nonnenstieg 8, 37075 Göttingen

Telefon: 0551-54724-0

Telefax: 0551-54724-21

www.cuvillier.de

Alle Rechte vorbehalten. Ohne ausdrückliche Genehmigung des Verlages ist es nicht gestattet, das Buch oder Teile daraus auf fotomechanischem Weg (Fotokopie, Mikrokopie) zu vervielfältigen.

1. Auflage, 2009

Gedruckt auf säurefreiem Papier

978-3-86727-848-5

To my parents.

Preface

This thesis is submitted as partial fulfilment of the Doctorate degree at the Dortmund University of Technology, Germany.

The project, granted by the Deutsche Forschungsgemeinschaft (DFG) with grant SA 700/7, has been carried out from October 2003 to December 2007 at the Department of Biochemical and Chemical Engineering, University of Dortmund, Germany, under the supervision of Prof. Dr. Gabriele Sadowski. I wish to thank her for giving me the opportunity to work on an interesting and challenging topic and for her scientific and personal support.

I would like to thank all my dear colleagues at the Chair of Thermodynamics for many years of enjoyable working atmosphere, especially Matthias Funke, who shared the office with me, Feely Tumakaka and Matthias Kleiner for their support concerning PC-SAFT, our secretary Gaby Mazur for her organisation skills and human touch, and Michael Görnert for two wonderful trips to Spain and Portugal. Special thanks are directed to our technician and laboratory personnel, Karl-Heinz Schulz and Susanne Richter for their inestimable help in the laboratory.

I wish to state my gratitude to Christoph Held, whose Diploma thesis I had the pleasure to supervise. I appreciate his commitment and thank him for the many fruitful discussions.

I express my special thanks to my dearest friend Felix Piltz who has accompanied me through thick and thin for over more than 10 years.

Three very important persons may not be missed out here. For all their love and support I am deeply indebted to my parents and my brother.

Many others have contributed to the success of this thesis, no matter whether on a scientific or on a personal level. To list them all would fill more than this page. However, I would like to mention Ms. Asli Azkan for her student thesis she wrote under my supervision, Prof. John Prausnitz for keeping an eye on me, Prof. Frederico Tavares for appreciable discussions about the potential of mean force, Prof. Jørgen Møllerup and Dr. Martin Breil for prompt support concerning electrolyte solutions.

Zusammenfassung

Mehr als 90% der Herstellungskosten für Aminosäuren, Peptide und Proteine fallen auf deren Reinigung zurück. Daher sind zuverlässige Informationen über das Phasenverhalten biologischer Systeme für die Auslegung von Trennstufen von zentraler wirtschaftlicher Bedeutung. In der Regel werden o. g. Produkte fermentativ in wässrigen Lösungen hergestellt, die außerdem noch Elektrolyte enthalten können. Das Phasenverhalten dieser Lösungen wird in besonderem Maße durch Faktoren wie Salztyp, Ionenstärke und pH bestimmt.

In dieser Arbeit wird zunächst ein auf der PC-SAFT Zustandsgleichung basiertes Modell entwickelt, mit dem thermodynamische Eigenschaften wässriger Elektrolytlösungen beschrieben werden können. Weiterhin wird das entstandene Modell zur Modellierung wässriger Aminosäure- bzw. Peptid-Systeme verwendet. Besonderes Augenmerk wird auf die gleichzeitige Beschreibung verschiedener Systemeigenschaften – Dichten, Dampfdrücke, Aktivitätskoeffizienten und Löslichkeiten – mit einer minimalen Anzahl an Modellparametern gelegt. Nach erfolgreicher Modellierung der binären Randsysteme, werden ternäre Wasser-Elektrolyt-Aminosäure Systeme auf Ihre Modellierbarkeit untersucht.

Zusätzlich werden die metastabile flüssig-flüssig Entmischung, der zweite osmotische Virialkoeffizient, Systemdichten und die Löslichkeit von Proteinen am Beispiel von Hühnereiweiß-Lysozym/NaCl Lösungen sowohl mit der PC-SAFT Zustandsgleichung als auch mit einem auf dem Potential of Mean Force (PMF) basierenden Ansatz modelliert. Hier zeigt sich die begrenzte Anwendbarkeit der PC-SAFT Zustandsgleichung bei solch komplexen Systemen. Qualitativ richtige Ergebnisse können hingegen mit dem PMF Ansatz erreicht werden.

Alle in dieser Dissertation behandelten Modelle wurden in FORTRAN implementiert. Die Auswertung der Ergebnisse erfolgte mit MATLAB[®].

Schlüsselbegriffe: Perturbation Theory, PC-SAFT, Potential of Mean Force, Elektrolyte (Alkalihalide, -hydroxide, -sulfate, -nitrate, Erdalkalisalze, Ammoniumchlorid), Aminosäuren (Glycin, Alanin, Serin, Prolin, Valin, Arginin, Lysin, Threonin, Histidin, α -/ β -/ γ -Aminobuttersäure, α -/ γ -Aminovaleriansäure), Peptide (Diglycin, Triglycin, Dialanin, Alanylglycin, Glycylalanin), Protein (Hühnereiweiß Lysozym), Dampfdruck, (mittlerer ionischer) Aktivitätskoeffizient, Dichte, Löslichkeit

Abstract

More than 90% of the production costs for amino acids, peptides, and proteins are attributed to their purification. Therefore, reliable information about phase behavior of biological systems is of essential financial importance for the design of separation units. In general, bioproducts are obtained by fermentation in aqueous solutions that may also contain electrolytes. The phase behavior of such solutions is particularly dependent on salt type, ionic strength, and pH.

In this thesis a model based on the PC-SAFT equation of state is developed for the description of thermodynamic properties of aqueous electrolyte solutions. This model is also applied for aqueous amino acid and peptide systems. The aim is to simultaneously describe various system properties – densities, vapor pressures, activity coefficients, and solubilities – with a minimum number of adjustable model parameters. After successful modeling of the binary systems, ternary water/electrolyte/amino acid systems are investigated.

Additionally, the meta-stable liquid-liquid coacervation in protein solutions as well as the second osmotic virial coefficients, system densities, and solubilities of proteins are scrutinized based on aqueous hen egg-white lysozyme/NaCl solutions. Both, the PC-SAFT model and a model based on potential of mean force (PMF) are tested for their applicability regarding such complex mixtures. It is shown that the PC-SAFT approach fails in the description of protein solutions whereas the PMF ansatz yields, at least, good qualitative agreement between model and experiment.

All models used for this thesis were implemented in FORTRAN. The evaluation of data was carried out with MATLAB[®].

Keywords: perturbation theory, PC-SAFT, potential of mean force, electrolyte (alkali halides, hydroxides, sulfates, nitrates, earth alkali salts, ammonium chloride), amino acid (glycine, alanine, serine, proline, valine, arginine, lysine, threonine, histidine, α -/ β -/ γ -aminobutyric acid, α -/ γ -aminovaleric acid), peptide (diglycine, triglycine, dialanine, alanylglycine, glycylalanine), protein (hen egg-white lysozyme), vapor pressure, (mean ionic) activity coefficient, density, solubility

Contents

1	Introduction	1
1.1	Aim of the Thesis	2
1.2	Structure of the Thesis	2
1.3	Investigated Systems	2
2	Thermodynamical Background	5
2.1	Basics	5
2.2	Calculation of Phase Equilibria	7
2.2.1	Vapor-Liquid and Liquid-Liquid Equilibria	7
2.2.2	Solid-Liquid Equilibria	9
2.3	Calculation of Thermodynamic Properties	11
2.3.1	Pressure	11
2.3.2	Chemical Potential and Fugacity Coefficients	12
2.3.3	Activity Coefficients and Reference States	13
3	Equations of State from Statistical Mechanics	17
3.1	Fundamentals	17
3.2	Radial Distribution Function	20
3.3	Relation of Thermodynamic Functions to $g(r)$	23
3.4	Intermolecular Potentials	23
3.5	Perturbation Theories	24
3.6	The PC-SAFT Equation of State	27
4	Potential of Mean Force	31
4.1	Interactions in Colloidal Dispersions	31
4.2	Global Phase Diagram of a Colloid System	33
4.3	Osmotic Pressure	33
4.4	Second Osmotic Virial Coefficient	35
4.5	PMF	35
4.6	Calculation of Phase Equilibria with a PMF Model	41
5	Electrolyte PC-SAFT (ePC-SAFT)	43
5.1	Electrolyte Systems	43
5.1.1	Introduction	43
5.1.2	Debye-Hückel (DH) Theory of Electrolyte Solutions	44

5.1.3	Augmented Electrolyte Theories	46
5.1.4	The ePC-SAFT Model	47
5.2	Amino Acid and Oligopeptide Solutions	47
6	Results: Low Molecular Weight Components	49
6.1	Modeling of Water	49
6.2	Modeling of Electrolyte Solutions with ePC-SAFT	50
6.2.1	Strategy for Parameter Estimation	51
6.2.2	Results	52
6.3	Modeling of Amino Acid and Peptide Solutions with ePC-SAFT	56
6.3.1	Parameter Estimation	57
6.3.2	Results for the Binary Systems	59
6.4	Modeling of Aqueous Electrolyte/Amino Acid Solutions	62
7	Results: Protein Systems	65
7.1	Modeling of Protein Solutions with ePC-SAFT	65
7.2	Modeling of Protein Solutions with PMF	68
8	Summary and Outlook	73
	Bibliography	75
	Appendix	
A	Symbols and Abbreviations	88
B	Electrolytes	93
C	Amino Acids and Peptides	100
D	Chemical Structures	121
E	Conversion of the Activity Coefficients	122
F	The Cross-Differential Equation	124
G	Activity Coefficients in Ternary Solutions	127
H	Electrolyte/Amino Acid Solutions	130

Chapter 1

Introduction

Amino acids are the building blocks for all life on earth. Albeit the almost infinite variety of species the number of amino acids forming proteins is limited to about 20. The majority of them are rather simple organic compounds with an amino group and an aliphatic, aromatic, or heterocyclic side chain (R) attached α to the carboxylic group. With the exception of the simplest amino acid glycine, all other amino acids are chiral compounds. In nature the L-form prevails. However, D-alanine, for example, is found in the cell membrane of bacteria.

Amino acids and their derivatives are of particular economical importance since they are utilized on a large scale as nutrition factors and flavor enhancers (e. g. glutamate). Additionally, many pharmaceuticals such as antibiotics, heart, cancer, and anti-HIV drugs are produced starting from amino acids. An excellent overview about production methods and the application of several amino acids is given by Kleemann et al.¹. Most production processes are based on white biotechnology – in other words, on fermentation and enzymatic technologies. The purification of the target product is achieved by crystallization from the filtered fermentation broth often containing also electrolytes and other by-products. For the design of separation units knowledge of thermodynamic data is indispensable. Therefore, since the beginning of the past century phase behavior in amino acid solutions has attracted the interest of many research groups especially with regard to its modeling. Activity coefficients as well as solubilities in aqueous amino acid solutions also containing electrolytes have been measured and described with models of varying complexity.

In addition to amino acids, peptides and proteins are economically highly valuable bi-products. Precipitation by addition of salts, non-ionic polymers, polyelectrolytes, or organic solvents is commonly used to isolate target proteins from solutions. Often two metastable liquid phases – one protein-rich and one protein-lean – form instead of the thermodynamically stable solid precipitate. The phase behavior is very complex and strongly depending on solution conditions such as ionic strength, salt type and pH. Although still far away from a rigorous quantitative modeling of the thermodynamics of complex protein solutions, qualitative agreement between model and experiment can already be achieved.

1.1 Aim of the Thesis

The scope of this thesis is twofold: Because solutions in biotechnology often contain salts, a model that can deal with charged species is essential. The Perturbed-Chain Statistical Association Theory (PC-SAFT) developed by Groß et al.² is extended by an electrolyte term in order to describe solution densities, vapor pressure depression, and mean ionic activity coefficients of aqueous electrolyte solutions. In a second step, phase behavior of binary water-amino acid (peptide) mixtures is calculated with the same model. Herewith, the foundation is laid for modeling the influence of electrolyte type and concentration on activity coefficient and solubility of amino acids and peptides in aqueous solutions.

Another aim is to model phase behavior in protein systems with an equation of state. The applicability of a rigorous approach such as PC-SAFT is investigated. Further, a model based on the McMillan-Mayer framework is applied to describe second osmotic virial coefficients of hen egg-white lysozyme in aqueous salt solutions as well as the meta-stable liquid-liquid demixing and the solubility.

1.2 Structure of the Thesis

After this introduction Chapter 2 provides the thermodynamic basics of phase equilibria calculations. Besides some fundamentals, Chapter 3 contains a detailed description of how equations of state, especially the PC-SAFT equation of state, are developed from statistical mechanics and perturbation theory. The concept of the radial distribution function and its relation to other thermodynamic functions is elucidated. Chapter 4 is dedicated to the potential of mean force ansatz and its theoretical application to colloidal dispersions. The extension of the PC-SAFT model to electrolyte systems follows in Chapter 5. Further, the method of modeling amino acid (peptide) solutions with electrolyte PC-SAFT (ePC-SAFT) is explained. Modeling results for electrolyte solutions, amino acid (peptide) solutions, and electrolyte/amino acid solutions are presented in Chapter 6 whereas Chapter 7 summarises the results for the protein systems. A summary of the thesis, conclusions, and an outlook for future work follow in Chapter 8.

The Appendix mainly comprises component model parameters and supplementary result figures.

1.3 Investigated Systems

The electrolyte PC-SAFT equation of state is used to model solution densities, vapor pressures, (mean ionic) activity coefficients and solubilities of following aqueous electrolyte, amino acid, and peptide solutions:

- salts containing

cations: Li^+ , Na^+ , K^+ , NH_4^+ , Mg^{2+} , Ca^{2+}

anions : F^- , Cl^- , Br^- , I^- , OH^- , NO_3^- , SO_4^{2-}

- glycine, DL-alanine, DL-serine, L-serine, L-proline, L-valine, L-arginine, L-lysine, DL-threonine, L-threonine, L-histidine
- α -ABA, β -ABA, γ -ABA*
- α -AVA, γ -AVA[†]
- diglycine, triglycine, dialanine, alanylglycine, glycyalalanine

As far as experimental data was available solubilities of amino acids and peptides were modeled.

The influence of amino acids on the mean ionic activity coefficient of salts was investigated for 17 electrolyte/amino acid systems (see Appendix H, pp. 130).

As an example of a protein system hen egg-white lysozyme/NaCl solutions were chosen.

*ABA: aminobutyric acid

[†]AVA: aminovaleric acid

Chapter 2

Thermodynamical Background

2.1 Basics

A mixture of chemical compounds can distribute to multiple phases (solid, liquid, gas). There will be an interchange of components between the coexisting phases until equilibrium is reached and all intensive properties do not change anymore. Intensive properties are those that do not depend on the size, mass, or shape of the phase, such as temperature, pressure, density, and composition. The equilibrium thermodynamics provides an abstract mathematical framework which quantitatively relates the variables describing the state of the system.

A system is completely characterized by the following function which contains the information of the first and second law of thermodynamics:

$$U = U(S, V, \mathbf{n}) \quad (2.1)$$

Eq. 2.1 is called thermodynamic potential or fundamental function of the internal energy with the entropy S and the volume V as the respective fundamental variables. The total differential of this function is

$$dU = \underbrace{\left(\frac{\partial U}{\partial S}\right)_{V, \mathbf{n}}}_{T} dS + \underbrace{\left(\frac{\partial U}{\partial V}\right)_{S, \mathbf{n}}}_{-P} dV + \sum_{i=1}^N \underbrace{\left(\frac{\partial U}{\partial n_i}\right)_{S, V, n_{j \neq i}}}_{\mu_i} dn_i \quad (2.2)$$

Here, the dependence of the internal energy on the amount of each component i is given by the partial differential quotient $\left(\frac{\partial U}{\partial n_i}\right)_{S, V, n_{j \neq i}}$ and is called chemical potential μ_i .

Equilibrium is reached when the entropy is maximized or in other words the internal energy is at its minimum, i. e.

$$dS = 0 \quad , \quad d^2S < 0 \quad (2.3)$$

$$dU = 0 \quad , \quad d^2U > 0 \quad (2.4)$$

For a system consisting of C components distributed in π phases this can be translated

into the three well-known phase equilibrium conditions:

$$T^{(1)} = T^{(2)} = \dots = T^{(\pi)} = T \quad (2.5)$$

$$P^{(1)} = P^{(2)} = \dots = P^{(\pi)} = P \quad (2.6)$$

$$\mu_i^{(1)}(T, P, \mathbf{n}^{(1)}) = \mu_i^{(2)}(T, P, \mathbf{n}^{(2)}) = \dots = \mu_i^{(\pi)}(T, P, \mathbf{n}^{(\pi)}) \quad \forall i \in C \quad (2.7)$$

Applying Legendre transformation three other fundamental equations can be derived from Eq. 2.2:

$$dH = d(U + PV) = TdS + VdP + \sum_{i=1}^N \mu_i dn_i \quad (2.8)$$

$$dG = d(H - TS) = -SdT + VdP + \sum_{i=1}^N \mu_i dn_i \quad (2.9)$$

$$dA = d(U - TS) = -SdT - PdV + \sum_{i=1}^N \mu_i dn_i \quad (2.10)$$

The fundamental variables for the enthalpy H are S and P . The Gibbs (free) energy (or free enthalpy) plays an important role in equilibrium thermodynamics since its fundamental variables T and P are easily accessible experimentally in contrast to the entropy, for example. Also the Helmholtz (free) energy A , with its fundamental variables T and V , is of major interest because many thermodynamic models (especially those derived from statistical mechanics) are written in terms of the Helmholtz energy.

A comparison of the coefficients of the total differential equations (Eqs. 2.2, 2.9-2.10) and their respective fundamental equations (not shown here) yields following differential quotients:

$$\left(\frac{\partial U}{\partial S}\right)_{V, n_i} = \left(\frac{\partial H}{\partial S}\right)_{P, n_i} = T \quad (2.11)$$

$$\left(\frac{\partial U}{\partial V}\right)_{S, n_i} = \left(\frac{\partial A}{\partial V}\right)_{T, n_i} = -P \quad (2.12)$$

$$\left(\frac{\partial A}{\partial T}\right)_{V, n_i} = \left(\frac{\partial G}{\partial T}\right)_{P, n_i} = -S \quad (2.13)$$

$$\left(\frac{\partial H}{\partial P}\right)_{S, n_i} = \left(\frac{\partial G}{\partial P}\right)_{T, n_i} = V \quad (2.14)$$

and

$$\left(\frac{\partial U}{\partial n_i}\right)_{S, V, n_j \neq i} = \left(\frac{\partial H}{\partial n_i}\right)_{S, P, n_j \neq i} = \left(\frac{\partial G}{\partial n_i}\right)_{T, P, n_j \neq i} = \left(\frac{\partial A}{\partial n_i}\right)_{T, V, n_j \neq i} = \mu_i \quad (2.15)$$

The equations shown above prove the fact that the knowledge of one thermodynamic potential suffices to derive all other properties of a system. Hence, without loss of generality we confine ourselves to dealing only with the Helmholtz energy A and its derivatives throughout this work.

2.2 Calculation of Phase Equilibria

2.2.1 Vapor-Liquid and Liquid-Liquid Equilibria

The equality of the chemical potential of each component in every phase (Eq. 2.7) can be reformulated as the isofugacity criterium

$$f_i^{(1)} = f_i^{(2)} = \dots = f_i^{(\pi)} \quad \forall i \in C \quad (2.16)$$

Within the scope of this work the number of phases is restricted to two. There are three concepts for the calculation of phase equilibria: $\varphi - \varphi$, $\gamma - \varphi$, and $\gamma - \gamma$. These are explained below.

$\varphi - \varphi$ Concept

Using the definition of the fugacity coefficient φ_i

$$\varphi_i \equiv \frac{f_i}{x_i P} \quad (2.17)$$

with x_i being the mole fraction of component i one obtains

$$(x_i \varphi_i)^{(1)} = (x_i \varphi_i)^{(2)} \quad \forall i \in C \quad (2.18)$$

The fugacity coefficients are complex functions of system temperature, volume or density, and composition: $\varphi_i = \varphi_i(T, v, \mathbf{x})$. Therefore, the compositions in each phase must be calculated iteratively. As an example, the iteration algorithm for an isobaric-isothermal flash VLE or LLE calculation is illustrated in Fig. 2.1. However, this concept is generally applicable (also in the critical phase region where liquid and gas phase have similar properties) as long as there are equations of state providing the fugacity coefficients for each phase.

$\gamma - \varphi$ Concept

When calculating VLE the fugacity of the liquid phase can also be described by an activity coefficient γ_i while the behavior of the vapor phase is still captured by the fugacity coefficient:

$$f_i^L = x_i^L \gamma_i P_{0i}^{LV} \varphi_{0i}^{LV} Poy = x_i^V \varphi_i^V P = f_i^V \quad (2.19)$$

P_{0i}^{LV} and φ_{0i}^{LV} are the vapor pressure and the fugacity coefficient of pure component i , respectively. The Poynting factor Poy captures the pressure dependence of the fugacity coefficient and is negligible (≈ 1) for pressures below 10 bar. Further, the ratio $\varphi_{0i}^{LV} / \varphi_i^V \approx 1$ at low pressures. Hence, Eq. 2.19 simplifies to

$$x_i^L \gamma_i P_{0i}^{LV} = x_i^V P \quad (2.20)$$

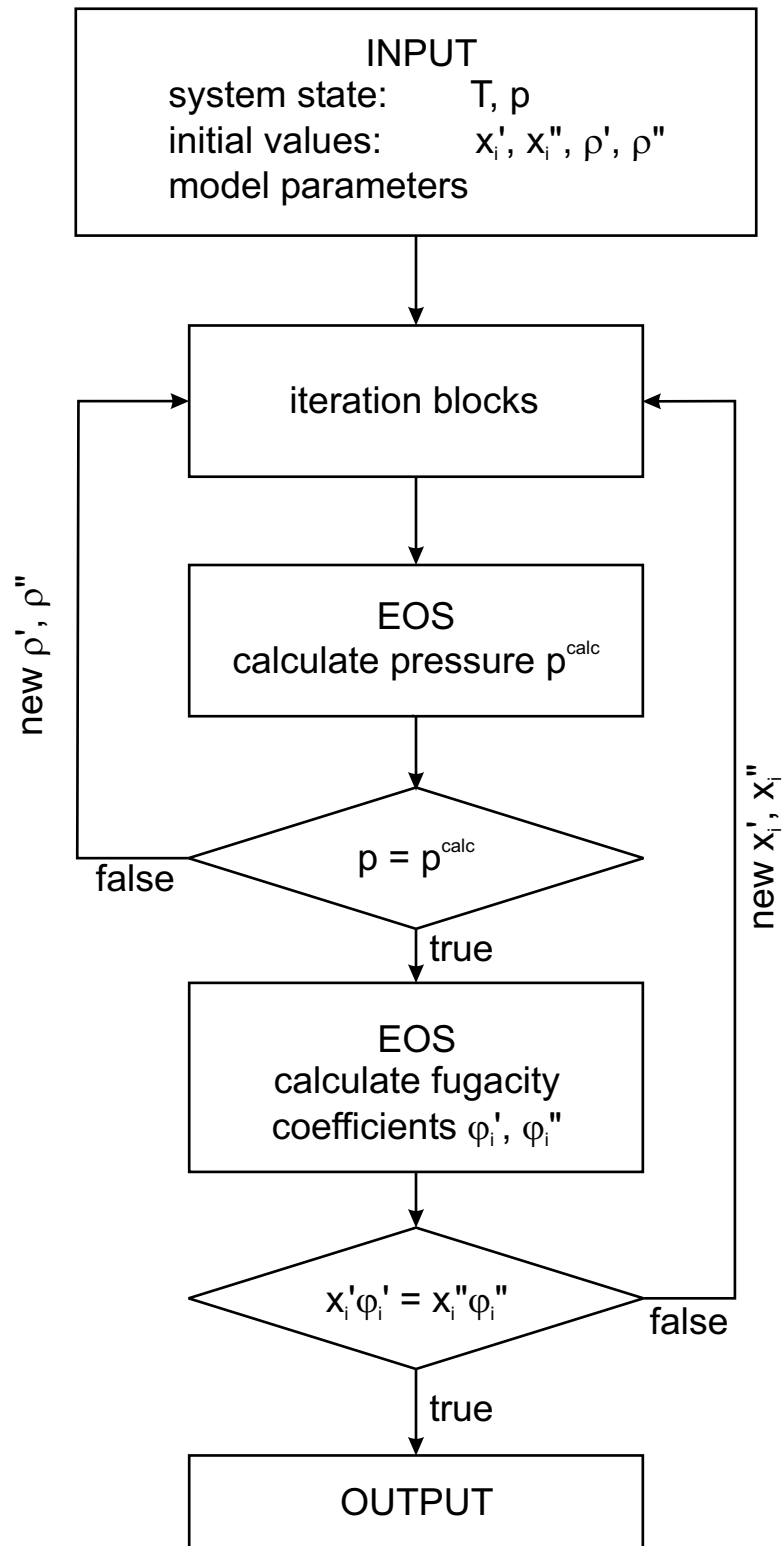


Fig. 2.1: Flowchart of an isobaric-isothermal VLE or LLE flash calculation for two phases ' and ''.

and at low concentration, i. e. in the limit of an ideal solution where $\gamma_i \approx 1$, to the well-known Raoult's law

$$x_i^L P_{0i}^{LV} = x_i^V P \quad (2.21)$$

The activity coefficient is obtained from g^E -models* or can as well be calculated with the help of an equation of state by the following definition

$$\gamma_i \equiv \frac{\varphi_i}{\varphi_{0i}} \quad (2.22)$$

One advantage of the $\gamma - \varphi$ concept is that for isothermal calculations and when the vapor pressure is given as a function of temperature (e. g. Antoine equation) the phase compositions are numerically easy to obtain. That is not the case for isobaric calculations. Phase equilibrium calculations at higher pressures with the $\gamma - \varphi$ concept are seldom performed because an equation of state is needed to evaluate the Poynting factor and the fugacities for Eq. 2.19. Hence, in this case it makes more sense to directly use the $\varphi - \varphi$ concept. Another shortcoming of the $\gamma - \varphi$ concept is that – based on different assumptions and simplifications for the liquid and the gas phase – the critical phase region is not well described.

$\gamma - \gamma$ Concept

For the description of LLE both liquid phases can be described with activity coefficients. This method is only applicable for pressure and density independent phase equilibria because g^E models generally are only able to capture the temperature and concentration dependence of the excess free energy. Nevertheless, due to the incompressibility of liquids, many binary mixtures reveal a negligible influence of the pressure on the phase equilibrium. Density effects due to temperature changes are also often neglected assuming similar thermal expansion coefficients for all components.

2.2.2 Solid-Liquid Equilibria

The fugacities of the solid (S) and the liquid (L) phase are formulated using activity coefficients:

$$f_i^S = x_i^S \gamma_i^S f_{0i}^S \quad (2.23)$$

$$f_i^L = x_i^L \gamma_i^L f_{0i}^L \quad (2.24)$$

where f_{0i}^S and f_{0i}^L are the (pure component) standard fugacities of the solid and the liquid, respectively. Rearranging Eqs. 2.23-2.24 one obtains the solubility of component i in the liquid phase

$$x_i^L = \frac{x_i^S \gamma_i^S f_{0i}^S}{\gamma_i^L f_{0i}^L} \quad (2.25)$$

*Remember: $g^E = k_B T \sum_i x_i \ln \gamma_i$.

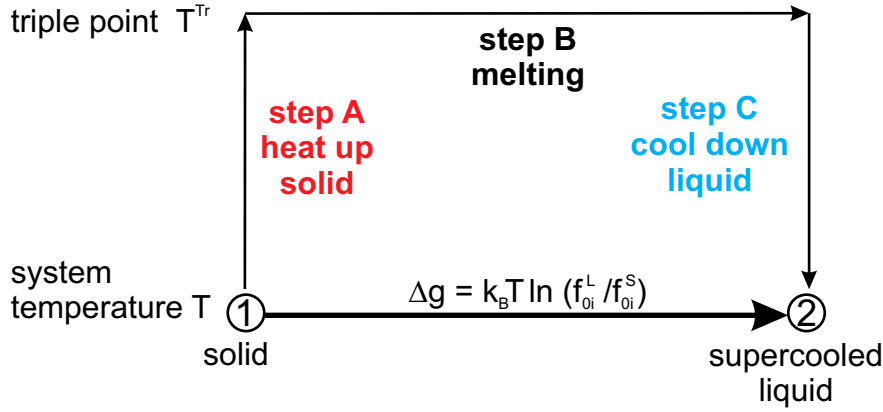


Fig. 2.2: Thermodynamic cycle for the calculation of the ratio f_{0i}^S/f_{0i}^L .

Unfortunately, the standard fugacities are not readily available, especially when the system temperature lies above the triple point of the crystallizing component and below the one of the other component. In this case ‘pure solid’ and ‘pure liquid’ represent hypothetical states. However, for the calculation of the solubility only the ratio f_{0i}^S/f_{0i}^L is of importance. One harnesses a thermodynamic cycle as illustrated in Fig. 2.2.

The specific Gibbs enthalpy change for the transition from pure solid ① to supercooled liquid ② at temperature T is given by

$$\Delta g = k_B T \ln \frac{f_{0i}^L}{f_{0i}^S} \quad (2.26)$$

In analogy to Eq. 2.10 in a closed system ($dn = 0$)

$$\Delta g = \Delta h - T \Delta s \quad (2.27)$$

where the change in enthalpy and entropy can be expressed as the sum of the changes for step A, step B, and step C:

$$\begin{aligned} \Delta h &= \int_T^{T_{0i}^{Tr}} c_{p,i}^S dT + \Delta h_{0i}^{Tr} + \int_{T_{0i}^{Tr}}^T c_{p,i}^L dT \\ &= \Delta h_{0i}^{Tr} + \int_{T_{0i}^{Tr}}^T \Delta c_{p,i} dT \end{aligned} \quad (2.28)$$

$$\begin{aligned} \Delta s &= \int_T^{T_{0i}^{Tr}} \frac{c_{p,i}^S}{T} dT + \frac{\Delta h_{0i}^{Tr}}{T_{0i}^{Tr}} + \int_{T_{0i}^{Tr}}^T \frac{c_{p,i}^L}{T} dT \\ &= \frac{\Delta h_{0i}^{Tr}}{T_{0i}^{Tr}} + \int_{T_{0i}^{Tr}}^T \frac{\Delta c_{p,i}}{T} dT \end{aligned} \quad (2.29)$$

Here, $\Delta c_{p,i}$ is the difference between the specific heat capacities of the solid and the liquid, respectively, i. e. $\Delta c_{p,i} = c_{p,i}^S - c_{p,i}^L$, and Δh_{0i}^{Tr} is the melting enthalpy at the triple point. Provided that the heat capacities are temperature independent between T and T_{0i}^{Tr} , one obtains

$$\ln \frac{f_{0i}^L}{f_{0i}^S} = \beta \Delta h_{0i}^{SL} \left(1 - \frac{T}{T_{0i}^{Tr}} \right) - \beta \Delta c_{p,i} (T_{0i}^{Tr} - T) + \frac{\Delta c_{p,i}}{k_B} \ln \frac{T_{0i}^{Tr}}{T} \quad (2.30)$$

Eq. 2.30 can be simplified assuming that the first term is the predominant one and that the others cancel out. Further, the triple point temperature is often substituted by the melting temperature T_{0i}^{SL} , hence Δh_{0i}^{Tr} becomes the melting enthalpy Δh_{0i}^{SL} at T_{0i}^{SL} . Finally one obtains an equation for the calculation of solubilities

$$-\ln \frac{f_{0i}^L}{f_{0i}^S} = \ln \frac{x_i^L \gamma_i^L}{x_i^S \gamma_i^S} = -\beta \Delta h_{0i}^{SL} \left(1 - \frac{T}{T_{0i}^{SL}} \right) \quad (2.31)$$

In case of a pure solid the activity of the solid becomes unity and Eq. 2.31 is rearranged to directly yield the solubility

$$x_i^L = \frac{1}{\gamma_i^L} \exp \left\{ -\beta \Delta h_{0i}^{SL} \left(1 - \frac{T}{T_{0i}^{SL}} \right) \right\} \quad (2.32)$$

2.3 Calculation of Thermodynamic Properties from Helmholtz Energy

In the following subsections it will be shown how to calculate the fugacity coefficients from an equation of state. The equation of state used in this work is given in terms of the residual Helmholtz energy. Here, ‘residual’ denotes the difference between a property of a real fluid and that of an ideal gas evaluated at the same T , V , and total number of molecules N . Hence,

$$A^{res}(T, V, N) = A(T, V, N) - A^{id}(T, V, N) \quad (2.33)$$

For convenience we define a dimensionless Helmholtz energy which is related to N

$$a(T, v, \mathbf{x}) \equiv \frac{A(T, V, N)}{Nk_B T} \quad (2.34)$$

2.3.1 Pressure

The pressure results from the partial derivative of the reduced Helmholtz energy with respect to the specific volume v at constant T and composition \mathbf{x} (in analogy to Eq. 2.13):

$$\left(\frac{\partial a}{\partial v} \right)_{T, \mathbf{x}} = -\beta P \quad (2.35)$$

$$\left(\frac{\partial (a^{id} + a^{res})}{\partial v} \right)_{T, \mathbf{x}} = -\beta (P^{id} + P^{res}) \quad (2.36)$$

with $\beta \equiv 1/k_B T$. Hence, the system pressure is

$$\beta P = \beta P^{id} - \left(\frac{\partial a^{res}}{\partial v} \right)_{T,x} \quad (2.37)$$

with $P^{id} = k_B T/v$. An often used thermodynamic quantity is the compressibility factor

$$Z = \frac{Pv}{k_B T} = 1 + Z^{res} \quad (2.38)$$

2.3.2 Chemical Potential and Fugacity Coefficients

For the calculation of phase equilibria according to Eq. 2.18 a relationship between the residual Helmholtz energy a^{res} , the fugacity coefficient φ_i and the chemical potential $\mu_i(T, V)$ is needed.

First we define the chemical potential as function of T and P :

$$\mu_i(T, P) = \mu_i^{id}(T, P) + k_B T \cdot \ln \frac{f_i}{x_i P} \quad (2.39)$$

In this case the standard state of the ideal gas is chosen to be at T and P . Since T , P , and V are linked variables following equality is valid at equilibrium:

$$\mu_i(T, P) = \mu_i(T, V) \quad (2.40)$$

Subtracting $\mu_i^{id}(T, V)$ on both sides of Eq. 2.40 and including the definition of the fugacity coefficient (Eq. 2.17) one obtains

$$\mu_i^{res}(T, V) = (\mu_i^{id}(T, P) - \mu_i^{id}(T, V)) + k_B T \cdot \ln \varphi_i \quad (2.41)$$

The term in brackets is equivalent to $(k_B T \cdot \ln Z)$ so that one finally gets an equation for the calculation of the fugacity coefficient from chemical potential and compressibility factor:

$$\begin{aligned} \ln \varphi_i &= \beta \mu_i^{res}(T, V) - \ln Z \\ &\quad \downarrow \text{(Eq. 2.15)} \\ &= \beta \left(\frac{\partial A^{res}}{\partial n_i} \right)_{T,v,n_{j \neq i}} - \ln Z \end{aligned} \quad (2.42)$$

It can be shown that the partial derivative can be replaced by³

$$\begin{aligned} \beta \left(\frac{\partial A^{res}}{\partial n_i} \right)_{T,v,n_{j \neq i}} &= a^{res} + Z^{res} + \left(\frac{\partial a^{res}}{\partial x_i} \right)_{T,v,x_{k \neq j}} \\ &\quad - \sum_j^C x_j \left(\frac{\partial a^{res}}{\partial x_j} \right)_{T,v,x_{k \neq j}} \end{aligned} \quad (2.43)$$

2.3.3 Activity Coefficients and Reference States

As already mentioned in Sec. 2.2.1 the activity coefficient is calculated as the ratio of the fugacity coefficient in the mixture and the one of the pure component[†]

$$\gamma_i \equiv \frac{\varphi_i}{\varphi_{0i}} \quad (2.22)$$

This definition is only meaningful if there exists an equation of state able to represent both the aggregate state of the mixture ($\rightarrow \varphi_i$) and the one of the pure component, i. e. the respective reference fugacity coefficient φ_{0i} . As an example, the activity coefficient of an amino acid in water shall be calculated. The solution is liquid while at the same conditions (T, P) the pure amino acid is solid. Hence, in this case the application of Eq. 2.22 is not feasible. In order to avoid this shortcoming one introduces a new standard state, the *hypothetical ideal solution*. The chemical potential of the solute i in this standard state is defined at system temperature, pressure, and at unit concentration $x_i = 1$. Transferred to the real solution that means that $\gamma_i \rightarrow 1$ for $x_i \rightarrow 0$, or in words: component i is infinitely diluted in the solvent system. We define the fugacity coefficient at infinite dilution (index ∞)

$$\varphi_i^\infty(\mathbf{n}) = \lim_{n_i \rightarrow 0} \varphi_i(\mathbf{n}) \quad (2.44)$$

or in terms of mole fractions

$$\varphi_i^\infty(\mathbf{x}) = \lim_{x_i \rightarrow 0} \varphi_i(\mathbf{x}, \frac{x_j}{x_k} = \text{const}) \quad (2.45)$$

where, $\frac{x_j}{x_k} = \text{const}$ denotes that the ratio of the mole fraction of each pair of components j and k ($j, k \neq i$) remains constant. For example, consider a ternary mixture at $x_1 = 0.5$, $x_2 = 0.3$, $x_3 = 0.2$. Then the fugacity coefficient at infinite dilution of component 1 is

$$\varphi_1^\infty = \varphi_1(x_1 = 0.0, x_2 = 0.6, x_3 = 0.4)$$

Having defined the fugacity coefficient at infinite dilution one obtains the so-called unsymmetric activity coefficient

$$\tilde{\gamma}_i \equiv \frac{\varphi_i}{\varphi_i^\infty} \left(= \frac{\gamma_i \cdot \varphi_{0i}}{\gamma_i^\infty \cdot \varphi_{0i}} \right) \quad (2.46)$$

Things get more involved if the solute is an electrolyte. Although one can define the activity coefficient of the single ion $\tilde{\gamma}_+$ and $\tilde{\gamma}_-$ and calculate them for example with the help of an equation of state, it is not possible to measure them separately. By potentiometric or vapor pressure measurements one always obtains a mean ionic activity coefficient (MIAC)

$$\tilde{\gamma}_\pm = (\tilde{\gamma}_+^{\nu_+} \cdot \tilde{\gamma}_-^{\nu_-})^{\frac{1}{\nu}} \quad (2.47)$$

[†]For the sake of better legibility the dependency of φ_i on T, P is omitted in the following, i. e. $\varphi_i = \varphi_i(T, P)$.

where ν_+ and ν_- are the stoichiometric coefficients of the cation and the anion, respectively, $\nu = \nu_+ + \nu_-$. In literature one will often find MIAC on a molal basis. The relation between the molal scale (index m) and the mole fraction scale (index x) is given as[‡]

$$\tilde{\gamma}_{\pm}^m = \frac{\tilde{\gamma}_{\pm}^x}{1 + \frac{M_W}{1000} \cdot \nu \cdot m_S} \quad (2.48)$$

where M_W is the molecular weight of the solvent (in our case water) in g/mol and m_S is the molality of the salt as weighed into solution in mol salt per kg of solvent. The mean ionic activity a_{\pm} of the salt is defined as $a_{\pm} = m_{\pm} \gamma_{\pm}$ with

$$m_{\pm} = (m_+^{\nu_+} m_-^{\nu_-})^{\frac{1}{\nu}} = m_S (\nu_+^{\nu_+} \nu_-^{\nu_-})^{\frac{1}{\nu}} \quad (2.49)$$

If not stated differently, the activity coefficients appearing in this work are unsymmetrically scaled and on molal basis. Hence, the index m will be omitted for the sake of better legibility.

Activity Coefficients in Amino Acid/Electrolyte Solutions

As mentioned above, MIAC in binary electrolyte solutions are easily determined by electrochemical methods. The procedure is somewhat more intricate when a second solute (e. g. an amino acid) is present in the electrolyte solution. By using ion selective electrodes (ISE) the ratio of the MIAC of the electrolyte in the ternary solution (index *ter*) to the one in the binary solution without amino acid but at same electrolyte molality (index *bin*) can be measured,[§]

$$\gamma_{\pm}^{ter} / \gamma_{\pm}^{bin}$$

The experimental method shall not be the issue here. The reader is referred to the literature: e. g. see Refs.^{4,5}

Unfortunately, the activity coefficient of the non-electrolyte solute cannot be measured directly. However, the ratio of the activity coefficient of the amino acid in the ternary solution to the one in the binary solution without electrolyte[¶]

$$\gamma_A^{ter} / \gamma_A^{bin}$$

[‡]For the derivation of this conversion formula see Appendix E.

[§]It shall be emphasized at this point that the reference state for the ratio of MIAC is not the infinite dilution but the (hypothetical) pure component. This is due to the fact that the infinite dilution in the binary solution is different from the one in the ternary (containing also an amino acid).

[¶]In analogy to $\gamma_{\pm}^{ter} / \gamma_{\pm}^{bin}$ the reference state for $\gamma_A^{ter} / \gamma_A^{bin}$ is also the pure component.

is related to the electrolyte's MIAC by the Gibbs-Duhem equation^{||}:

$$\nu \int_{m_{\pm}=0}^{m_{\pm}} \left(\frac{\partial \ln \gamma_{\pm}^{ter}}{\partial m_A} \right)_{m_{\pm}} dm_{\pm} = \ln \left(\frac{\gamma_A^{ter}}{\gamma_A^{bin}} \right)_{m_{\pm}} \quad (2.50)$$

Hence, measured electrolyte activity coefficients can – at least theoretically – be converted to activity coefficients of the amino acid. This approach has been widely applied by Khoshkbarchi et al.⁶ However, the applicability of this concept is questionable. A discussion can be found in Appendix G.

^{||}This equation is also called cross-differential equation. Its derivation can be found in Appendix F.

Chapter 3

Equations of State from Statistical Mechanics

3.1 Fundamentals

Many equations of state have been developed in the past centuries – van der Waals EOS and Peng Robinson EOS, just to mention two of them. They describe the thermodynamic properties of pure liquids and gases and their mixtures. Equations of state quantify the dependency of the system pressure on system volume, temperature, and composition. Further, they allow the calculation of fugacity coefficients. Equations of state can be derived on the basis of the (classical canonical*) partition function Q by using the well-known relationship

$$A(T, V, N) = -k_B T \ln Q(T, V, N) \quad (3.1)$$

The partition function is obtained by summation over all possible energy states in a system of N particles at coordinates $\mathbf{r}^N = [\mathbf{r}_1 \dots \mathbf{r}_N]$:

$$Q = \frac{1}{N! \Lambda^{3N}} (q_v q_r q_e)^N \underbrace{\int_V \exp \{-\beta U_N(\mathbf{r}^N)\} d\mathbf{r}^N}_{\text{configuration integral } \Phi} \quad (3.2)$$

Here, $\Lambda = \sqrt{\frac{h^2}{2\pi m k_B T}}$ is the de Broglie wavelength, q_v, q_r, q_e are the contributions from vibrational, rotational, and electron movements of the molecules, respectively. These terms are negligible when dealing with spherically symmetric molecules and shall be omitted further on for the sake of simplicity. U_N is the internal energy arising from interactions between the molecules. Assuming that the intermolecular interactions are pair-wise additive, i. e. they consist solely of pair terms, U_N can be written as

$$U_N = u_{12} + u_{23} + \dots + u_{ij} = \sum_{i < j}^N u_{ij} \quad (3.3)$$

*A classical canonical ensemble is an ensemble of energy states at equal temperature, volume, and number of molecules.

Hence, the integrand of the configuration integral Φ becomes

$$\exp\{-\beta U_N(\mathbf{r}^N)\} = \exp\left\{-\beta \sum_{i<j}^N u(r_{ij})\right\} = \prod_{i<j}^N \exp\{-\beta u(r_{ij})\} \quad (3.4)$$

In general, the pair potential $u(r)$ approaches 0 at large separations ($r \rightarrow \infty$), where molecules do not 'feel' each other anymore, and to infinity at small separations which prevents molecular overlap. For further calculations it is convenient to define the so-called Mayer f -function that approaches zero at large separations and has a defined limit at small separations:

$$f(r) \equiv \exp\{-\beta u(r)\} - 1, \quad \begin{cases} \lim_{r \rightarrow 0} f(r) = -1 \\ \lim_{r \rightarrow \infty} f(r) = 0 \end{cases} \quad (3.5)$$

Inserting Eq. 3.5 into Eq. 3.4 leads to

$$\exp\{-\beta U_N(\mathbf{r}^N)\} = \prod_{i<j}^N [1 + f(r_{ij})] . \quad (3.6)$$

Exemplarily, for $N = 3$ molecules interacting pair-wise this product may be expanded (writing $f_{ij} \equiv f(r_{ij})$)

$$\begin{aligned} (1 + f_{12})(1 + f_{13})(1 + f_{23}) &= 1 + f_{12} + f_{13} + f_{23} + \dots \\ &\dots + f_{12}f_{13} + f_{12}f_{23} + f_{13}f_{23} + \dots \\ &\dots + f_{12}f_{13}f_{23} \end{aligned} \quad (3.7)$$

Keeping in mind the expansion in Eq. 3.7 and neglecting terms of higher order (i. e. the indirect interaction of two particles over a third one) the configurational integral is rewritten as

$$\begin{aligned} \Phi &= \int_V \exp\{-\beta U_N(\mathbf{r}^N)\} d\mathbf{r}^N \\ &= \int_V \prod_{i<j}^N [1 + f_{ij}] d\mathbf{r}^N \\ &= \int_V \left[1 + \sum_{i<j} f_{ij} + \dots \right] d\mathbf{r}^N \end{aligned} \quad (3.8)$$

This integral can be split up into its addends. The term of zeroth order is simply $\Phi_0 = V^N$. As there is no interaction involving only one atom the next order is two. Since the indices are only dummy variables all second order terms give the same contribution. From statistical considerations one can derive that there are $N(N - 1)/2$ binary combinations,

hence

$$\begin{aligned}
\Phi_2 &= \frac{N(N-1)}{2} \int_V f_{ij} d\mathbf{r}^N \\
&= \frac{N(N-1)}{2} V^{N-2} \int_V f(r) d\mathbf{r}_1 d\mathbf{r}_2 \\
&= \frac{N(N-1)}{2V^2} V^N V \int_V f(r) d\mathbf{r}
\end{aligned} \tag{3.9}$$

The first factor is simply $\rho_N^2/2$, the second is equal to Φ_0 and V is the integral over $d\mathbf{r}_2$. The two terms Φ_0 and Φ_2 contribute to an expansion of the configurational integral $\Phi = \Phi_0(1 + \Phi_2/\Phi_0 + \dots)$ [†]. Considering the relationship between the Helmholtz free energy and the configurational integral as given in Eq. 3.1 and approximating the logarithm by its power series one obtains

$$\begin{aligned}
A &= \underbrace{-k_B T \ln[V^N/N! \Lambda^{3N}]}_{A^{id}} - k_B T \ln[1 + \Phi_2/\Phi_0 + \dots] \\
&= A^{id} - \frac{\rho_N^2 V k_B T}{2} \int_V f(r) d\mathbf{r} + \dots
\end{aligned} \tag{3.10}$$

This is now a power series in terms of the density for the Helmholtz free energy. Differentiation (Eq. 2.13) directly leads to the corresponding power series for the pressure:

$$\beta P = \rho_N - \frac{\rho_N^2}{2} \int_V f(r) d\mathbf{r} + \dots \tag{3.11}$$

By comparison of Eq. 3.11 to the well-known virial expansion of the pressure in terms of density

$$\beta P = \sum_{i=1}^{\infty} B_i^* \rho_N^i \tag{3.12}$$

one sees that the first term $B_1^* = 1$ corresponds to the ideal gas expression while the second virial coefficient can be calculated by

$$\begin{aligned}
B_2^* &= -\frac{1}{2} \int_V f(r) d\mathbf{r} \\
&= -2\pi \int_0^{\infty} [\exp\{-\beta u(r)\} - 1] r^2 dr
\end{aligned} \tag{3.13}$$

We will come back to this quantity in Sec. 4.4.

The pressure expansion in terms of density derived so far reduces the many-body problem to the sum of two-body, three-body, etc. problems. Such a decomposition is only applicable in the low density region, i. e. in gaseous fluids. In liquids each molecule is in permanent interaction with a large number of its surrounding neighbors. Therefore, more sophisticated techniques which account for the structure of the fluid have to be used. The next section is

[†]This kind of expansion is called Padé approximation.

devoted to a central idea included in most of the theories for liquids: the radial distribution function.

3.2 Radial Distribution Function

The radial distribution function $g(r, \rho_N)$ gives the probability to find a molecule at distance r in an infinitesimally narrow annulus of width dr from a randomly chosen center molecule when the whole system has the global density ρ_N (see Fig. 3.1). In other words $g(r, \rho_N)$ is the ratio between local and global density.[‡]

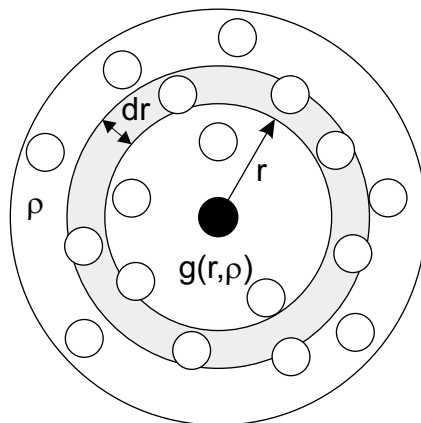


Fig. 3.1: Illustration of the radial distribution function $g(r, \rho_N)$.

The radial distribution function can be calculated by either molecular simulation or by numerical or analytical calculations on the basis of statistical mechanics. The first method is based upon computer simulations of a model system containing N molecules in a volume V with system density $\rho_N = N/V$. The molecules are characterized by their shape (spheres, chains, ...), size (σ) and intermolecular potential ($u(r)$: hard-sphere, LJ-potential, ...). Either by random displacement (Monte Carlo simulation) or by solving the Newtonian equations (Molecular Dynamics) a large amount of new system configurations (typically $10^5 - 10^6$) are generated and the frequency of occurrence of intermolecular distance r between two particles is averaged over all configurations yielding directly $g(r)$.

The second method consists in solving integral equations to calculate $g(r)$. Making simplifying assumptions it is possible to solve these integrals analytically. Due to the simplifications the models cannot reach the accuracy of molecular simulations. There is a trade-off between the lower accuracy when solving the integral equations and the time-consuming simulations.

As mentioned before, $g(r)$ gives the probability of finding the center of a molecule at distance r from a reference particle. For hard spheres with diameter σ it is obvious that $g(r < \sigma) = 0$ since there cannot be any intersection between the two spheres. At infinite

[‡]For convenience we write $g(r)$ instead of $g(r, \rho_N)$ keeping in mind the dependency of g on the global density ρ_N .

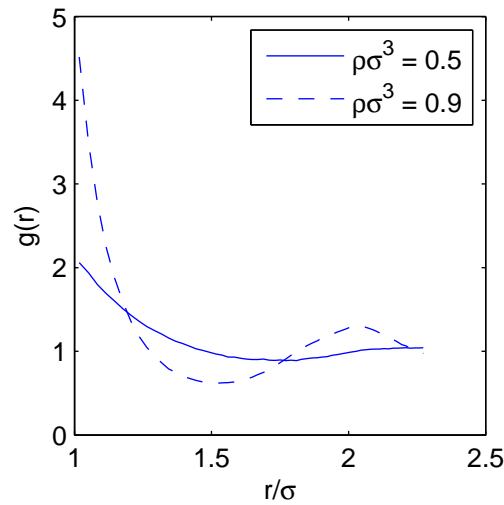


Fig. 3.2: Hard-sphere radial distribution function $g(r)$ at two different reduced densities. Data taken from Ref.⁷

distance the probability of finding another molecule approaches unity, hence the local density approaches the bulk value.

Here, the influence of the origin molecule is negligible. Fig. 3.2 shows the curve progression of $g(r)$ at different system densities for hard spheres. Especially at high densities the local density in the direct vicinity of the center molecule is much higher than the global density. This clearly shows that $g(r)$ is a direct measure for the interdependence of two molecules. The value at contact distance, more precisely the right limit $g(r = \sigma^+) = \lim_{r \rightarrow \sigma^+} g(r)$, plays an important role in perturbation theories (see Sec. 3.5).

For convenience the function

$$h(r) \equiv g(r) - 1 \quad (3.14)$$

is defined. This so-called correlation function describes the difference between the local and the global density. Therefore, it reflects the mutual influence of two molecules.

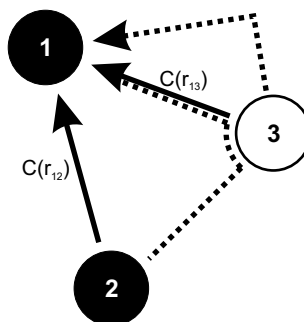


Fig. 3.3: Direct (—) and indirect (---) correlation of three molecules.

Most approaches for the calculation of $g(r)$ or $h(r)$ are based on the Ornstein-Zernicke

equation[§]. Both authors suggested in 1914 to split up the correlation function $h(r_{12})$ between two molecules 1 and 2 into one direct part $c(r_{12})$ and one indirect part (see Fig. 3.3). $c(r_{12})$ is consequently named direct correlation function and accounts for the interactions that arise directly from particle 1 towards particle 2. Furthermore, there is a collateral influence of 2 towards 1 which is mediated through a third molecule 3 either directly or indirectly. This ‘detour’ effect is accounted for averaging over all possible position configurations of 3 weighted by the system density ρ_N . The correlation function is then

$$h(r_{12}) = c(r_{12}) + \rho_N \int_V c(r_{13})h(r_{23}) d\mathbf{r}_3 \quad (3.15)$$

Eq. 3.15 is called Ornstein-Zernicke equation and gives the definition for the direct correlation function $c(r)$. Unfortunately, Eq. 3.15 is implicit and can only be solved if $c(r)$ is expressed in terms of $h(r)$ or $g(r)$. For short-range interactions between the molecules Percus and Yevick proposed following approximation⁸:

$$c(r) = g(r)[1 - \exp\{\beta u(r)\}] \quad (3.16)$$

Inserting Eq. 3.16 into Eq. 3.15 and defining

$$y(r) = g(r) \exp\{\beta u(r)\} \quad (3.17)$$

and

$$f(r) = \exp\{-\beta u(r)\} - 1 \quad (3.5)$$

yields the Percus-Yevick (PY) integral equation for the calculation of $h(r)$ or $g(r)$ respectively:

$$y(r_{12}) = 1 + \rho_N \int_V f(r_{13})y(r_{13})h(r_{23}) d\mathbf{r}_3 \quad (3.18)$$

Another integral equation, the so-called hypernetted-chain (HNC) equation, is obtained by setting

$$c(r) = g(r) - 1 - \ln g(r) - \beta u(r) \quad (3.19)$$

and yields

$$\ln y(r_{12}) = \rho_N \int_V [h(r_{13}) - \ln g(r_{13}) - u(r_{13})]h(r_{23}) d\mathbf{r}_3 \quad (3.20)$$

Both approaches presented above have been used for analytical or numerical evaluation of the radial distribution function for hard spheres, hard chains, LJ-molecules and the results have more or less successfully been compared to molecular simulations (see Ref.³ pp. 129f).

3.3 Relation of Thermodynamic Functions to $g(\mathbf{r})$

The intermolecular potential energy between two randomly chosen molecules at r and $r + dr$ is simply $u(r) \cdot \rho_N g(r) \cdot 4\pi r^2 dr$. After integration over all possible positions r and

[§]Original papers see: L. Ornstein and F. Zernike. *Proc. Kon. Akad. Wet. Amsterdam*, 19: 132, 1917; L. Ornstein and F. Zernicke. *Phys. Z.*, 19: 134, 1918.

accounting for the commutability of the molecules by multiplying with $N/2$, the internal energy of the system is given by

$$U = \frac{N\rho_N}{2} \int_0^\infty u(r) \cdot g(r) \cdot 4\pi r^2 dr \quad (3.21)$$

Applying Eq. 2.13 gives the so-called *pressure equation*

$$-\beta \left(\frac{\partial U}{\partial V} \right)_{S,N} = \frac{P}{k_B T} = \rho_N - \frac{\rho_N^2}{6k_B T} \int_0^\infty r \left(\frac{\partial u(r)}{\partial r} \right) \cdot g(r) \cdot 4\pi r^2 dr \quad (3.22)$$

An alternative function is the *compressibility equation*

$$k_B T \left(\frac{\partial \rho_N}{\partial P} \right)_T = 1 - \rho_N \int_0^\infty [g(r) - 1] 4\pi r^2 dr \quad (3.23)$$

Both Eq. 3.22 and Eq. 3.23 allow the calculation of the pressure directly from the intermolecular potential $u(r)$ and the radial distribution function $g(r)$. However, the integrals can only be solved – after some simplifications – for a few model systems such as the hard-sphere system. Although these simple systems do not reflect reality sufficiently well, they have been of major interest in the past decades. A series of equations of state are based on perturbation theory. This topic will be addressed in Section 3.5.

3.4 Intermolecular Potentials

In this section the most common intermolecular potentials are presented. The simplest form is the already mentioned hard-sphere (hs) potential. Due to the hard core the spheres repel each other at contact. Otherwise they do not ‘feel’ their neighbors. The curve progression and the function of the hs potential are given in Fig. 3.4a. To account for attractive forces (negative values of $u(r)$) the square-well (sw) potential provides a simple and in most cases analytically manageable alternative. Like the hs-molecule the sw-molecule has an invariant diameter and exerts a constant attractive force (potential depth u_0) within σ and $\lambda\sigma$ (Fig. 3.4b). If the box length approaches zero then the molecules stick together when they collide due to an extremely strong but short-ranged attraction (Fig. 3.4c). The Lennard-Jones (LJ) potential (Fig. 3.4d) is best suited to represent the real interactions between molecules, especially at high pressure since it also accounts for soft repulsion at $r < \sigma$. However, since the application of the LJ potential leads to analytically unsolvable integral expressions, in many cases one harks back to the sw-potential.

3.5 Perturbation Theories

As mentioned above, many equations of state are based on perturbation theory. Therefore, a short explanation of its main principals shall be given here. The idea behind a perturbation theory is to find an approximate solution to a problem by starting from an exactly solvable related problem and then adding terms that account for deviations from

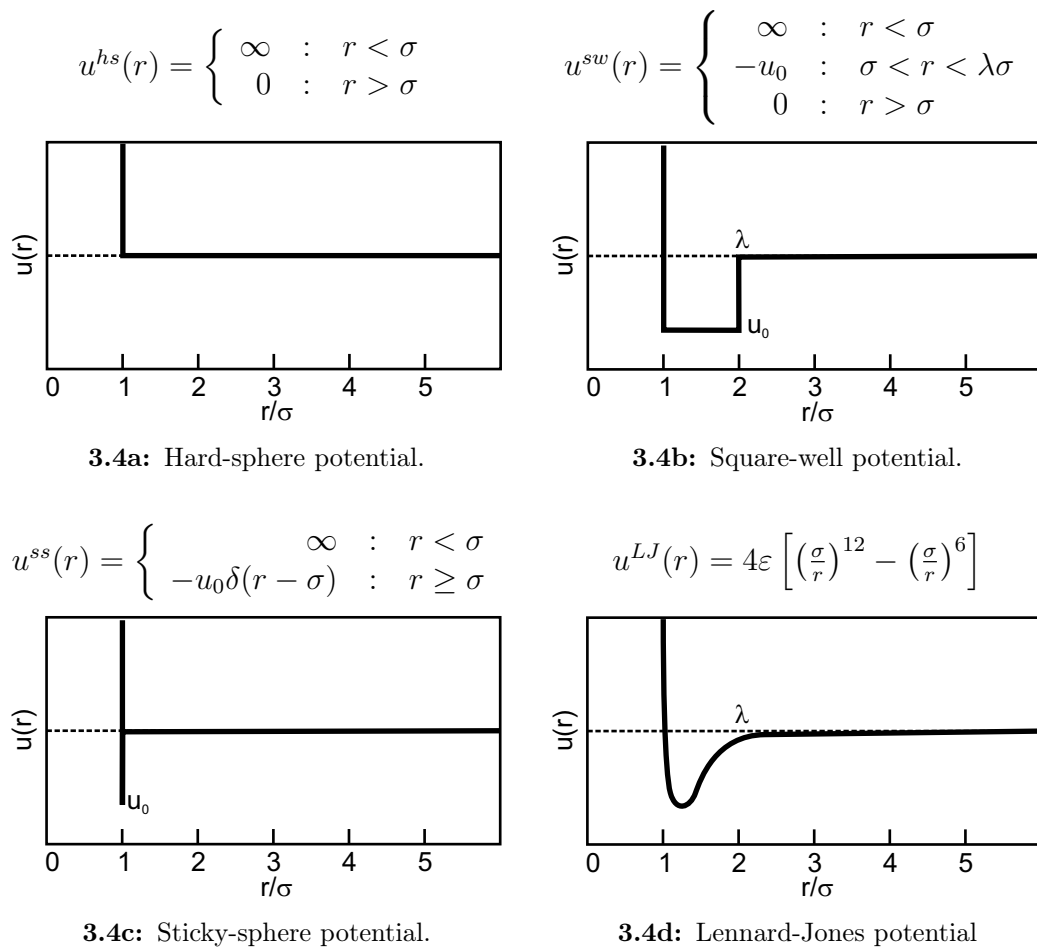


Fig. 3.4: Intermolecular potentials.

the exact solutions. Transferred to equations of state that means that one starts from a reference system (e. g. hard-sphere) and adds terms to account for deviations from the reference system. The basis of modern perturbation theories was developed by Zwanzig in the early 1950s^{9,10}. He considered spherical molecules with a Lennard-Jones interaction potential. This total potential energy is divided into a repulsive (reference) and an attractive (perturbation) part,

$$U(r) = U^{ref}(r) + U^{pert}(r) \quad (3.24)$$

The residual free energy of the system is therefore also split into a reference and a perturbation part which is expanded in terms of β

$$\begin{aligned} A^{res} &= A^{ref} + A^{pert} \\ &= A^{ref} + \omega_1 + \beta\omega_2 + \mathcal{O}(\beta^2) \end{aligned} \quad (3.25)$$

ω_1 and ω_2 are perturbation terms of first and second order, respectively[¶]. There are several approaches for their calculations¹²⁻¹⁴. In the following the Barker-Henderson Theory is discussed in more detail since it provides the basis for the equations of state (PC-SAFT and PMF-model) used in this work. Under the assumption that the total energy is the sum of pair potentials (Eq. 3.3) ω_1 is easily obtained as

$$\omega_1 = \frac{\rho_N}{2} \int_0^\infty u^{pert}(r) g^{ref}(r) 4\pi r^2 dr \quad (3.29)$$

Note that the radial distribution function is the one of the reference system. The derivation of the second-order term is a little bit more involved because it includes three- and four-body distribution functions. Barker and Henderson¹² give an approximated term for ω_2

$$\omega_2 = -\frac{\rho_N}{4} \int_0^\infty [u^{pert}(r)]^2 \left(\frac{\partial \rho_N}{\partial P} \right) g^{ref}(r) 4\pi r^2 dr \quad (3.30)$$

This is the so-called *macroscopic compressibility approximation*. A better approach is obtained replacing $\left(\frac{\partial \rho_N}{\partial P} \right) g^{ref}$ by $\left(\frac{\partial [\rho_N \cdot g^{ref}]}{\partial P} \right)$ yielding the *local compressibility approximation*:

$$\begin{aligned} a^{res} = a^{ref} &+ \frac{\rho_N \beta}{2} \int_0^\infty u^{pert}(r) g^{ref}(r) 4\pi r^2 dr \\ &- \frac{\rho_N \beta}{4} \int_0^\infty [u^{pert}(r)]^2 \left(\frac{\partial [\rho_N \cdot g^{ref}(r)]}{\partial P} \right) 4\pi r^2 dr \end{aligned} \quad (3.31)$$

Finally, an appropriate separation of the interaction potential in a reference and a perturbation part is necessary. Barker and Henderson investigated Lennard-Jones spheres. They suggested to split up the potential into a positive (repulsive) and a negative (attractive) part as illustrated in Fig. 3.5. As reference they used the hard-sphere system. Since the hard sphere is not an integral part of the Lennard-Jones potential (as it is for the square-well potential), an effective hard-sphere diameter must be chosen. Barker and Henderson

[¶]This power series is obtained inserting the perturbation potential (Eq. 3.24) into Eq. 3.1. It results that the perturbation free energy is given by

$$A^{pert} = -k_B T \ln \langle \exp\{-\beta U_N^{pert}\} \rangle \quad (3.26)$$

where $\langle \rangle$ denotes a statistical average. The power series in terms of β is then

$$A^{pert} = \sum_{n=1}^{\infty} \frac{\omega_n}{n!} (-\beta)^{n-1} \quad (3.27)$$

where the coefficients ω_n are functions of $\langle (U_N^{pert})^n \rangle$. Further, replacing the exponential function in Eq. 3.26 by its power series one obtains

$$\exp\{-\beta A^{pert}\} = \exp \left\{ \sum_{k=0}^{\infty} \frac{\beta_k}{k!} \langle (U_N^{pert})^k \rangle \right\} \quad (3.28)$$

Comparison of like coefficients in Eq. 3.27 and Eq. 3.28 yields the coefficients ω_n , e. g. $\omega_1 = \langle U_N^{pert} \rangle$ ¹¹.

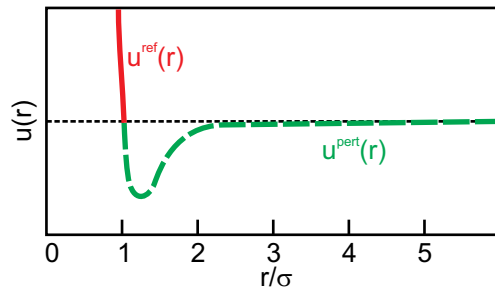


Fig. 3.5: Separation of the Lennard-Jones potential into a reference part (—) and a perturbation part (---) according to Barker and Henderson.

suggested the following expression for a temperature-dependent hard-sphere diameter

$$\sigma_{hs} = \sigma_{LJ} \int_0^1 [1 - \exp\{-\beta u(x)\}] dx, \quad x = r/\sigma_{LJ} \quad (3.32)$$

Thereby, the soft-core repulsion behavior of real fluids can be accounted for.

A whole family of equations of state was developed on the basis of Eqs. 3.31 and 3.32. Either the integrals were calculated analytically or they were approximated by power series of varying order. For example, Alder et al.¹⁵ suggested a fourth-order expression for the dispersion energy a^{disp}

$$a^{disp} = \sum_{i=1}^4 \sum_{j=1}^9 A_{ij} \left(\frac{\varepsilon}{k_B T} \right)^i \left(\frac{\eta}{\tau} \right)^j \quad (3.33)$$

where $\eta = \frac{\pi}{6} \sigma^3 \rho_N$ is a dimensionless density and $\tau = \frac{\pi}{6} \sqrt{2}$ is the packing fraction at closest packing. The authors fitted the constants A_{ij} to computer simulation data of square-well molecules. Chen and Kreglewski¹⁶ used experimental density and virial coefficient data of argon, instead, to allow a better description of real substances. This led to the BACK (Boublik-Alder-Chen-Kreglewski) equation of state. Chapman et al.^{17,18} and Huang and Radosz^{19,20} followed a similar approach to develop the well-known SAFT (Statistical Association Fluid Theory) equation of state. The kernel of their work is the application of Wertheim's first-order thermodynamic perturbation theory (TPT1)^{21–26} in order to account for the concatenation of hard-sphere segments to chains and for associative effects such as hydrogen bonding between molecules. However, the dispersion term is inconsistently still based on a hard-sphere reference system.

To circumvent this shortcoming Groß and Sadowski^{2,27,28} developed an equation of state whose reference state is the hard-chain instead of the hard-sphere. This implies that in the Barker-Henderson integrals in Eq. 3.31 the hard-sphere radial distribution function must be replaced by a hard-chain distribution function. Hence, this equation of state is called Perturbed-Chain SAFT (PC-SAFT). However, in analogy to the proceeding of Chen and Kreglewski, Groß et al. substituted the integrals by power series in terms of temperature T , density η , and segment number m_{seg} and fitted the model constants to experimental data of the alkane homologous series. They obtained an equation of state which is in particular

suited for the description of polymer systems. The following section is dedicated to the PC-SAFT EOS. Its extension to charged molecules will be discussed in Chapter 5.

3.6 The PC-SAFT Equation of State

As already mentioned in Sec. 3.5, the PC-SAFT equation of state is based on a second-order perturbation theory. For non-associating fluids the residual Helmholtz energy is given by summing the free energy of the reference fluid (hard chain) and the perturbation term which reflects the dispersive interactions

$$a^{res} = a^{hc} + a^{disp} \quad (3.34)$$

Three parameters are necessary to describe the molecule: the temperature-independent segment diameter σ_i , the segment number $m_{seg,i}$, and the dispersion energy ε_i/k_B .

Hard-Chain Term

Starting point for the description of a hard-chain fluid is a system of hard spheres that each possess two sticky association sites. The bonds are irreversibly formed between two adjacent spheres. The influence of the next neighbor is not included in the theory. The hard-chain term in the PC-SAFT model is inherited from the SAFT model of Chapman et al.¹⁷:

$$a^{hc} = \bar{m}_{seg} \cdot a^{hs} - \sum_i x_i (m_{seg,i} - 1) \cdot \ln g_{ii}^{hs}(d_{ii}) \quad (3.35)$$

Here \bar{m}_{seg} is the mean segment number given by

$$\bar{m}_{seg} = \sum_i x_i m_{seg,i} \quad (3.36)$$

The segment-based free energy of a hard-sphere system is given by Boublik²⁹ and Mansoori et al.³⁰ as

$$a^{hs} = \frac{1}{\zeta_0} \left[\frac{3\zeta_1\zeta_2}{1-\zeta_3} + \left(\frac{\zeta_2^3}{\zeta_3^2} - \zeta_0 \right) \cdot \ln(1-\zeta_3) \right] \quad (3.37)$$

where

$$\zeta_n = \frac{\pi}{6} \rho_N \sum_i x_i m_{seg,i} \cdot d_i^n \quad \text{with } n = \{0, 1, 2, 3\} \quad (3.38)$$

Note that ζ_3 corresponds to the reduced density (packing fraction). In analogy to the temperature-dependent diameter proposed by Barker and Henderson (Eq. 3.32) the temperature-dependent segment diameter d_i for the PC-SAFT EOS is defined as

$$d_i = \sigma_i (1 - 0.12 \cdot \exp\{-3\beta\varepsilon_i\}) \quad (3.39)$$

The radial distribution function value at contact needed in Eq. 3.35 is

$$g_{ij}^{hs}(d_{ij}) = \frac{1}{1-\zeta_3} + \left(\frac{d_i d_j}{d_i + d_j} \right) \frac{3\zeta_2}{(1-\zeta_3)^2} + \left(\frac{d_i d_j}{d_i + d_j} \right)^2 \frac{2\zeta_2^2}{(1-\zeta_3)^3} \quad (3.40)$$

Dispersion Term

The free energy dispersion contribution is

$$\begin{aligned} a^{disp} &= -2\pi\rho_N \cdot I_1(\zeta_3, \bar{m}_{seg}) \cdot \overline{m^2\varepsilon\sigma^3} \\ &\quad - \pi\rho_N \cdot \bar{m}_{seg} C_1 \cdot I_2(\zeta_3, \bar{m}_{seg}) \cdot \overline{m^2\varepsilon^2\sigma^3} \end{aligned} \quad (3.41)$$

For the compressibility term and the double sums following abbreviations were introduced

$$C_1 = \left(1 + Z^{hc} + \rho_N \left(\frac{\partial Z^{hc}}{\partial \rho_N} \right) \right)^{-1} \quad (3.42)$$

$$\overline{m^2\varepsilon\sigma^3} = \sum_i \sum_j x_i x_j m_{seg,i} m_{seg,j} (\beta\varepsilon_{ij}) \sigma_{ij}^3 \quad (3.43)$$

$$\overline{m^2\varepsilon^2\sigma^3} = \sum_i \sum_j x_i x_j m_{seg,i} m_{seg,j} (\beta\varepsilon_{ij})^2 \sigma_{ij}^3 \quad (3.44)$$

In order to describe mixtures the one-fluid-theory is applied, i. e. a hypothetical fluid with the same properties as the mixture is parameterized using adequate mixing rules. The Berthelot-Lorenz mixing rules are used for the combination of two different segment types, i. e.

$$\sigma_{ij} = \frac{\sigma_i + \sigma_j}{2} \quad (3.45)$$

$$\varepsilon_{ij} = \sqrt{\varepsilon_i \varepsilon_j} \cdot (1 - k_{ij}) \quad (3.46)$$

The binary interaction parameter k_{ij} is an optional adjustable parameter fitted to mixture properties. The integrals of the perturbation theory have been replaced by potential series according to

$$I_1(\zeta_3, \bar{m}_{seg}) = \sum_{i=0}^6 a_i(\bar{m}_{seg}) \cdot \zeta_3^i \quad (3.47)$$

$$I_2(\zeta_3, \bar{m}_{seg}) = \sum_{i=0}^6 b_i(\bar{m}_{seg}) \cdot \zeta_3^i \quad (3.48)$$

The coefficients a_i and b_i depend on the mean segment number

$$a_i(\bar{m}_{seg}) = a_{0i} + \frac{\bar{m}_{seg} - 1}{\bar{m}_{seg}} a_{1i} + \frac{\bar{m}_{seg} - 1}{\bar{m}_{seg}} \frac{\bar{m}_{seg} - 2}{\bar{m}_{seg}} a_{2i} \quad (3.49)$$

$$b_i(\bar{m}_{seg}) = b_{0i} + \frac{\bar{m}_{seg} - 1}{\bar{m}_{seg}} b_{1i} + \frac{\bar{m}_{seg} - 1}{\bar{m}_{seg}} \frac{\bar{m}_{seg} - 2}{\bar{m}_{seg}} b_{2i} \quad (3.50)$$

The model constants a_{0i} , b_{0i} , etc. have been fitted to experimental data of the alkane homologue series³¹ and are tabulated in Ref.²

Association Term

For molecules that exhibit strong anisotropic attractive interactions (e. g. hydrogen bonding) an association term is added to the residual Helmholtz energy

$$a^{res} = a^{hc} + a^{disp} + a^{assoc} \quad (3.51)$$

According to Wertheim's TPT1 model^{21–26} two molecules i and j each having two off-center association sites A and B can interact with each other via a square-well potential of depth $\varepsilon^{A_i B_j}$ and range $r^{A_i B_j}$ (see Fig. 3.6). The latter parameter is proportional to the so-called association volume $\kappa^{A_i B_j}$ which is commonly preferred. Hence, the association term introduces two new pure-component parameters. Due to steric incompatibility certain configurations of molecules and bonds are not allowed:

- Each association site can form only one single bond.
- Two molecules can only form a single bond. A double bond is prohibited.
- Two association sites on the same molecule cannot form a bond, i. e. ring formation is not allowed.
- Two association sites of the same type cannot form a bond (e. g. A—A is not possible).

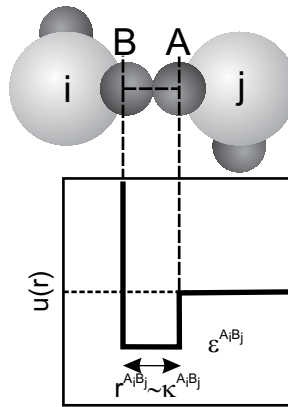


Fig. 3.6: Square-well potential between two association sites A and B .

The association contribution for a mixture of components is given by^{||}

$$a^{assoc} = \sum_i x_i \sum_{A_i}^{\forall \text{sites on } i} \left(\ln X^{A_i} + \frac{1 - X^{A_i}}{2} \right) \quad (3.52)$$

^{||}Here the summation index A_i denotes a site on molecule i and the summation is over all sites on the molecule regardless of the type.

The fraction of non-bonded molecules i at site A_i must be calculated iteratively using

$$X^{A_i} = \left(1 + \sum_j x_j \sum_{B_j}^{\forall \text{sites on } i} X^{B_j} \cdot \Delta^{A_i B_j} \right)^{-1} \quad (3.53)$$

where $\Delta^{A_i B_j}$ denotes the bonding strength given by

$$\Delta^{A_i B_j} = g_{ij}^{hs}(d_{ij}) \cdot \kappa^{A_i B_j} \cdot \sigma_{ij}^3 [\exp\{\beta \varepsilon^{A_i B_j}\} - 1] \quad (3.54)$$

To avoid numerical difficulties when dealing with compounds having a large amount of sites (e. g. polymers) one can rewrite Eqs. 3.52-3.53 under the assumption, that all association sites on a molecule have the same association parameters³²:

$$a^{assoc} = \sum_i x_i \sum_{A_i}^{\forall \text{site types}} N^{A_i} \left(\ln X^{A_i} + \frac{1 - X^{A_i}}{2} \right) \quad (3.55)$$

$$X^{A_i} = \left(1 + \sum_j x_j \sum_{B_j}^{\forall \text{site types}} N^{B_j} X^{B_j} \cdot \Delta^{A_i B_j} \right)^{-1} \quad (3.56)$$

Here, N^{A_i} denotes the number of association types A on molecule i . Note that the summation is over the association types and not over the association sites as in Eqs. 3.52-3.53. For the cross-association the mixing rules of Wohlbach and Sandler are used

$$\varepsilon^{A_i B_j} = \frac{\varepsilon^{A_i B_i} + \varepsilon^{A_j B_j}}{2} \quad (3.57)$$

$$\kappa^{A_i B_j} = \sqrt{\kappa^{A_i B_i} \kappa^{A_j B_j}} \cdot \left(\frac{\sqrt{\sigma_i \sigma_j}}{\sigma_{ij}} \right)^3 \quad (3.58)$$

Chapter 4

Potential of Mean Force

4.1 Interactions in Colloidal Dispersions

All the considerations for pure components made in Chapter 3 can be extended to mixtures in a straightforward way. Within the scope of this work one main focus is directed to colloidal dispersions such as protein solutions. The often charged macromolecules are very big compared to the range of typical interaction potentials. Therefore, the interactions may be approximated by a hard-sphere potential. Neglecting the small solvent molecules in a first step the hard-sphere system represents the behavior of colloidal solutions quite well. For a more realistic description, besides the interactions between alike molecules (colloid-colloid, solvent-solvent) the unlike pairs (colloid-solvent) must be included as well. This is a challenging task due to the complicated structure of the solvent particles especially when electrolytes are involved. They lead to nontrivial screening effects. A common approach in order to reduce complexity is to incorporate all solvent-solvent and solvent-colloid interactions into the colloid-colloid potential. This modified potential is obtained by statistical averaging with respect to all possible configurations of the solvent molecules. Hence, it is called ‘potential of mean force’ (PMF)*. Note, that applying this ‘trick’ the many-component system has been reduced to one containing only a pure species floating in a medium other than vacuum. Despite the analogy to a low-pressure pure gas phase the interactions between two solute molecules can be of different character. This shall be shown by an example: Two molecules at fixed separation may attract each other in free space. However, when they are surrounded by small solvent particles the macromolecules have to displace the solvent molecules from their path. The net colloid-colloid interaction may then become repulsive if the work for the displacement is higher than the work gained by the approach.

Before presenting some of the PMF commonly encountered in literature it shall be shown how the phase behavior of colloidal dispersions depends on the shape of the interaction potential and, further, how the second osmotic virial coefficient is linked to the PMF.

*In the following, the symbol w is used for the PMF in order to distinguish it from the potential in vacuo.

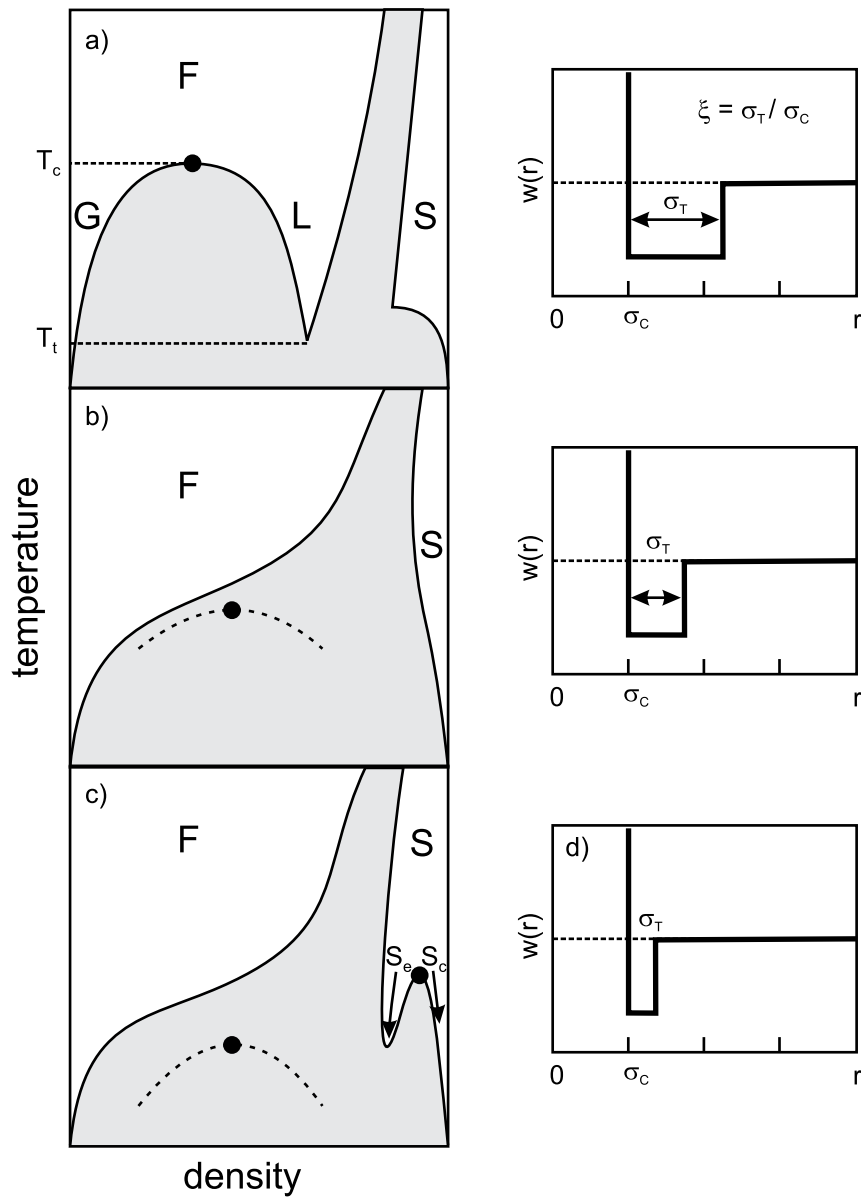


Fig. 4.1: Schematic phase diagrams as the ratio ξ decreases (from top to bottom). T_c and T_t are the critical and the triple point temperature, respectively. The phase types are denoted with **F**luid, **G**as, **L**iquid, and **S**olid, respectively. For very short-ranged attractive potentials two solid phases S_e and S_c coexist below a solid-solid critical point. The dashed curve represents a meta-stable vapor-liquid phase transition which maps into a liquid-liquid transition for real colloid systems.

4.2 Global Phase Diagram of a Colloid System

Although the microscopic nature of colloidal suspensions is very complicated, given the many possible interaction mechanisms, the net intermolecular potentials have two features in common: hard-core repulsion and usually a very short-ranged attractive or repulsive tail. The topology of the phase diagram is highly affected by the ratio ξ of the range of the tail σ_T and the hard-core diameter σ_C ($\xi = \sigma_T/\sigma_C$)³³. For large ξ , i. e. for long-ranged tails, the phase diagram shows a typical behavior of a simple system such as a noble gas (Fig. 4.1a). This type of phase diagram exhibits two first-order phase transitions. The first transition from solid to liquid phase is an inherent property of any hard-core system. The second vaporization transition emanates from the attractive tail. When ξ is decreased the critical point T_c is shifted to lower temperatures. If ξ goes below a certain value, T_c becomes lower than the triple point temperature T_t and, hence, the vapor-liquid transition becomes meta-stable (dashed curve in Fig. 4.1b) giving way to a second-order phase transition, i. e. sublimation.

An analogous phase behavior has been found for colloidal suspensions, e. g. protein solutions. The proteins have a large diameter compared to the range of their interaction potentials. Hence, they exhibit a phase diagram as depicted in Fig. 4.1b. The fluid-solid transition of the model system corresponds to the liquidus line. The vapor-liquid transition maps into a liquid-liquid coacervation. Here, two distinct liquid phases are formed: one protein-rich, the other protein-poor (see e. g. Ref.³⁴).

A further decrease of the attractive tail range leads to a solid-solid phase transition (Fig. 4.1c). Such behavior occurs in some metallic systems³⁵ but has not been measured for colloid dispersions.

4.3 Osmotic Pressure

Many processes in nature are dominated by the phenomenon osmotic pressure. For example, trees utilize this effect to suck water from their roots up to the leaves. Consider a system divided by a semi-permeable membrane in two parts, one containing a pure solvent, the other containing the same solvent and a solute as shown in Fig. 4.2. The membrane is permeable only to the solvent (w) but not to the solute (s). Nature aims at equilibration of the solute's concentration in both phases. Hence, solvent molecules will penetrate the membrane and pressure will raise in the double-prime phase until thermodynamic equilibrium is reached.

Since the solute is only present on one side of the membrane, the equilibrium condition can only be formulated for the solvent. Besides the equality of temperature in both phases, the chemical potential of the solvent must also be equal

$$\mu'_w = \mu''_w \quad (4.1)$$

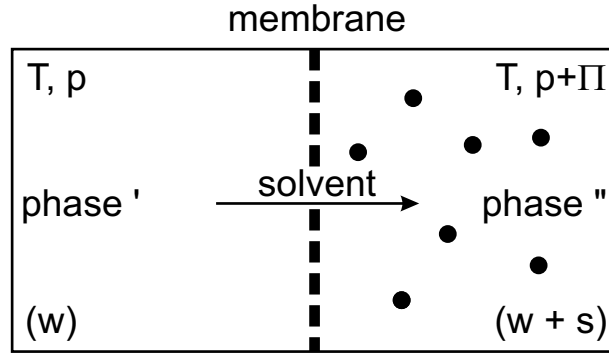


Fig. 4.2: Diagram of an osmotic cell. The membrane is permeable only to the solvent (w) but not to the solute (s).

The chemical potentials in both phases are

$$\mu'_w = \mu_{0w}(T, p) \quad (4.2)$$

$$\mu''_w = \mu_{0w}(T, p) + \int_{\mu_{0w}(T, p)}^{\mu_{0w}(T, p+\Pi)} d\mu_w + k_B T \ln a''_w(T, p + \Pi) \quad (4.3)$$

a''_w is the activity of the solvent in the double-prime phase. Combining Eqs. 4.1-4.3 and rearranging leads to

$$\int_{\mu_{0w}(T, p)}^{\mu_{0w}(T, p+\Pi)} d\mu_w = -k_B T \ln a''_w(T, p + \Pi) \quad (4.4)$$

The left side can be replaced by

$$\int_{\mu_{0w}(T, p)}^{\mu_{0w}(T, p+\Pi)} d\mu_w = \int_p^{p+\Pi} v_{0w} dp \quad (4.5)$$

and hence – assuming an incompressible solvent, i. e. the specific volume $v_{0w} \neq v_{0w}(p)$ – one yields

$$\begin{aligned} \int_p^{p+\Pi} v_{0w} dp &= -k_B T \ln a''_w(T, p + \Pi) \\ \rightarrow \beta \Pi &= -\frac{1}{v_{0w}} \ln a''_w(T, p + \Pi) \end{aligned} \quad (4.6)$$

At low solute concentrations the activity can be approximated by the concentration and the specific volume of the solvent equals the reciprocal system density so that Eq. 4.6 reduces to

$$\beta \Pi = -\rho \ln x''_w = -\rho \ln(1 - x''_s) \quad (4.7)$$

Further the logarithm can be expressed by its Taylor series as $\ln(1 - x) \approx -x$ yielding

$$\beta\Pi = \rho x_s'' \quad \text{or} \quad \beta\Pi = \rho_s \quad (4.8)$$

with ρ_s being the solute's number concentration in $1/\text{m}^3$. Eq. 4.8 is called *van't Hoff* equation for osmotic pressure Π . It is similar to the ideal-gas equation. Remember, the main assumptions made for the derivation of van't Hoff's equation are that the solution is very dilute and that the solvent is incompressible.

4.4 Second Osmotic Virial Coefficient

In Sec. 3.1 it was shown how the system pressure is linked to the intermolecular potential between two molecules in vacuo. A formalism for the calculation of the second virial coefficient was derived. A similar approach is followed when dealing with pseudo one-component systems such as colloid solutions. McMillan and Mayer[†] showed that the pressure of an imperfect gas directly maps into the osmotic pressure of a solution (see also Refs.^{37,38})

$$\beta\Pi = \sum_{i=1}^{\infty} B_i \rho_s^i = \rho_s + B_2 \rho_s^2 + \dots \quad (4.9)$$

Therefore, the second osmotic virial coefficient can be calculated using Eq. 3.13, replacing the potential u by the PMF w (see Sec. 4.5), hence

$$B_2 = -2\pi \int_0^{\infty} [\exp\{-\beta w(r)\} - 1] r^2 dr \quad (4.10)$$

The second osmotic virial coefficient is experimentally accessible by osmometry or light-scattering measurements. The measured coefficients can be used to identify the inter-colloidal interaction mechanisms and to fit model parameters.

4.5 PMF

In this section the main focus lies on the potentials of mean force that capture the different interaction mechanisms in colloidal solutions. There exists a vast literature concerning the PMF. Pioneering work has been done by Derjaguin and Landau³⁹ and Verwey and Overbeek⁴⁰. The so-called DLVO theory is based on the assumption that the single potentials are independent from each other and additive. The DLVO theory comprises hard-sphere contributions w_{hs} , electrostatic repulsion w_{elec} and dispersive attraction w_{disp} . Other potential forms have been developed in order to account for further intermolecular effects.

[†]Note that the independent variables in the McMillan-Mayer framework³⁶ are temperature, volume, solute mole number, and (constant) chemical potential of the solvent $(T, V, \mathbf{n}_s, \mu_w)$. Instead, in the classical (Lewis-Randall) framework the independent variable set is (T, V, \mathbf{n}) or (T, P, \mathbf{n}) . The McMillan-Mayer framework is best suited for calculations of the osmotic pressure because – as was shown in the derivation in Sec. 4.3 – the solvent chemical potential is equal on both sides of the membrane.

Hard-Sphere Potential w_{hs}

The hs-potential of mean force is equivalent to the version for molecules in vacuo (compare Fig 3.4a). The respective potential is given by

$$w_{hs}(r) = \begin{cases} \infty & : r \leq \sigma \\ 0 & : r > \sigma \end{cases} \quad (4.11)$$

Note that this potential is inherently part of many PMF models and can be omitted explicitly when the lower integration bound (Eq. 4.10) is set to the particle's diameter σ instead of zero.

Dispersion

In DLVO theory attractive forces between two colloids are described by a van der Waals type term. The attractive dispersion potential $w_{disp}(r)$ is calculated from Hamaker's theory⁴¹:

$$w_{disp}(r) = \begin{cases} \infty & : r \leq \sigma \\ -\frac{H}{12} \left\{ \frac{\sigma^2}{r^2 - \sigma^2} + \frac{\sigma^2}{r^2} + 2 \ln\left(1 - \frac{\sigma^2}{r^2}\right) \right\} & : r > \sigma \end{cases} \quad (4.12)$$

or

$$w_{disp}(r) = \frac{H}{36} \left(\frac{\sigma}{r}\right)^6 \quad : r \gg \sigma \quad (4.13)$$

Note that Eq. 4.12 is not defined at $r = \sigma$ and the limit is $-\infty$. Therefore, when evaluating the integral (Eq. 4.10) the lower integration limit must be chosen to be $\sigma + \delta$, where δ is mostly one order of magnitude smaller than the hard-core diameter. The value of δ has a big influence on the calculated thermodynamic properties (osmotic virial coefficients, phase equilibria). Although there are expressions to approximatively calculate Hamaker constants H from solvent and particle quantum mechanical properties (e. g. Ref.⁴²) they are commonly regressed from experimental data such as second osmotic virial coefficients^{43,44}. For bovine α -chymotrypsin Coen et al.⁴⁵ have regressed Hamaker constants using 4 models of varying complexity. Model (1) includes DLVO potential, model (2) additionally accounts for charge-dipole and dipole-dipole interactions, and model (3) also considers osmotic effects (see below). When using model (1) Hamaker constants at low ionic strengths (0.01 M) are higher than expected and strongly pH-dependent. This indicates that attractive forces not accounted for in DLVO theory are represented by the higher value for the Hamaker constant. Model (2) provides Hamaker constants which are much less pH-dependent and a magnitude lower than for model (1). The inclusion of osmotic-attraction potential (model (3)) does not significantly affect Hamaker constants at low ionic strengths. Model (4) additionally accounts for the charge fluctuation on the protein surface due to ion binding. Here, the Hamaker constants show only little dependency on solution pH. According to Nir⁴⁶ $H \approx 1 - 2 k_B T$ and Hamaker constants for various globular proteins have similar values as H is directly proportional to protein density, which is similar for most proteins. Nonetheless, Coen et al. obtained $H \approx 5 - 10 k_B T$ at low ionic

strength. The higher values indicate additional attractive forces independent from ionic strength and pH maybe due to hydrophobic interactions or hydrogen bonding which are not accounted for explicitly in the models⁴⁷.

Electrostatic Potential w_{elec}

Equally charged particles repel each other according to Coulomb's law ($u(r) = q^2/4\pi\epsilon_0r$ in vacuo). In a dielectric medium the potential becomes $w(r) = q^2/4\pi\epsilon r$, where $\epsilon = \epsilon_0\epsilon_r$. ϵ_0 is the permittivity in vacuo and ϵ_r is the relative permittivity of the medium. The surrounding countercharges (in form of ions) screen the charges on the macromolecules. This screening is described by a Debye-Hückel term so that the electrostatic potential due to charge-charge interactions becomes

$$w_{q-q}^{DLVO}(r) = \begin{cases} \infty & : r \leq \sigma \\ \frac{q^2(1/r) \exp[-\kappa(r-\sigma)]}{4\pi\epsilon (1+\kappa\sigma/2)^2} & : r > \sigma \end{cases} \quad (4.14)$$

where

$$\kappa = \sqrt{(2e^2N_A I)/(k_B T \epsilon)} \quad (4.15)$$

is the inverse Debye length and $I = \frac{1}{2}(z_{an}^2\rho_{an} + z_{cat}^2\rho_{cat})$ the ionic strength of the solution, respectively. The superscript (DLVO) denotes that this equation is part of the DLVO theory. Eq. 4.14 was derived using a mean field approximation assuming that the electrolyte ions can be treated as point charges. Strictly speaking this assumption is only valid at low ionic strengths ($< 0.1 M$)⁴¹. The Debye-Hückel theory will be addressed in more detail in Chapter 5.1. An alternative expression for charge-charge interactions was suggested by Sogami and Ise (SI)⁴⁸

$$w_{q-q}^{SI}(r) = \begin{cases} \infty & : r \leq \sigma \\ \frac{1}{\beta} z^2 L_B \left[\frac{\sinh(\kappa a)}{\kappa a} \right]^2 \left[\frac{1+\kappa a \coth(\kappa a)}{r} - \frac{\kappa}{2} \right] \exp[-\kappa r] & : r > \sigma \end{cases} \quad (4.16)$$

where $L_B = \beta e^2/4\pi\epsilon$ is the Bjerrum length and $a = \sigma/2$.

Both DLVO and SI theory are based on linearized Poisson-Boltzmann equations and Debye-Hückel theory. Charge distributions on the macroion's surface cannot be assessed. The main differences between the models are that for DLVO theory the solution volume is assumed to be unaffected by pressure and by charges of the ions while this is not the case for SI theory. Further, the SI potential is able to describe attraction between like-charged ions whereas DLVO theory needs a van der Waals dispersion term as described above to account for attractive forces⁴⁸. However, comparison with molecular dynamics simulations shows that SI theory clearly underestimates repulsive interaction forces between macroions⁴⁹.

Till here a uniform charge distribution on the macromolecule has been assumed. More accurate models also account for charge-dipole ($q - \mu$), charge-induced dipole ($q - i\mu$), dipole-dipole ($\mu - \mu$) and induced dipole-dipole ($\mu - i\mu$) interactions. The respective potentials are listed below⁴³ (valid for $r > \sigma$):

$$w_{q-\mu} = -\frac{2}{3}\beta \frac{q^2\mu^2}{(4\pi\varepsilon)^2r^4} \cdot \left\{ \frac{3(1+\kappa r)\exp[-\kappa(r-2a)]}{(1+\kappa a)[2+2\kappa a+(\kappa a)^2+(1+\kappa a)(\varepsilon_s/\varepsilon)]} \right\}^2 \quad (4.17)$$

$$w_{q-i\mu} = -\frac{q^2\alpha}{(4\pi\varepsilon)^2r^4} \xi(r) \quad (4.18)$$

$$w_{\mu-\mu} = -\frac{2}{3}\beta \frac{\mu^4}{(4\pi\varepsilon)^2r^6} \cdot \left\{ \frac{3^4[2+2\kappa r+(\kappa r)^2]^2 \exp[-2\kappa(r-2a)]}{[2+2\kappa a+(\kappa a)^2+(1+\kappa a)(\varepsilon_s/\varepsilon)]^4} \right\} \quad (4.19)$$

$$w_{\mu-i\mu} = -\frac{2\mu^2\alpha}{(4\pi\varepsilon)^2r^6} \xi(r) \quad (4.20)$$

where the $\xi(r)$ are unknown screening parameters expected to be near unity and ε_s is the dielectric constant at the surface of the macromolecule.

For the dipole-dipole interaction potential Coen et al.⁴⁵ and Striolo et al.⁵⁰ provide a slightly different equation:

$$w_{\mu-\mu} = -\frac{9}{2}\beta \frac{\mu^4}{(4\pi\varepsilon)^2r^6} \cdot \left\{ \frac{[(2+2\kappa r+(\kappa r)^2)^2+2(1+\kappa r)^2] \exp[-2\kappa(r-a)]}{[2+2\kappa a+(\kappa a)^2+(1+\kappa a)(\varepsilon_s/\varepsilon)]^4} \right\} \quad (4.21)$$

Vilker et al.⁵¹ also give a deviant version of Eq. 4.20, where the factor 3^4 is replaced by 3, the exponential term is $\exp[-2\kappa(r-a)]$ and the exponent of the denominator is 2 instead of 4:

$$w_{\mu-\mu} = -\frac{2}{3}\beta \frac{\mu^4}{(4\pi\varepsilon)^2r^6} \left\{ \frac{3[2+2\kappa r+(\kappa r)^2]^2 \exp[-2\kappa(r-a)]}{2+2\kappa a+(\kappa a)^2+(1+\kappa a)(\varepsilon_s/\varepsilon)} \right\}^2 \quad (4.22)$$

ε_s is the dielectric constant at the surface of the macroion. According to Phillies et al.⁵² $\varepsilon_s \approx 4$ compared to $\varepsilon_{water} \approx 80$. Some authors do not use a consistent definition of the parameter ε . In order to obtain correct units, e. g. in Eq. 4.20 either ε_s should be substituted by $\varepsilon_0\varepsilon_s$ or in the denominator of the last term ε should be replaced by ε_r .

It is difficult to retrace which author provides the correct version of the dipole-dipole and charge-dipole interaction potential. However, numerical investigation of Vilker et al.'s equation (Eq. 4.22) for the dipole-dipole interaction shows that there must be a misprint in the corresponding paper (Ref.⁵¹). For solutions containing no salt (ionic strength $I = 0$ mM) $\kappa = 0$ and Eq. 4.22 yields a screening factor (in curly brackets) greater than 1. This is not consistent with the purpose of the screening factor, namely to decrease the dipole-dipole potential in the presence of small ions.

Typically, Boltzmann averages of the screened charge-charge, orientation-(angle)-averaged charge-dipole and dipole-dipole interactions are first calculated separately and then summed

up to obtain the overall interaction potential. This procedure is not exact as angle-averaged charge-dipole and dipole-dipole interactions are strongly non-additive and interlinked⁵⁰. The following model has been proposed to calculate the potential of mean force including the strong coupling of respective interactions⁵³:

$$w_{elec}(r) = w_{q-q}(r) + w_{q-\mu}(r) + w_{\mu-\mu}(r) + w_p(r) \quad (4.23)$$

with w_{q-q} as in Eq. 4.14,

$$w_{q-\mu}(r) = -2k_B T \ln \left[\frac{1}{\alpha_1} \sinh \alpha_1 \right] \quad (4.24)$$

$$w_{\mu-\mu}(r) = -k_B T \frac{2\alpha_2^2 + \alpha_3^2}{9} \quad (4.25)$$

$$w_p(r) = -k_B T \ln \frac{18(4 + 4 \cosh \alpha_3 + e^{2\alpha_2} + 8 \cosh \alpha_1 + e^{-2\alpha_2} \cosh 2\alpha_1)}{(9 + 8 \cosh \alpha_1 + \cosh 2\alpha_1)(12 + 4 \cosh \alpha_3 + 2 \cosh 2\alpha_2)} \quad (4.26)$$

$$\begin{aligned} \alpha_1 &= \beta \frac{(ze)\mu}{4\varepsilon_0\varepsilon_r r^2} S_1 \\ \alpha_2 &= \beta \frac{\mu\mu}{4\varepsilon_0\varepsilon_r r^3} S_2 \\ \alpha_3 &= \beta \frac{\mu\mu}{4\varepsilon_0\varepsilon_r r^3} S_3 \end{aligned} \quad (4.27)$$

$$\begin{aligned} S_1 &= \frac{3(1 + \kappa r) \exp[-\kappa(r - 2a)]}{(1 + \kappa a)[2 + 2\kappa a + (\kappa a)^2 + (1 + \kappa a)(\varepsilon_s/\varepsilon)]} \\ S_2 &= \frac{9(1 + \kappa r + \frac{(\kappa r)^2}{2})^2 \exp[-\kappa(r - 2a)]}{[2 + 2\kappa a + (\kappa a)^2 + (1 + \kappa a)(\varepsilon_s/\varepsilon)]^2} \\ S_3 &= \frac{9(1 + \kappa r) \exp[-\kappa(r - 2a)]}{[2 + 2\kappa a + (\kappa a)^2 + (1 + \kappa a)(\varepsilon_s/\varepsilon)]^2} \end{aligned} \quad (4.28)$$

$w_p(r)$ is a correction term accounting for the non-additivity of the respective electrostatic potentials.

Osmotic Effects

When dealing with colloid solutions containing salt at high concentrations, the excluded volume of the salt ions theoretically should not be neglected. Two macroions approaching contact displace the small salt ions from the spacing between the large molecules. This causes an ion concentration imbalance and thus a net impulse on the two macromolecules towards each other (see Fig 4.3). The result is a stronger attractive interaction between the colloids⁴¹. However, numerical investigations have shown that calculated B_2 and phase equilibria are little affected by the osmotic contribution to the PMF.

A possible potential for osmotic-attractive interactions was presented by Asakura and

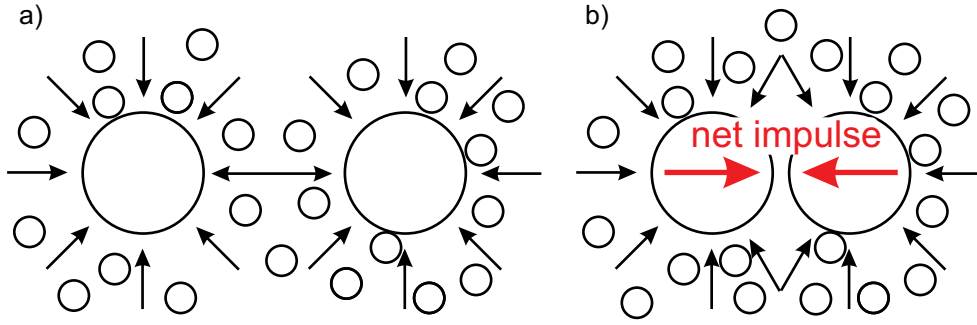


Fig. 4.3: Osmotic effects at high salt concentrations and short intercolloidal distance. **a)** Large distance between two colloids: The small ions can hit the macromolecule from all sides. The net impulse on each colloid is zero. **b)** Short distance between two colloids: The space between the colloids cannot be penetrated by the small ions. The net impulse exerted on the colloids is directed towards each other causing attraction between the macromolecules.

Oosawa⁵⁴:

$$w_{osmo}(r) = \begin{cases} \infty & : r < \sigma \\ -\frac{4}{3}\pi\tilde{\sigma}^3(\rho_{ion}k_B T) \left[1 - \frac{3r}{4\tilde{\sigma}} + \frac{r^3}{16\tilde{\sigma}^3}\right] & : \sigma \leq r \leq 2\tilde{\sigma} \\ 0 & : r \geq \sigma_{mi} \end{cases} \quad (4.29)$$

where $\tilde{\sigma} = (\sigma + \sigma_{ion})/2$, $\sigma_{ion} = (z_{an}\sigma_{cat} + z_{cat}\sigma_{an})/(z_{an} + z_{cat})$ is the valence-weighted mean ionic hydration diameter, and ρ_{ion} is the total ion number concentration. Eq. 4.29 is derived by approximating the osmotic pressure difference by the ideal osmotic pressure of the electrolyte solution ($\Pi_{id} = \rho_{ion}k_B T$). The ion diameters are dependent on the thickness of the hydration layer and related to the ion's position in the lyotropic series⁵⁵.

Yukawa Potential w_{Yuk}

A simple but very useful model potential is the Yukawa potential of the form

$$w_{Yuk}(r) = \begin{cases} \infty & : r < \sigma \\ -\varepsilon\frac{\sigma}{r} \exp\{k\sigma(1 - \frac{r}{\sigma})\} & : r \geq \sigma \end{cases} \quad (4.30)$$

where ε and k are, respectively, the magnitude of the attraction and the screening length that provides a measure for the range of the forces. The Yukawa potential shows similarities to a screened charge-charge potential (compare e. g. to w_{q-q}^{DLVO}) and is thus suitable to describe qualitatively colloidal systems containing electrolytes. Phase behavior of Yukawa systems have been investigated e. g. by Tavares et al.⁵⁶.

4.6 Calculation of Phase Equilibria with a PMF Model

Once the form of the PMF is known, one obtains the Helmholtz free energy of the colloidal system applying a perturbation theory, e. g. as already explained in Sec. 3.5. For the fluid phase a second-order Barker-Henderson theory (macroscopic compressibility approach) is applied while for the solid phase a first-order approach has turned out to be sufficiently accurate.

In case of a pure component the chemical potential is directly obtained by

$$\beta\mu = a + Z \quad (4.31)$$

Note that a already includes the contribution of the ideal gas for the fluid phase or of the ideal crystal for the solid phase, respectively. This contribution is given by

$$a^{id} = \ln C + \ln \eta - 1 \quad (4.32)$$

The exact value of constant C is irrelevant for equilibrium calculations because it is independent from the phase type (fluid/solid) and it appears on both sides of the respective equations. Different reference systems and radial distribution functions have to be chosen for the fluid and the solid phase.

The Fluid Phase

The hard-sphere reference is described by the well-known Carnahan-Starling⁵⁷ equation

$$a^{hs,CS} = \frac{4\eta - 3\eta^2}{(1 - \eta)^2} \quad (4.33)$$

$$Z^{hs,CS} = \frac{1 + \eta + \eta^2 - \eta^3}{(1 - \eta)^3} \quad (4.34)$$

The differential $\left(\frac{\partial \rho_N}{\partial P}\right)$ needed for the second-order term is given by

$$\left(\frac{\partial \rho_N}{\partial P}\right) = \frac{(1 - \eta)^4}{1 + 4(\eta + \eta^2 - \eta^3) + \eta^4} \quad (4.35)$$

Further, the radial distribution function from Chang and Sandler⁵⁸ is implemented.

The Solid Phase

The contributions for the hard-sphere crystal reference (fcc structure) are proposed by Velasco et al.⁵⁹

$$a^{hs,fcc} = -3 \ln \left(1 - \left(\frac{\eta}{\tau} \right)^{\frac{1}{3}} \right) - 3 \ln 2 \quad (4.36)$$

$$Z^{hs,fcc} = \frac{1}{1 - \left(\frac{\eta}{\tau} \right)^{\frac{1}{3}}} \quad (4.37)$$

The radial distribution function for the solid is based on equations of Kincaid and Weis⁶⁰. Combination of Eqs. 3.25, 3.29,3.30, and 4.31-4.36 provides the mathematical framework for the calculation of phase diagrams.

Chapter 5

Electrolyte PC-SAFT (ePC-SAFT)

5.1 Electrolyte Systems

5.1.1 Introduction

Since the beginnings of the last century many researchers have concentrated their efforts in correlating and predicting phase equilibria in electrolyte solutions. In 1923 Debye and Hückel⁶¹ published one of the pioneering papers dealing with aqueous electrolyte solutions. They considered a system of hard spheres in a dielectric continuum and calculated the contribution to the system energy for charging up the spheres. Their model is often treated as an excess Gibbs energy model; however, what they developed was an electrostatic contribution to the Helmholtz energy when charging hard spheres at constant temperature, volume and chemical potential of the solvent. Their development includes the background potential as well as the self potential. The latter is also known as the Born potential which is independent of the configuration as long as we are dealing with pure solvents.

g^E -models like the local composition NRTL activity coefficient model by Chen et al.⁶² and its extensions^{63–65} or other group contribution models^{66,67} have been applied to correlate activity coefficients of single-salt and mixed-salt electrolyte solutions. However, one disadvantage of excess Gibbs enthalpy models is that they need many adjustable parameters, some of them being temperature-dependent or even concentration-dependent. Further, g^E -models are not able to predict densities. Equation of state (EOS) models circumvent these crucial disadvantages. Several models based on equations of state were extended to electrolyte systems. Fürst and Renon⁶⁸ combined the nonelectrolyte EOS of Schwartzen-truber et al. with a mean spherical approximation (MSA) long-range term to account for the electrostatic interactions. Wu and Prausnitz⁶⁹ presented an electrolyte equation of state based on the Peng-Robinson EOS (PREOS) which itself already accounts for hard-core and dispersion interactions. They added a Born energy term for charging up the uncharged reference system in a continuous medium of given permittivity, a Coulombic term to account for electrostatic interactions between the ions, and further an association term to consider hydrogen bonds between the water molecules. Myers et al.⁷⁰ followed a similar approach using the ideal gas mixture as a reference system, considering also the

Born energy to discharge the ions in vacuum and then recharging them in the dielectric medium. Both approaches yield good agreement with experimental vapor pressure data. However, they are based on the semi-empirical PREOS which is known to fail when predicting liquid densities.

A series of electrolyte equations of state are based on perturbation theories. Many models of this kind are based on the SAFT approach. To describe electrolyte solutions, Galindo et al.^{71,72} have successfully extended the SAFT-VR EOS⁷³ to electrolyte solutions by using an additive electrostatic term for the Helmholtz free energy obtained from the solution of the Ornstein-Zernicke equation for the restricted primitive model (RPM) with the MSA closure. Their model yields good results for vapor pressures and liquid densities of aqueous solutions of monovalent ions. Ji et al.⁷⁴ have coupled the SAFT1 EOS with a similar RPM model. They calculate osmotic and activity coefficients of some alkali salts and their mixtures in water.

In this work the PC-SAFT model is extended to electrolyte solutions. Whereas the hard-core, dispersion, and association interactions are already taken into account by the original PC-SAFT, the charging of the ions is considered by the Debye-Hückel (DH) term. Therefore, the DH term will be discussed in detail in the following section.

5.1.2 Debye-Hückel (DH) Theory of Electrolyte Solutions

Debye and Hückel⁶¹ considered diluted electrolyte solutions and regarded the solvent (water) as a dielectric continuum. This assumption is feasible as the amount of water molecules is much greater than the total amount of ions. The ions are treated as hard spheres which can approach each other to distance a_i . This value is equivalent to an ion diameter. Debye and Hückel proposed a contribution to the Helmholtz free energy for charging up a hard-sphere system. This kind of model, where the ions are considered as charged spheres and the solvent is implicitly regarded as a dielectric continuum, is referred to as primitive model (PM). It should be denoted that the original DH theory was developed as a primitive model and not as a restricted primitive model (RPM). Both types of model consider the size of the ions but in the RPM the diameters of all ion species are equal.

The starting point for the treatment of charged particles is the Poisson equation:

$$\nabla^2 \Phi_{out}(r) = -\frac{\rho}{\varepsilon} \quad (5.1)$$

where $\Phi_{out}(r)$ is the electric potential in dependency of the distance r from the center of an arbitrarily chosen ion. The index *out* denotes that Eq. 5.1 is valid outside the ionic sphere of diameter a_i . ρ is the volumetric charge density, and ε is the dielectric constant of the medium.

Following the Boltzmann principle, ρ itself can be expressed by

$$\rho = N_A \sum_i q_i c_i \exp(-\beta q_i \Phi_{out}) \quad (5.2)$$

where q_i and c_i are the charge (in C) and the number concentration of ion i , respectively. Combining Eqs. 5.1 and 5.2 yields the Poisson-Boltzmann differential equation which – in order to be easily solved – is linearized

$$\begin{aligned}\nabla^2\Phi_{out} &= \frac{\beta N_A}{\varepsilon} \sum_i q_i^2 c_i \Phi_{out} \\ &= \kappa^2 \Phi_{out}, \quad \text{with } \kappa^2 = \frac{\beta N_A}{\varepsilon} \sum_i q_i^2 c_i\end{aligned}\quad (5.3)$$

κ is called the inverse Debye screening length and has the unit of reciprocal meter (compare also Eq. 4.15). The differential Eq. 5.3 leads to the solution

$$\Phi_{out}(r) = \frac{A}{r} e^{-\kappa r} + \frac{A'}{r} e^{\kappa r} \quad \text{for } r \geq a_i \quad (5.4)$$

where obviously $A' = 0$ as the potential $\Phi_{out}(r)$ has to vanish for infinite distance r . This solution is valid for $r \geq a_i$. The internal region of the ionic sphere (index *in*) is regarded as a continuum of given permittivity with a point charge at the center. Here, the centers of the surrounding ions are excluded and the Poisson equation (Eq. 5.1) simplifies to Laplace's equation, namely

$$\nabla^2\Phi_{in} = 0 \quad (5.5)$$

and thus the electric potential is given by

$$\Phi_{in}(r) = \frac{q_i}{4\pi\varepsilon} \frac{1}{r} + B \quad \text{for } r \leq a_i \quad (5.6)$$

The first term of Eq. 5.6 is the self potential often denoted as the Born potential. The two constants A and B are obtained taking into consideration the boundary conditions that at $r = a_i$ both Φ_{in} and Φ_{out} as well as their gradients $\left(\frac{\partial\Phi_{in}}{\partial r}\right)$ and $\left(\frac{\partial\Phi_{out}}{\partial r}\right)$ must be identical, respectively. Hence,

$$A = \frac{q_i}{4\pi\varepsilon} \frac{e^{\kappa a_i}}{1 + \kappa a_i} \quad \text{and} \quad B = -\frac{q_i}{4\pi\varepsilon} \frac{\kappa}{1 + \kappa a_i} \quad (5.7)$$

Constant B represents the potential of the point charge in the center of the ion sphere. Therefore, the potential energy of one ion relative to its environment is given by

$$u_i = q_i B = -\frac{q_i^2}{4\pi\varepsilon} \frac{\kappa}{1 + \kappa a_i} \quad (5.8)$$

and the potential energy of the whole system becomes

$$\begin{aligned}
 U^{\text{elec}} &= \sum_i \frac{N_i}{2} u_i \\
 &= - \sum_i \frac{N_i q_i^2}{8\pi\epsilon} \frac{\kappa}{1 + \kappa a_i} \\
 &= - \frac{\kappa}{8\pi\epsilon} \sum_i \frac{N_i q_i^2}{1 + \kappa a_i}
 \end{aligned} \tag{5.9}$$

To obtain an expression for the Helmholtz free energy the following standard thermodynamic relationship is used

$$d\left(\frac{A}{T}\right) = U d\left(\frac{1}{T}\right) - \frac{P}{T} dV + \frac{1}{T} \sum_i \mu_i dn_i \tag{5.10}$$

At constant volume and composition the molar electrostatic Helmholtz free energy becomes^{4,61}

$$a^{\text{elec}} = - \frac{\beta}{4\pi\epsilon} \sum_i \frac{x_i q_i^2}{3} \kappa \chi_i \tag{5.11}$$

where

$$\chi_i = \frac{3}{(\kappa a_i)^3} \left[\frac{3}{2} + \ln(1 + \kappa a_i) - 2(1 + \kappa a_i) + \frac{1}{2}(1 + \kappa a_i)^2 \right] \tag{5.12}$$

and x_i is the mole fraction of ion i .

5.1.3 Augmented Electrolyte Theories

The original DH theory can be enhanced by considering more accurate descriptions of both, the non-ionic and the ionic interactions. The non-electrostatic corrections may consist in adding an attractive interaction to the hard-sphere repulsion. The electrostatic interactions may be described more accurately, for example, by using a quadratic series expansion of Eq. 5.2. These kind of extensions to both ionic and non-ionic contributions assume implicitly that the respective interactions are decoupled. In reality, this is not the case. The use of integral equation theories provides an alternative without assuming the decoupling of these effects⁷². For example, the solution of the Ornstein-Zernicke equation for charged particles with the mean spherical approximation closure for the RPM and PM can be found in Refs.^{75,76} In his Diploma Thesis Held⁷⁷ has compared several ionic contributions (DH, MSA, PM, RPM) in combination with the PC-SAFT EOS. He has shown that none of the more complex electrolyte terms yields markedly better results than the mathematically rather simple DH model.

5.1.4 The ePC-SAFT Model

In this work, the PC-SAFT EOS is extended to also account for the interaction of charged molecules, hereafter referred to as ePC-SAFT. The grade of complexity is restricted to the PM of Debye and Hückel keeping in mind that the long-term objective is not to optimise the equation of state for electrolyte solutions but rather to find a meaningful basis for the description of aqueous amino acid, polypeptide, and protein solutions containing electrolytes. The ePC-SAFT model considers the following contributions:

$$a^{res} = a^{hc} + a^{disp} + a^{assoc} + a^{elec} \quad (5.13)$$

The respective equations for the residual Helmholtz free energy contributions to hard-chain repulsion a^{hc} , dispersion a^{disp} , and association a^{assoc} are summarized in Sec. 3.6 and in Ref.² The contribution due to charging up the system a^{elec} is calculated by Eq. 5.11. The electrostatic contributions for pressure and chemical potential are obtained by standard thermodynamics:

$$\frac{p^{elec}}{k_B T} = - \left(\frac{\partial a^{elec}}{\partial v} \right)_{T, \mathbf{N}} = - \frac{\kappa \rho_N}{24\pi k_B T \varepsilon} \sum_k x_k q_k^2 \sigma_k \quad (5.14)$$

$$\frac{\mu_j^{elec}}{k_B T} = \left(\frac{\partial A^{elec}/k_B T}{\partial N_j} \right)_{T, V, N_i \neq N_j} = - \frac{q_j^2 \kappa}{24\pi k_B T \varepsilon} \left[2\chi_j + \frac{\sum_k x_k q_k^2 \sigma_k}{\sum_k x_k q_k^2} \right] \quad (5.15)$$

with

$$\sigma_k = \left(\frac{\partial(\kappa \chi_k)}{\partial \kappa} \right)_{T, \mathbf{N}} = -2\chi_k + \frac{3}{1 + \kappa a_k} \quad (5.16)$$

Here, the pressure and density dependency of the dielectric constant of water is neglected since the values of ε_r in the temperature range of 278-373 K and at $p = 1$ kPa compared to the values at $p = 1$ MPa differ only at the second decimal place.

The original PC-SAFT model for associating, uncharged molecules has 5 parameters, namely: the segment number, the segment diameter, the dispersion energy, the association energy, and the association volume. The DH term does not require any additional adjustable parameter since the charge of the ions is given by their valence.

Also non-primitive (NP) models should be mentioned in this context. For example, Seyfkar et al.⁷⁸ couple the NP-MSA with the Boublik-Mansoori-Carnahan-Starling-Leland hard sphere EOS as the reference system to calculate MIAC of several salt solutions. Zhao et al.⁷⁹ extend the SAFT-VR EOS with a NP-MSA electrolyte contribution and compare their results with MC simulations.

5.2 Amino Acid and Oligopeptide Solutions

Since the early years of the last century vapor pressures, densities, solubilities, and activity coefficients of amino acids and peptides in various solutions have been measured, correlated, and modeled.

Two main approaches have been followed for the description of thermodynamic properties

of amino acid and polypeptide solutions: g^E -models and equations of state. Khoshkbarchi and Vera⁸⁰ give an excellent overview of the thermodynamic models – g^E -models and equation of states (EOS) – applied in recent years to calculate activity coefficients and solubilities of amino acids in aqueous solutions. For example, Kuramochi et al.⁸¹ used the UNIFAC model combined with a Pitzer-Debye-Hückel term for the long-ranged electrostatic interactions to calculate activity coefficients in aqueous solutions containing amino acids, sugar, and inorganic salts. Nass⁸² applied the Electrolyte NRTL theory to model amino acid solubilities of L-alanine, L-serine, and L-threonine.

Equations of state of varying complexity have been applied to amino acid solutions. Khoshkbarchi and Vera present a primitive model based on first order perturbation theory for the correlation of activity coefficients and solubilities of some amino acids and oligopeptides (up to trimers) in water^{80,83,84}. In a primitive model the solvent (in this case water) is only considered implicitly by its dielectric constant. The amino acids and peptides were modeled as Lennard-Jones spheres which also exhibit dipole-dipole interactions (Stockmayer fluid). The model of Khoshkbarchi and Vera needs three pure-component parameters, namely the sphere diameter, the dispersion energy, and the dipole moment. While the first two are fitted to experimental data, the third is calculated by means of quantum mechanics. In their model Khoshkbarchi and Vera include the pH-dependence of the solubilities. Therefore, the pKa values of the carboxylic and the amino group of the amino acids must be known in addition to the standard entropy and enthalpy of melting.

Simple models are based on a spherical shape of the molecules. This assumption may be justified for molecules like small amino acids. Aiming at the description of more complex biological systems, where the molecules exhibit a rod-like structure, segment based models appear to be more appropriate. The model by Liu et al.⁸⁵ is also based on perturbation theory but treats the solvent as discrete molecules. Further, the molecules are described as chains of Lennard-Jones spheres with dipole moment. The reference system consists of a hard-sphere mixture; chain formation, dispersion, and dipole-dipole interactions are taken into account as perturbation terms. Four pure-component parameters (segment number, segment diameter, dispersion energy, and dipole moment) are fitted to correlate activity coefficients and solubilities of some amino acids and dipeptides in aqueous solutions. Fuchs et al.⁸⁶ have applied the PC-SAFT EOS to model solubilities of glycine, DL-alanine, and DL-methionine in water-alcohol solutions at varying pH.

The solutions examined within the scope of this thesis are restricted to single-solvent (water) solutions of amino acids and oligopeptides.

Chapter 6

Results: Low Molecular Weight Components

6.1 Modeling of Water

To be able to calculate vapor pressures and densities of aqueous solutions, the main component, namely water, has to be modeled as accurately as possible. Groß and Sadowski²⁸ fitted PC-SAFT model parameters to vapor pressure and density data in a temperature range from the triple point to the critical point. Although the overall performance of the model with respect to vapor pressures and densities is very good, the density deviations at low temperature are remarkable.

Since the long-term objective is to describe phase equilibria in aqueous solutions of biological components the temperature range of interest is restricted to $T = 273 - 373$ K. In order to obtain better agreement between experimental and modeled data the parameter set for water is refitted to experimental data in this temperature range using a nonlinear least squares algorithm⁸⁷. The parameters are summarized in Tab. 6.1. Although a four-site model would best reflect the physics of water molecules it was demonstrated earlier that a two-site (2B) approach yields better agreement between model and reality²⁸. Another advantage of using only two association sites instead of four is the decrease in computational time. The density anomaly at about 280 K cannot be reproduced by any state-of-the-art equation of state (see Fig. 6.1, dashed line). Therefore, a temperature-dependent segment diameter is introduced here for the component water:

$$\sigma^* = \sigma + t_1 \cdot \exp\{t_2 \cdot T\} + t_3 \cdot \exp\{t_4 \cdot T\} \quad (6.1)$$

σ^* is the temperature-dependent segment diameter and the t_i are four additionally adjustable parameters. The relative mean deviation* for the densities and for the vapor pressures are 0.015% and 0.60%, respectively. The excellent agreement between calculated

*The relative mean deviation is calculated by $RMD = \frac{1}{N} \sum_i^N \left| 1 - \frac{Model_i}{Expt_i} \right|$, where N is the number of data points.

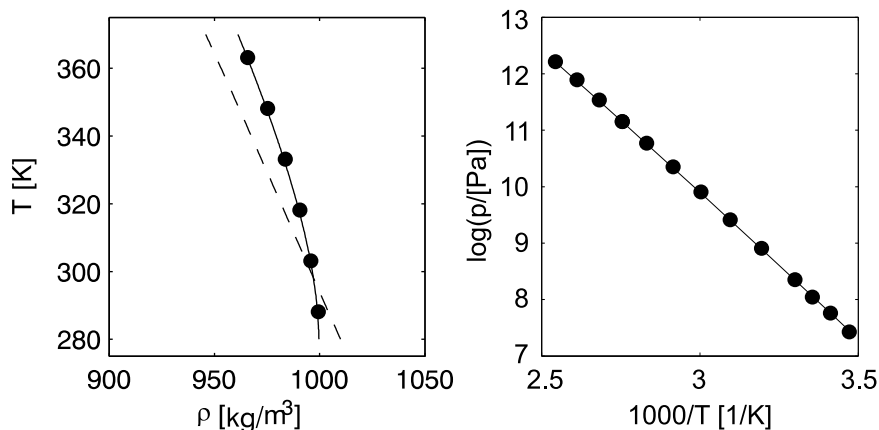


Fig. 6.1: Liquid phase densities (left) and vapor pressures (right) of pure water calculated with ePC-SAFT (line). The symbols represent experimental data⁸⁸. The dashed line is calculated with a T-independent segment diameter.

and experimental data for the T-dependent water model is shown in Fig. 6.1.

Tab. 6.1: ePC-SAFT parameters for water.

segment number	$(m_{seg}/M) = 0.06687$	$[-]$
segment diameter	$\sigma = 2.7927$	$[\text{Å}]$
	$t_1 = 10.11$	$[\text{Å}]$
	$t_2 = -0.01775$	$[K^{-1}]$
	$t_3 = -1.417$	$[\text{Å}]$
	$t_4 = -0.01146$	$[K^{-1}]$
dispersion energy	$\varepsilon = 353.9449$	$[K]$
association sites	$N = 2$	$[-]$
association energy	$\varepsilon^{A_i B_j} = 2425.6714$	$[K]$
association volume	$\kappa^{A_i B_j} = 0.45090$	$[-]$

6.2 Modeling of Electrolyte Solutions with ePC-SAFT

For the calculation of vapor pressures and densities of electrolyte solutions several assumptions have to be made. A reasonable approximation within the temperature range of this work ($T < 373$ K) is that the vapor phase above the solution consists of pure water only since the dissolved inorganic salts considered here are nonvolatile. A proof for the validity of this assumption is given e. g. by Parisod and Plattner⁸⁹. At $T = 653$ K they measured a NaCl concentration of less than 0.1 % in the vapor phase of a H_2O –NaCl solution.

The considered salts are regarded as strong electrolytes, i. e. they fully dissociate into the respective cations and anions. The ions are treated as charged hard spheres ($m_{seg} = 1$) with diameter σ_j (j refers to ions) which mutually interact solely by hard-core and electrostatic forces. The diameter is equivalent to the distance of closest approach a_j . Dispersive


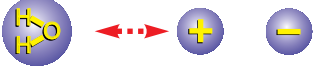

interaction	hard chain	dispersion	association	electrostatic
	✓	✓	✓	✗
	✓	✓	✗	✗
	✓	✗	✗	✓

Fig. 6.2: Interaction matrix: interactions in an aqueous electrolyte solution accounted for in the ePC-SAFT model.

interactions reign exclusively between water–water (ε_{11}) and water–ion pairs (ε_{1j}), hence $\varepsilon_{jj} = 0$. Association is considered only among water molecules.

In the ePC-SAFT model the water molecules are considered explicitly in the hard-chain, the association and the dispersion terms. The interactions arising from the polarity and polarisability of the water molecules and their effect on the electrical potential in the solution are implicitly accounted for by the dielectric constant of water. The interactions in the water-salt system are summarized in Fig. 6.2. The temperature-dependent dielectric constant of water is calculated applying the correlation of Floriano and Nascimento⁹⁰ and setting the pressure to 100 kPa.

6.2.1 Strategy for Parameter Estimation

Two main concepts for modeling electrolyte solutions are found in the literature. The majority of electrolyte models is based on a salt-specific approach. Albeit more flexible and in some cases more accurate than an ion-specific model, the number of adjustable parameters increases linearly with the number of electrolyte systems. Further, mixtures of salts with a common ion (e. g. H_2O -NaCl-KCl) are difficult to describe on a physically sound basis. For the given example, the chloride ion of the sodium chloride would have other parameters than the chloride ion of the potassium chloride. An ion-specific approach appears to be more convenient circumventing the above mentioned shortcoming. Here, the parameters are fixed for each ion, i. e. the chloride in NaCl is the same as in KCl. Another advantage is that the number of parameters increases less than linearly with the number of electrolyte systems. For example, 6 parameter sets suffice to describe 9 alkali halides. In order to obtain a consistent parameter set, the ion parameters must be fitted simultaneously to experimental data of all the considered salts. That makes the estimation procedure slow and susceptible to numerical difficulties. The optimizer, which uses a gradient-based algorithm, may get stuck at a suboptimal parameter set depending on the initial values

provided by the user. The objective functions to be minimized contemporaneously are

$$OF_1 = \sum_i^{NP} \left[1 - \frac{\tilde{\gamma}_i^{calc}}{\tilde{\gamma}_i^{exp}} \right]^2 \quad (6.2)$$

and

$$OF_2 = \sum_i^{NP} \left[(\rho_i^{calc} - \rho_{i,w}^{calc}) - (\rho_i^{exp} - \rho_{i,w}^{exp}) \right]^2 \quad (6.3)$$

where $\rho_{i,w}^{calc}$ and $\rho_{i,w}^{exp}$ are the calculated and experimental densities of pure water at the same T and P as the salt solution. Using the form of OF_2 is more convenient than taking the ratio of the density differences because it avoids the mathematically unfavorable division by small numbers at very dilute solution conditions. Another drawback of the ion-approach is that – strictly speaking – when salts with new ion types are added all parameters of the extended ion matrix must be refitted. Since the ion parameters have been fitted to aqueous solution data they implicitly include information about the solvent water. Hence, the ion parameters may be used only in combination with the water parameters given in Tab. 6.1.

6.2.2 Results

The parameters to be fitted for each ion are its hydrated diameter σ_j and its dispersion energy ε_j when interacting with water. Note that ε_j is a pure component value of the respective ion j . The dispersion energy between water ($i = 1$) and an ion j is calculated using the standard vdW mixing rule $\varepsilon_{ij} = (\varepsilon_i \varepsilon_j)^{0.5} (1 - k_{ij})$. All binary parameters k_{ij} are set to zero. Nevertheless, it should be emphasized that the obtained parameters are only valid for aqueous solutions since the dielectric constant of water is used in the a^{elec} term. Adding or exchanging the solvent will lead to a different behavior of the ions.

Since there is no vapor pressure or density data available for the pure ions their parameters must be obtained from aqueous solutions. First, vapor pressure and density data of solutions containing only one of the respective salts were used for the parameter estimation^{91,92}. The investigated salts were alkali halides $AnCat$ with $Cat = \{Na^+, Li^+, K^+\}$ and $An = \{Cl^-, Br^-, I^-\}$. Further, the sulfate ion being part of Li_2SO_4 , Na_2SO_4 , and K_2SO_4 was chosen as an example of a bivalent anion. With the obtained electrolyte parameters vapor pressures and densities of single-salt and mixed-salt solutions could be calculated with good accuracy. However, mean ionic activity coefficients (MIAC) calculated with the same parameter sets showed high deviations from experiment. This is not surprising, because the vapor pressure depression obeys Raoult's law to a large extent and, thus, is not sensitive enough for a parameter estimation. Therefore, in a second step ionic parameters were fitted to densities and MIAC resulting in an excellent description of all three data sets⁷⁷, densities, vapor pressures, and MIAC as demonstrated in Fig. 6.3 for the arbitrarily chosen salt NaI.

Additionally, salts containing F^- , OH^- , NH_4^+ , and NO_3^- and the bivalent cations Mg^{2+} and

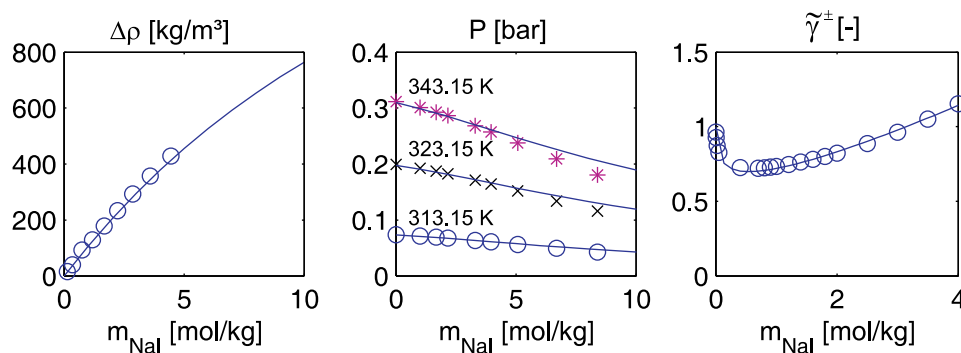


Fig. 6.3: Densities, vapor pressures, and MIAC of NaI. The symbols represent experimental data, the lines are calculated with the ePC-SAFT EOS. The vapor pressures have been predicted with the ePC-SAFT EOS.

Ca^{2+} were considered. Tab. B.1 in Appendix B summarises the optimized ion parameters. An excerpt is given in Tab. 6.2. Figs. B.1-B.6 show the modeling results for 24 alkali salts. The good performance of the ePC-SAFT model is reflected in low deviations averaged over all modeled salts of 0.94%, 4.69%, and 10.81% for densities, vapor pressures, and MIAC, respectively. However, the MIAC of the sulfates are an exception. This may be due to ionic association, detectable by conductance measurements⁹³. Ion pairing effects are not implemented in the ePC-SAFT model. Vapor pressures for LiBr are reproduced with an exceptionally high average deviation of about 30%. This appears odd because the more sensitive MIAC are modeled accurately suggesting that the measured VLE data should be regarded as questionable. The average deviations between modeled and experimental data for all salts are summarized in Tab. B.2.

Tab. 6.2: ePC-SAFT parameters for the alkali halide ions (excerpt from Tab B.1). The segment number is set to unity. For comparison the Pauling ionic diameter σ_j^P (e. g. Ref⁹⁴) are tabulated as well. The hydration free energies ΔG^{hydr} are taken from Ref.⁹⁵

ion	molar mass M [g/mol]	diameter σ_j^P [Å]	diameter σ_j [Å]	disp. energy ε_j [1/K]	valence z_j [-]	hydration energy ΔG^{hydr} [kJ/mol]
Li^+	6.94	1.20	1.818	2697.280	+1	-531
Na^+	22.99	1.90	2.412	646.050	+1	-416
K^+	39.10	2.66	2.970	271.052	+1	-334
F^-	19.00	2.72	1.613	648.313	-1	-510
Cl^-	35.45	3.62	3.058	47.288	-1	-367
Br^-	79.90	3.90	3.457	60.222	-1	-336
I^-	126.90	4.32	3.932	80.435	-1	-291

It is worthwhile to scrutinise the trends of the ion parameters in order to test their physical relevance. The segment diameters follow the same trend as the Pauling diameters. The cation diameters are larger than the Pauling diameters indicating the formation of a tightly bound hydration sheath. Contrariwise, the anion diameters are about 0.4 Å smaller than their Pauling diameters. The dispersion energies, which reflect the interactions between water and ions, decrease in the sequence $\text{Li}^+ > \text{Na}^+ > \text{K}^+$ by an order of magnitude.

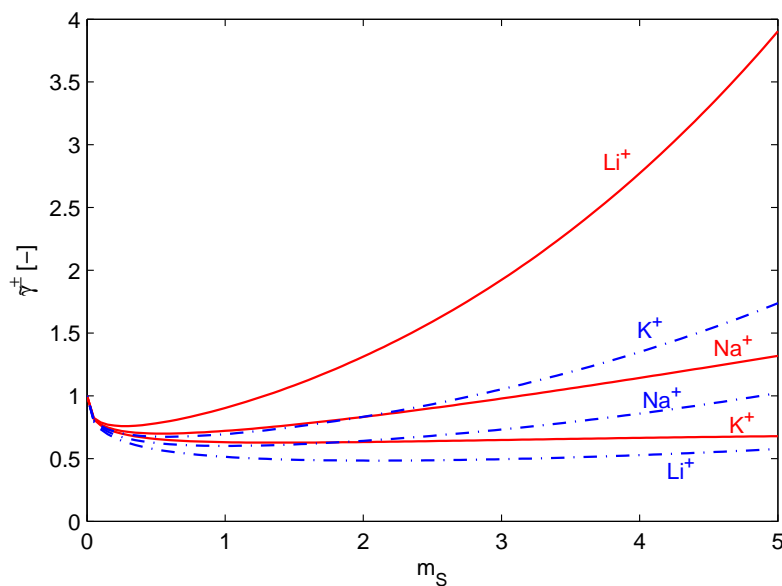


Fig. 6.4: MIAC of alkali iodides (—) and hydroxides (---) at 298.15 K calculated with ePC-SAFT. The values are ordered in the sequence $\tilde{\gamma}_{LiAn}^{\pm} > \tilde{\gamma}_{NaAn}^{\pm} > \tilde{\gamma}_{KAn}^{\pm}$ for the iodides and, reversely, $\tilde{\gamma}_{KAn}^{\pm} > \tilde{\gamma}_{NaAn}^{\pm} > \tilde{\gamma}_{LiAn}^{\pm}$ for the hydroxides. This behavior is mapped quantitatively by the ePC-SAFT model. Experimental data not shown for the sake of clarity.

This is consistent with the trend of the hydration free energies ΔG^{hydr} . The more negative the value the more intense are the water-ion interactions. The bivalent cations Ca^{2+} and Mg^{2+} reveal very high dispersion energies reflecting their two positive charges distributed over a relatively small ion sphere (i.e. high charge density) allowing extensive hydration. The interactions between (halide) anions and water are markedly weaker than it is the case with the cations. This is due to the larger size of the anions and, therefore, smaller charge density. The anion dispersion energies are smaller than the cation dispersion energies which is consistent with the fact, that the anions are only weakly hydrated. Especially the anions NO_3^- and SO_4^{2-} have very low dispersion energies because the oxygen atoms prevent extensive hydration (see Ref.⁹⁶, p. 122). Therefore, their dispersion energies are set to 0. The sulfate ion has a very small fitted diameter (2.55 Å) which may compensate for the vanishing dispersion energy value. An exception to the rule is the F^- ion which also reveals a fitted ion diameter which is about 1.1 Å smaller than the Pauling value.

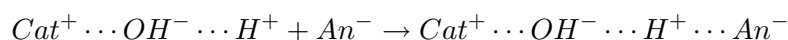
That the fluoride breaks ranks suggests that it undergoes water-ion interactions not considered in the ePC-SAFT model. Dielectric relaxation measurements⁹⁷ of aqueous fluoride solutions prove that the fluoride ion is strongly hydrated, which explains the high dispersion value of about 650 K.

That the fluorides exhibit a ‘special’ behavior can also be shown for the MIAC. The same is valid for the hydroxide ion. The MIAC of the alkali chlorides, bromides, and iodides follow the sequence $\tilde{\gamma}_{LiAn}^{\pm} > \tilde{\gamma}_{NaAn}^{\pm} > \tilde{\gamma}_{KAn}^{\pm}$. This trend is reversed for the fluorides and hydroxides. Fig. 6.4 illustrates this behavior for iodides and hydroxides. Here, two effects

seem to be superposed: The MIAC of the hydroxides are higher than those of the iodides. However, there must be another effect which decreases the MIAC for LiOH and NaOH. A possible explanation for this phenomenon is given by Harned and Robinson⁹³: The cation Cat^+ is surrounded by distorted water molecules



where the dotted lines represent linkages due to ion-solvent forces. The positive partial charge of the hydrogen atom attracts the anion An^- which then docks to the hydration shell. This effect is more pronounced for strong proton acceptors such as the small fluoride anion or the hydroxide. The interaction may be represented as



This kind of reaction is equivalent to ion pairing mediated by water molecules in the first hydration sheath resulting in a reduction of free ions and, hence, a lower activity coefficient. This effect is more pronounced for stronger hydrated cations, i. e. for the Li^+ which has the highest charge density. Since the K^+ is only weakly hydrated the MIAC of KI is lower than that of KOH. The ePC-SAFT is able to capture above-mentioned effects quantitatively.

Mixed Electrolyte Solutions

Vapor-pressures of solutions containing the mixtures NaCl/KBr and NaBr/KCl, respectively, were predicted and the calculated data was compared to experimental data⁹⁸. As can be seen in Tab. 6.3 the ePC-SAFT EOS can easily handle such systems without any readjustment of the ion parameters and without introducing any binary parameter k_{ij} . The average relative deviation of the vapor pressures is about 1%.

Tab. 6.3: Comparison of predicted vapor-pressures and experimental data of aqueous NaCl–KBr and NaBr–KCl solutions. Exp. data taken from Ref.⁹⁸.

T [K]	NaCl + KBr					NaBr + KCl				
	NaCl [m]	KBr [m]	p_{exp} [kPa]	p_{mod} [kPa]	Δp [%]	NaBr [m]	KCl [m]	p_{exp} [kPa]	p_{mod} [kPa]	Δp [%]
303.15	1.500	1.498	3.77	3.76	0.28	1.5020	1.4980	3.77	3.76	0.28
303.15	2.000	1.999	3.59	3.59	0.08	1.9990	2.0020	3.60	3.59	0.34
308.15	1.496	1.502	4.99	4.97	0.36	1.5010	1.4990	5.01	4.97	0.74
308.15	2.001	1.998	4.80	4.74	1.22	2.0010	1.9980	4.79	4.74	0.96
313.15	1.501	1.498	6.58	6.51	1.04	1.4980	1.5000	6.60	6.51	1.29
313.15	1.998	2.001	6.30	6.21	1.49	1.9990	1.9990	6.32	6.21	1.72
318.15	1.002	0.999	8.93	8.83	1.09	1.0030	0.0090	8.91	9.18	2.98
318.15	1.499	1.501	8.53	8.45	0.95	1.4970	1.5030	8.55	8.45	1.12
318.15	2.000	2.001	8.18	8.05	1.62	1.9990	2.0010	8.20	8.06	1.75
323.15	0.499	0.498	11.95	11.83	1.03	0.4990	0.5010	11.94	11.83	0.95
323.15	0.998	1.004	11.49	11.36	1.10	1.0020	0.9990	11.49	11.37	1.06
323.15	1.496	1.501	11.02	10.87	1.39	1.4990	1.4990	11.00	10.87	1.14
323.15	1.999	1.998	10.50	10.35	1.46	2.0030	1.9980	10.49	10.36	1.26
328.15	0.496	0.503	15.20	15.09	0.72	0.5010	0.5000	15.20	15.09	0.72
328.15	1.001	0.999	14.59	14.50	0.63	0.9970	1.0040	14.60	14.50	0.66
328.15	2.001	1.998	14.01	13.19	5.88	1.5010	1.5020	14.00	13.87	0.96
328.15	1.502	1.497	13.33	13.86	3.95	2.0020	1.9990	13.33	13.20	0.94
333.15	0.499	0.502	19.17	19.10	0.37	0.5030	0.4970	19.17	19.10	0.35
333.15	1.000	1.001	18.48	18.35	0.72	1.0020	1.0000	18.48	18.35	0.68
333.15	1.499	1.502	17.71	17.53	1.04	1.4990	1.5030	17.71	17.54	0.94
333.15	1.997	1.998	16.93	16.68	1.50	1.9980	2.0010	16.91	16.70	1.24

6.3 Modeling of Amino Acid and Peptide Solutions with ePC-SAFT

Within the ePC-SAFT framework each of the 20 amino acids and peptides is treated as a chain consisting of identical spheres. In analogy to the 2B-model of water (comp. Sec. 6.1), the amino and the carboxylic group have each one association site (see Fig. 6.5) mimicking the proton donor site (acidic group) and the proton acceptor site (amino group). Amino and carboxylic groups in the residue R are also considered. For instance, serine ($R = -CH_2 - OH$) exhibits one additional proton donating site. For the sake of reducing the number of adjustable parameters, both association-site types are assumed to have the same energy and volume parameters. When two amino acids form a peptide bond, two association sites are eliminated due to polycondensation (compare Fig. 6.5).

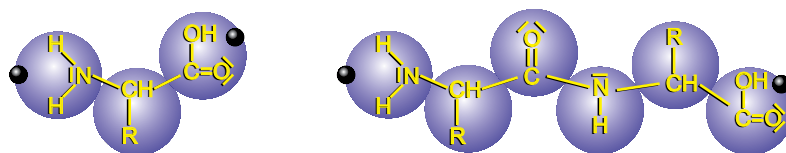


Fig. 6.5: Schematic representation of an amino acid (left) and a peptide (right). The amino and the carboxylic group are modeled by each one association site (black spheres). The residue R may also have association sites. The peptide backbone has only two association sites, one proton donor site and one proton acceptor site. When two amino acids form a peptide bond two association sites are eliminated due to polycondensation.

Although amino acids and peptides in solution (without pH adjustment) are mainly present as zwitterions, no charge-charge interactions are included in the model. Also, the interactions emanating from the large dipole moment are not considered. Numerical investigation has shown that including the dipole-dipole interactions in the EOS does not lead to an ameliorated performance of the model. The interactions accounted for in the ePC-SAFT EOS are summarized in Fig. 6.6.

interaction	hard chain	dispersion	association	electrostatic
	✓	✓	✓	✗
	✓	✓	✓	✗
	✓	✓	✓	✗

Fig. 6.6: Interaction matrix: interactions in an aqueous amino acid/peptide solution accounted for in the ePC-SAFT model.

6.3.1 Parameter Estimation

Only little experimental data is available for vapor pressures of pure amino acids (see e. g. Ref.⁹⁹) and peptides as they decompose before sublimation. Fuchs et al.⁸⁶ have used such data for the parameter regression for DL-methionine. They state that the relative mean deviations are fairly large since the absolute vapor pressures are very low (down to 4 Pa). Moreover, at ambient temperature the amino acids are solids. Hence, for the pure-component parameter estimation one harks back on binary (aqueous) solution data such as densities, vapor pressure depression, activity coefficients in solution and solubilities. In this work, the five ePC-SAFT parameters (segment number, segment diameter, dispersion energy, association energy, and association volume) are regressed to experimental density and activity coefficient data at 298.15 K. Afterwards, melting enthalpy and melting temperature are fitted to solubility data. In order to describe all 4 data types with only one parameter set a binary interaction parameter k_{ij} has to be introduced. Summing up, a total of 8 parameters is necessary for modeling the above-mentioned thermodynamic properties of amino acids and peptides in aqueous solutions. Since chiral molecules such as amino acids reveal pronounced differences in their solubility behavior, as far as experimental data is available, melting enthalpy and melting temperature are given for the L and DL form.

PC-SAFT parameters for glycine, alanine, serine, proline, valine, methionine, and some oligopeptides have already been fitted by Fuchs et al.⁸⁶ and Cameretti et al.¹⁰⁰ to aqueous solution densities, vapor pressures and solubilities. Although they achieved good agreement between model and experiment, activity coefficients cannot be described with the obtained parameters. Therefore, new parameters have been fitted to experimental density, activity coefficient, and solubility data. Further, the association site number has been decreased from two to one association site per type. This has the advantage of reduced computation time without decreasing the accuracy of the model. Furthermore, this procedure is consistent with the modeling of water with a 2B-approach. Fig. 6.7 clearly shows the deficiency of the old parameter set for the calculations of activity coefficients: while experimental activity coefficients are < 1 the model predicts $\tilde{\gamma}_A > 1$. Additionally, with the new parameter estimation strategy results are ameliorated also for vapor pressures and solubilities.

For the homopolypeptides diglycine and triglycine the majority of the pure-component parameters of glycine can directly be inherited as suggested by Cameretti et al.¹⁰⁰. However, in order to reproduce activity coefficient data of the glycine-peptides the segment number and the k_{ij} -parameter have to be refitted to experimental data. Of course, the melting properties cannot be inherited either. This approach also yields reasonable results for dialanine. For the heteropolypeptides alanyl-glycine and glycylalanine the whole set of parameters has to be regressed. Although these peptides are different in structure, solution densities and activity coefficients are identical within measurement uncertainty. Presumably, this is not the case for the solubilities, because here the steric orientation of the peptide residues plays a predominant role for the insertion of a molecule into the crystal structure.

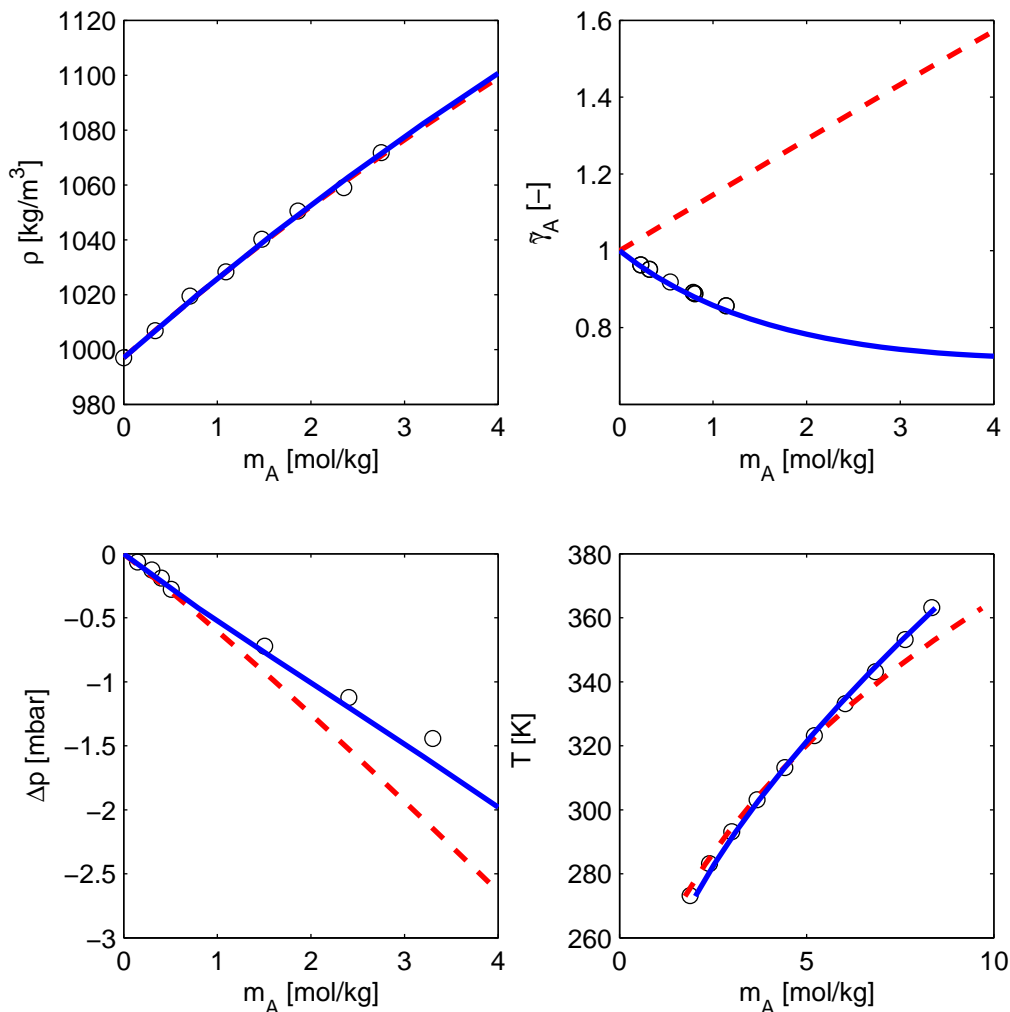


Fig. 6.7: Densities, activity coefficients, vapor pressure depressions and solubilities of glycine solutions. Symbols represent experimental data at 298.15 K (except for solubilities), lines are calculated with the ePC-SAFT EOS. The dashed lines have been calculated with the parameter set adjusted to densities, vapor pressures and solubilities as described in Ref.¹⁰⁰ The continuous lines have been obtained with the new parameter set fitted to densities, activity coefficients and solubilities as presented in this work.

For the aminobutyric acids and the aminovaleric acids the ePC-SAFT parameters were first fitted to the γ -form. Then, all parameters but segment number, dispersion energy, and binary interaction parameter were inherited to the β and α -types. m_{seg} , ε and k_{ij} were readjusted to experimental data. The incentive for this procedure is twofold: Firstly, the number of adjustable parameters is reduced decreasing computation time. Secondly, the obtained parameters may reveal physically relevant trends. Indeed, a closer look at the parameters of the aminobutyric acids shows that the segment number slightly decreases from α -ABA to γ -ABA indicating a more compact molecular structure of the γ -ABA in water.

The 20 amino acids and peptides considered in this work as well as their chirality are listed in Appendix C, Tab. C.1. Their parameters are summarized in Tab. C.2. It is noted that the melting temperatures appear to have lost their physical meaning because they are much higher than the decomposition temperatures of the amino acids. That is to be the compromise one has to accept when using a simple model for the solution properties given by Eq. 2.32.

6.3.2 Results for the Binary Systems

Densities, vapor pressures, activity coefficients, and solubilities of the considered amino acids and peptides can be reproduced by the model with good accuracy. The corresponding plots are given in Appendix C. In the following, the interactions between the amino acids and the solvent will be discussed by examining the trends of the activity coefficients for various series of amino acids and peptides.

Homologous Series: Glycine – Alanine – α -ABA – α -AVA

These amino acids have charged head groups (COO^- and NH_3^+) attached to the side chain tail. Hence, two antagonistic interaction types dominate in aqueous amino acid solutions: hydrophilic and hydrophobic. The former leads to attractive water-amino acid interactions and low solute activity coefficients. The latter provokes water-amino acid repulsions and hence stronger attractive interactions between the amino acids (high solute activity coefficients). This is reflected by the increase of the activity coefficients from glycine to α -AVA shown in Fig. 6.8. Interestingly, the activity coefficients of α -ABA and α -AVA do not differ much suggesting that for residue chains longer than two carbons the balance between hydrophilic and hydrophobic interactions is already completely shifted towards the mutual attraction between the amino acid side chains.

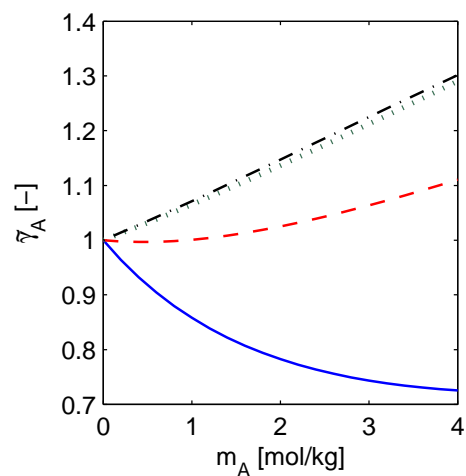


Fig. 6.8: Modeled activity coefficients of glycine (—), alanine (---), α -ABA (···), α -AVA (— · —). With increasing chain length in the residue the activity coefficient increases. Experimental data are omitted for the sake of clarity.

Homologous Series: α -ABA – β -ABA – γ -ABA / α -AVA – γ -AVA

The influence of the location of the amino group on the intermolecular interactions becomes clear when investigating amino acids of same chain length. In the α -ABA both the carboxyl and the amino group are attached to the α -carbon. Hence, the dipole moment is comparatively small. In the β -ABA the amino group position is shifted by one carbon atom. Therefore, the β -ABA reveals a larger dipole moment and an effectively shorter hydrophobic tail. The same holds for γ -ABA. It can be expected that larger dipole moments lead to increased solvation effects and, thus, to decreased activity coefficients. Indeed, this assumption is corroborated by experimental observation (see Fig. 6.9) – up to 4 m the activity coefficients follow the trend $\tilde{\gamma}_{\alpha\text{-ABA}} > \tilde{\gamma}_{\beta\text{-ABA}} > \tilde{\gamma}_{\gamma\text{-ABA}}$ – and also by the fact that the dispersion energies of the aminobutyric acids are ranked as $\varepsilon_{\alpha\text{-ABA}} > \varepsilon_{\beta\text{-ABA}} > \varepsilon_{\gamma\text{-ABA}}$ (see Tab. C.2). The same considerations are also valid for the aminovaleric acids.

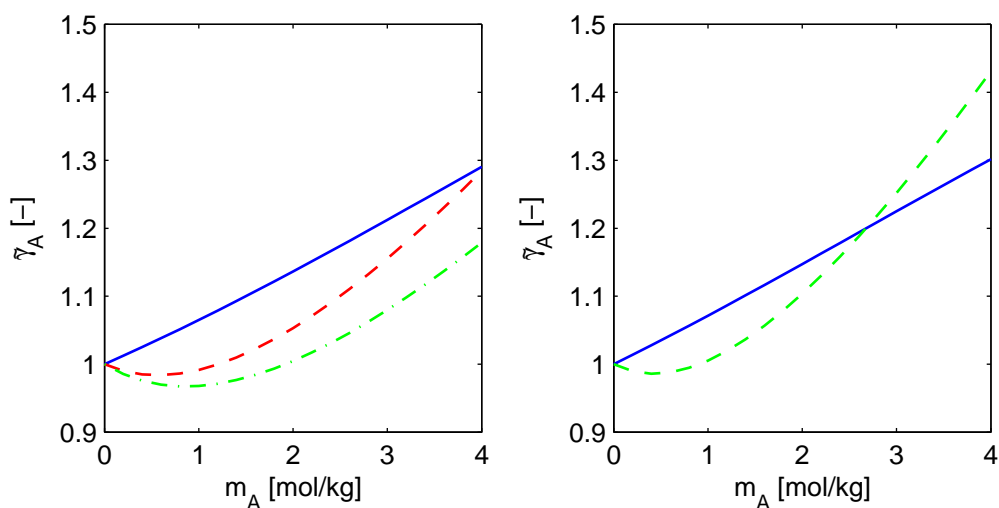


Fig. 6.9: Modeled activity coefficients of (left) α -ABA (—), β -ABA (---), γ -ABA (- · -), and (right) α -AVA (—), γ -AVA (- · -). The amino group is shifted from the α -carbon to the γ -carbon increasing the dipole moment of the molecule. Experimental data omitted for the sake of clarity.

The activity coefficients of β -ABA, γ -ABA, and γ -AVA show a minimum at about 1 mol/kg. The reason for this could be that at low solute concentrations the solute-solvent interactions (solvation) due to the amino acid's large dipole moment dominate whereas at high solute concentrations the hydrophobic solute-solute interactions become increasingly important. Here, less water molecules are available in order to provide complete solvation.

Homologous Series: Glycine – Diglycine – Triglycine

Despite the growing backbone length of the glycine peptides the activity coefficients decrease in contrast to the series glycine-alanine- α -ABA- α -AVA (see Fig. 6.10). This behavior can be attributed to the hydrophilic (polar) peptide group inserted per integrated glycine. In this case the hydrophilic character of the oligopeptide controls the phase behavior leading to enhanced solute-solvent interactions.

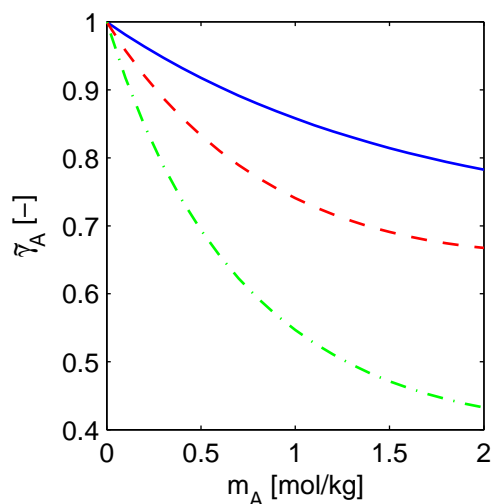


Fig. 6.10: Modeled activity coefficients of glycine (—), diglycine (---), and triglycine (-·-·). The activity coefficients decrease with increasing chain peptide length. Experimental data omitted for the sake of clarity.

Influence of Temperature on Activity Coefficients of Glycine and Alanine

The influence of temperature on the activity coefficients of amino acids shall be investigated using the examples of glycine and alanine. The increase in activity coefficients of both glycine and alanine with increasing temperature indicates that solvation becomes less favorable. The solvation process is exothermic¹⁰¹. Hence, according to LeChatelier's

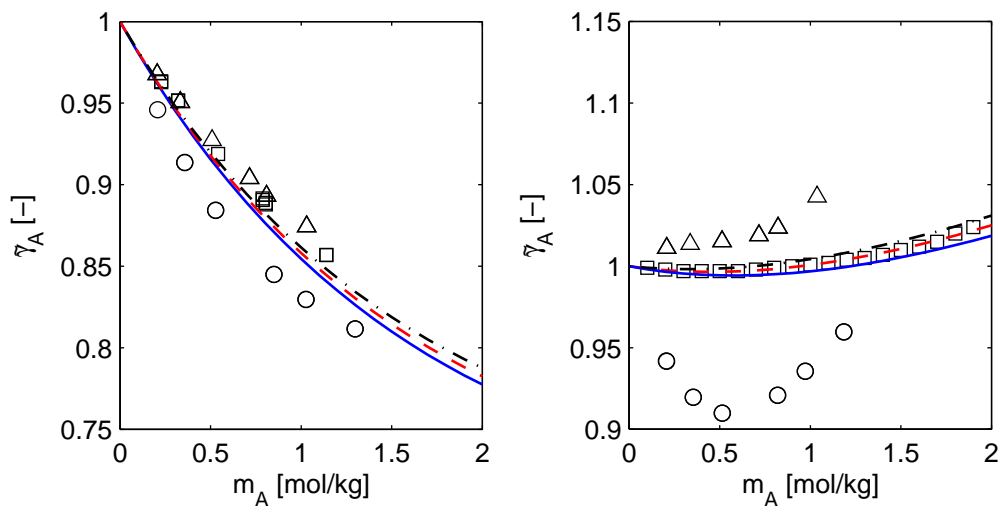


Fig. 6.11: Activity coefficients of glycine (left) and alanine (right) at 293.15 K (—, ○), 298.15 K (---, □), and 303.15 K (-·-·, △). The activity coefficients increase with increasing temperature. Experimental data taken from Refs^{102,103}.

principle, the amino acids will be less solvated at elevated temperatures. This trend can be reproduced qualitatively by the ePC-SAFT EOS (see Fig. 6.11). However, quantitative

agreement between model and experiment could not be achieved.

6.4 Modeling of Aqueous Electrolyte/Amino Acid Solutions

To this point, binary aqueous mixtures have been investigated. Model parameters have been fitted for electrolytes and amino acids as well as for small peptides. The ePC-SAFT model has successfully been applied for the calculation of thermodynamic properties of such systems. In the following the, applicability of the model and some extensions for aqueous electrolyte/amino acid solutions will be briefly discussed.

As described in Sec. 2.3.3 on p. 14, the ratio of the MIAC of the electrolyte in the ternary solution to the one in the solution without the amino acid (in the following abbreviated as ratio of MIAC) can be assessed by electrochemical potential measurements. Such measurements have been performed and interpreted especially by the group of Khoshkbarchi et al. for several electrolyte/amino acid systems (see e. g. Refs.^{5,6,104–106}).

From their measurements they conclude that at low salt concentrations the effect of the amino acid on the MIAC of the electrolyte is more pronounced than at high ionic strength. This can be seen in Fig. 6.12 using the example of NaNO_3 -serine solutions.

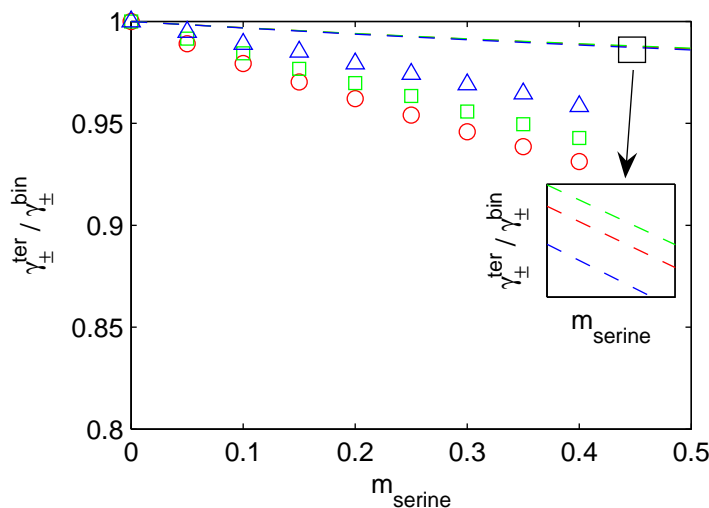


Fig. 6.12: Ratio of the MIAC of NaNO_3 in a NaNO_3 -serine solution to the one in a solution without amino acid at (\circ) 0.1, (\square) 0.3, and (\triangle) 0.7 m NaNO_3 . Experimental data taken from Ref.¹⁰⁷ Calculations (dashed lines) with ePC-SAFT without introduction of further binary interaction parameters revealing a reversed trend.

At constant amino acid molality the MIAC has its highest deviation from 1 at low ionic strength. Here, electrostatic interactions exceed the non-electrostatic, short-ranged interac-

tions. Instead, long-ranged electrostatic interactions are screened at high salt concentration and short-ranged interactions prevail, especially those between the hydrophobic backbone of the amino acid or peptide. Further, ion pairing between the dipolar, zwitterionic amino acid and the salt ions leads to an additional reduction of electrostatic forces. According to Soto-Campos et al.⁶ the formation of these ion-pair complexes is of physical type rather than of chemical type. The importance of this conclusion will become clear below.

The experimental data is compared to values predicted with the ePC-SAFT EOS. Without introducing any further binary interaction parameters the ratio of MIAC cannot be described properly as shown again by the example of serine in NaNO_3 solutions depicted in Fig. 6.12.

While experimental ratios increase with increasing salt content, the modeled data shows the inverse trend. Further, the respective curves are less spread than it is the case with the experiment. These facts indicate that there must be interactions between amino acid and electrolyte ions not yet accounted for in the model. That there is a strong interaction between amino acid and ions can be demonstrated by the ‘preferential interaction parameter’ as described by Shimizu¹⁰⁸. The quintessence of his work is that ions are tightly bound to the first hydration shell of the biomolecule. There are two ways of implementing this knowledge in the model.

The first and presumably easiest way is to introduce a binary interaction parameter k_{ij} between the amino acid and the ions (equal value for cation and anion) which addresses the dispersion energy between them. However, this procedure has turned out to be inappropriate for several electrolyte/amino acid systems[†] unless the k_{ij} is not considered to be dependent on salt molality[‡], which is per se a serious drawback. Nevertheless, the ratios of the MIAC can be modeled in this way as shown in Fig. 6.13 (left), again for serine in NaNO_3 solutions. More systems are given in Appendix H.

Further, k_{ij} assumes high absolute values < -0.3 . Last not least, solubilities of the amino acid predicted with this approach do not match experimental data (Fig. 6.13, right and Appendix H)

As explained above, due to the zwitterionic form of amino acids in solution, it is most probably that the charged functional groups (carboxylic group and amino group) interact with the ions. Although this interaction is surely of electrostatic type, the Debye-Hückel term already implemented in the ePC-SAFT EOS is not readily applicable. The reason is that this term was developed for spherical molecules and not for segmented ones as the modeled amino acids. The discussion shall be stopped at this point and be referred to future work.

[†]Systems considered were combinations of NaCl , KCl , NaNO_3 , KNO_3 , NaBr , and KBr with glycine, alanine, valine, serine, and diglycine. Appendix H contains the fitted k_{ij} values as well as plots of the MIAC ratios and the solubilities.

[‡]Khoshkbarchi and Vera¹⁰⁶ propose a k_{ij} dependent on amino acid concentration. Its value is rather high and can be > 0.4 depending on the investigated system.

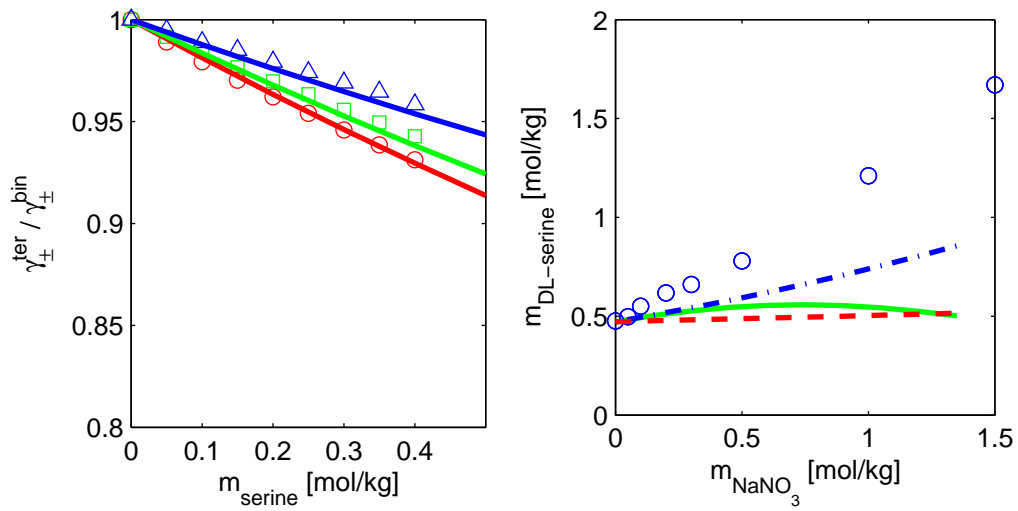


Fig. 6.13: Left: Ratio of the MIAC of NaNO₃ in a NaNO₃-serine solution to the one in a solution without amino acid at (\circ) 0.1, (\square) 0.3, and (\triangle) 0.7 m NaNO₃. Experimental data taken from Ref.¹⁰⁷ Calculations (continuous lines) with ePC-SAFT using a binary interaction parameter between amino acid and salt ions dependent on salt molality, $k_{ij} = -0.3183 + 0.2053 \cdot m_s$. Right: Solubilities of DL-serine in NaNO₃-solutions at 298.15 K vs. salt molality. Experimental data (\circ) taken from Ref.¹⁰⁹ The lines are calculated without k_{ij} ($- -$), with constant k_{ij} ($-$), and with ($- \cdot -$) $k_{ij}(m_s)$ between ion and amino acid, respectively.

Chapter 7

Results: Protein Systems

7.1 Modeling of Protein Solutions with ePC-SAFT

Rigorous thermodynamic modeling of aqueous protein solutions is a challenging task as will become clear in this section. Some aspects concerning the modeling of the meta-stable liquid-liquid demixing in protein solutions with the ePC-SAFT EOS are addressed. Solutions of HEW lysozyme will serve as an example.

The simplest protein system consists of four components, namely the solvent (water), the (charged) protein, and an electrolyte which dissociates into its cation and anion. This system is highly asymmetric concerning the molecule sizes. Solvent and ions have a diameter of about 3-4 Å. The macromolecule's diameter is one order of magnitude larger, in the case of lysozyme about 34 Å. All species exhibit a spherical shape and the segment numbers are unity or at least very close to one*. For a first approximation the salt ions shall be neglected. In terms of mole numbers of each species, the system consists of few macromolecules solvated in an ocean of solvent molecules†. Hence, the mixture properties should be dominated by the solvent. Applying the standard one-fluid mixing rule for the diameter

$$\sigma_{ij} = \frac{\sigma_i + \sigma_j}{2} \quad (3.58)$$

will lead to a large value which is not characteristic for that component making up most of the solution: the solvent (compare Fig. 7.1). This causes serious problems when calculating the density of a protein solution. Fig. 7.2 (continuous line) shows that calculated solution densities erroneously decrease with increasing protein concentration.

One method to circumvent the problems emanating from highly asymmetric molecule sizes is to consider the macromolecule as a chain of smaller segments. As depicted in Fig. 7.2, solution densities can be described perfectly when $m_{seg,P} = 1000$ and $\sigma_P = 2.68\text{Å}$. However, the main task is to model the liquid-liquid phase transition. Again, the considered system is restricted to the macromolecule and the solvent water. Due to the relatively high

*Water has a segment number of $m_{seg} \approx 1.2$.

†Due to the high molecular mass (17 kDa) in a lysozyme solution at a concentration of 1 mg/mL the molar ratio of protein to water is about $1:10^6$.

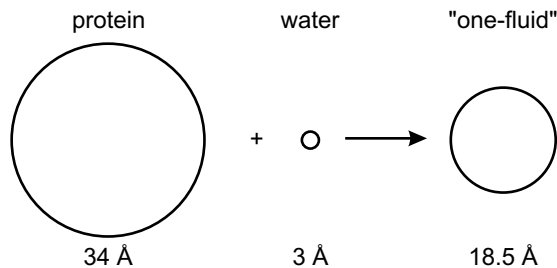


Fig. 7.1: Arithmetic mean of protein and water diameter as calculated with the standard mixing rule in ePC-SAFT.

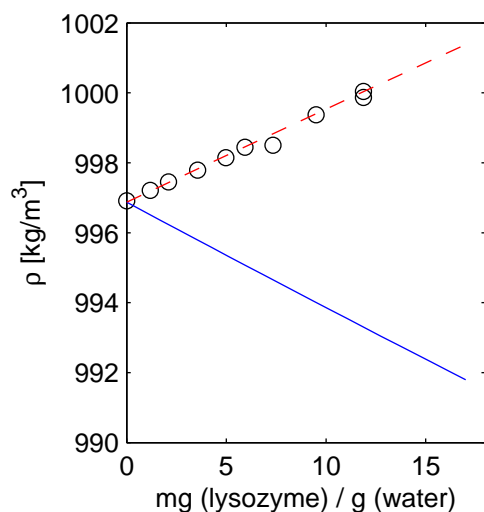


Fig. 7.2: Densities of HEW lysozyme solutions (no salts added). Experimental data (o) (own measurements), the continuous line (—) is calculated with the ePC-SAFT EOS setting the protein diameter $\sigma_P = 34 \text{ \AA}$. The dispersion energy of the protein has only a marginal influence on the calculated densities and is set to an arbitrary value of $\varepsilon_P/k_B = 500 \text{ K}$. The dashed curve (---) is calculated with $m_{seg,P} = 1000$ and $\sigma_P = 2.68 \text{ \AA}$. Both parameters are fitted to experimental density data.

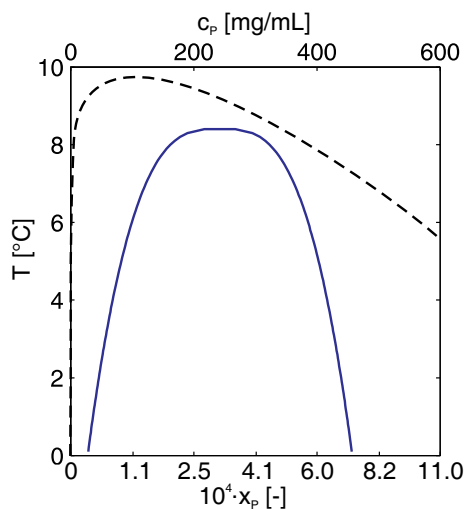


Fig. 7.3: Liquid-liquid phase equilibria of HEW lysozyme in a 510 mM NaCl solution containing NaAc buffer at pH 4.5 (—). The experimental data was correlated with $T^{cloud} = T^{crit} \left[1 - A \left(\frac{c^{crit} - c_p}{c^{crit}} \right)^{1/\beta} \right]$ as explained in Ref.¹¹⁰ The dashed line represents qualitatively a typical polymer/solvent system.

molecular mass of the protein (17 kDa) it can be expected that the calculated phase behavior will resemble that of a polymer-solvent mixture as depicted in Fig. 7.3 by a dashed line. The concentration of dissolved polymer in the solvent-rich phase is very low (mole fraction $x_P \ll 10^{-6}$). The miscibility gap is relatively large and highly asymmetric. Experimental data of protein systems reveal a different behavior. Here, both phases contain considerable amounts of protein as shown in Fig. 7.3.

The question arises, whether the ePC-SAFT approach in principle is able to capture such a behavior. A parameter study shall clarify the sensitivity of the locus of the binodal

Tab. 7.1: ePC-SAFT parameters for cyclohexane.

segment number	$m_{seg} = 2.53$	$[-]$
segment diameter	$\sigma = 2.85$	$[\text{\AA}]$
dispersion energy	$\varepsilon = 278.11$	$[K]$

on each adjustable parameter. An imaginary component P is mixed with water. As a starting point the parameters for component P are set to those of cyclohexane (Tab. 7.1). Cyclohexane and water are immiscible at room temperature and exhibit a LLE.

The segment number of P is increased from 2.5 to 32 keeping σ and ε constant. This change leads to a significant shift of the left branch of the binodal by more than 20 orders of magnitude to infinitesimal small mole fractions whereas the right branch is almost unaffected (compare Fig. 7.4). Compared to that segment diameter and dispersion energy have a minor effect on the equilibrium. As has been shown before, a high segment number is

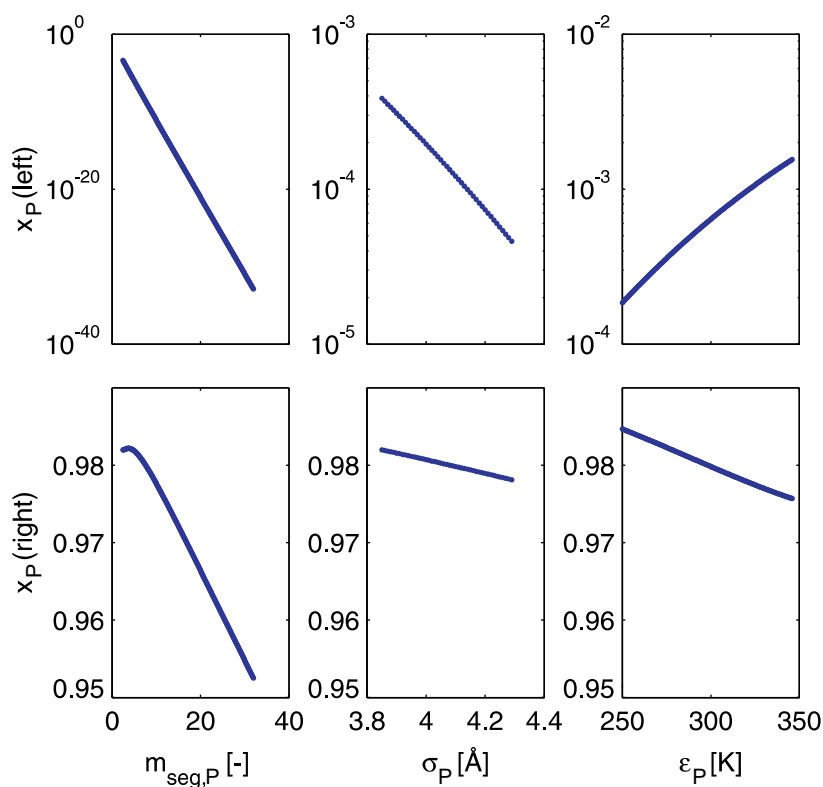


Fig. 7.4: Influence of the pure component parameters on the loci of the left and right branch of the phase boundary line expressed in mole fractions of component P . The segment number has the most pronounced influence on the left branch.

necessary in order to reproduce the densities of aqueous protein solutions. However, large segment numbers implicate practically complete immiscibility of the protein in the solvent, i. e. one phase will consist of almost pure solvent. This is in clear contrast to experimental data.

A conclusion may be that phase equilibria in protein solutions cannot be described with the state-of-the-art PC-SAFT approach. One reason may be that the PC-SAFT EOS was developed to reproduce the phase behavior of long rod-shaped molecules. Proteins instead possess a compact (tertiary) structure although the backbone consists of concatenated amino acids. Further, the charge distribution on the protein's surface is not only affected by the solution pH but also by the surrounding salt ions¹¹¹. This complicates a rigorous modeling.

7.2 Modeling of Protein Solutions with PMF

The thermodynamic description of protein solutions fails when using a model based on the Lewis-Randall framework, i. e. when the solvent is discretely taken into account. Hence, the complexity of the real system is reduced switching to the McMillan-Mayer framework where the solute is treated as a pseudo-pure component floating in a continuum of given permittivity.

Second Osmotic Virial Coefficient, Liquid-Liquid Transition and Solubility

Second osmotic virial coefficients (B_2) have been measured by osmometry or static light-scattering for a couple of protein solutions containing different salts at varying pH.^{43,51,112–116} PMF models of diverse complexity were used to correlate and reproduce the measured values in dependency on salt type and concentration, and solution pH. However, simple theories like the DLVO theory often fail because they contain only information about the ionic strength of the solution but not about specific interactions between the electrolyte and the protein (e. g. ion binding). Hofmeister discovered in the 1880s that the salting-out behavior of proteins is highly affected by the ion's type. E. g. at equal ionic strength NaSCN leads to a more pronounced salting-out than NaCl. The effectiveness of the ions in precipitating (negatively charged) proteins follows the so-called Hofmeister series $\text{Cs}^+ > \text{Rb}^+ > \text{K}^+ > \text{Na}^+ > \text{Li}^+$ for monovalent cations, $\text{Ba}^{2+} > \text{Sr}^{2+} > \text{Ca}^{2+} > \text{Mg}^{2+}$ for divalent cations, and $\text{SCN}^- > \text{I}^- > \text{ClO}_4^- > \text{NO}_3^- > \text{HCOO}^- > \text{Cl}^- > \text{F}^-$ for monovalent anions⁹⁵. These series also reflect the sequence of the ions' polarizability corroborating the assumption that this ion property plays an important role in the protein's phase behavior. And indeed, MC calculations show that the higher the polarizability the more attractive are the contributions to the mean force between two macroions¹¹⁷. Boström et al.¹¹⁸ include a salt-specific contribution to the PMF, a polynomial ansatz which already comprises the electrostatic interactions usually covered by a Debye-Hückel term. They use MC data for HEW lysozyme in aqueous solutions of NaCl, NaI, and NaSCN at 0.2 M salt concentration to fit the polynomial coefficients. They achieve at least qualitative agreement with experimental phase equilibria data. Such an approach could be extended to more salts and especially should include a salt-concentration dependency.

In this work, the original DLVO theory as described in Chapter 4.5 including Eqs. 4.11, 4.14, and 4.12 is used and compared to a more sophisticated approach by Bratko et al.⁵³.

Tab. 7.2: Model parameters for lysozyme. The net charge is dependent on solution pH. The equation is regressed to literature data¹¹¹.

molar mass	$M = 17000$	[g/mol]
segment diameter	$\sigma = 34.4$	[Å]
charge	$q(pH) = 0.375 \cdot pH^2 - 6.124 \cdot pH + 32.5$	[-]
dipole moment	$\mu_D = 400$	[D]
Hamaker constant	$H = 7.575$	[$k_B T$]
Stern-layer thickness	$\delta = 1.4$	[Å]

Their electrostatic contribution is given by Eq. 4.23 including interactions emanating from the large dipole moments of the proteins. As model system aqueous solutions of HEW lysozyme containing NaCl are investigated. The lysozyme parameters are summarized in Tab. 7.2. Although the formula weight of lysozyme is about 14.4 kDa static light scattering measurements yield a higher molecular mass. This may be caused by impurities and water or salt molecules bound to the protein surface. Further, the dipole moment of lysozyme is arbitrarily chosen to be 400 Debye instead of 180 Debye, a mean value found in the literature^{119,120}.

One should keep in mind that the dipole moment as well as the effective protein charge strongly depend on solution pH, ionic strength, and also the electrolyte type in solution. Further, the patchy charge distribution on the protein's surface reduces electrostatic repulsion¹²¹ and the overall charge of a protein fluctuates when another protein molecule approaches¹²². Both, the DLVO and the Bratko model, are based on spherically uniform charge distributions and do not account for fluctuations. Hence, strictly speaking, it is not feasible to set dipole moment and net protein charge to fixed values.

The pH dependence of the lysozyme net charge has been measured for KCl solutions at low ionic strength and modeled up to 2 M¹¹¹. The charges vary about ± 1 with respect to the ionic strength. This has already a marked influence on calculated B_2 and phase equilibria. Since there are no correlations for the lysozyme net charge in NaCl solutions, the data for KCl is used instead. The Hamaker constant is regressed to experimental B_2 data. The obtained value of $H = 7.575 k_B T$ is somewhat higher than the values predicted by Lifshitz theory¹²³. This discrepancy can be explained by the fact that the van der Waals term must compensate for any error introduced in the other terms, in this case the electrostatic contributions. As a consequence, the Hamaker constant is very sensitive to solution conditions such as pH and ionic strength. The dielectric constant of the solvent water is set to $\epsilon_r = 80$, which approximately corresponds to the value at 298.15 K.

While it is possible to achieve quantitative agreement between experimental B_2 and those calculated by means of a PMF approach, the models fail at the description of phase equilibria such as the experimentally observed meta-stable liquid-liquid demixing in protein solutions and the solubilities. Fig. 7.5 shows that second osmotic virial coefficients for lysozyme in NaCl solutions at pH 4.5 and 7, respectively, can be described quantitatively by both the DLVO and the Bratko model.

It surprises that the DLVO approach, albeit simpler, performs better than the Bratko

model at low ionic strength[‡].

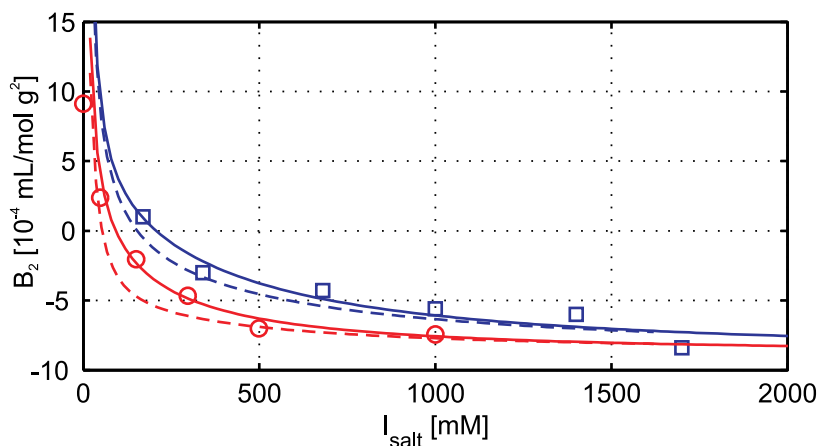


Fig. 7.5: The second osmotic virial coefficient of lysozyme in NaCl solutions at pH 7 (o) and pH 4.5 (□) vs. ionic strength. Calculations of phase equilibria with the DLVO model (—, —) and the Bratko model (---, ---).

Experimental data shows that the solubility of the tetragonal form of lysozyme decreases with increasing ionic strength due to enhanced screening of protein charges by salt ions. Further, as illustrated in Fig. 7.6, the solubility line lies above the meta-stable liquid-liquid region.

Using the same parameter set as for the description of B_2 , calculation of the liquid-liquid and liquid-solid transitions leads to phase boundary lines which lie about 50 K below the experimental values (see Fig. 7.6), indicating that the model net intermolecular potential is not attractive enough. Qualitative agreement is achieved concerning the dependency of the critical demixing temperature T_{crit} on ionic strength: a lower salt content leads to a decrease of T_{crit} . This can be explained by the higher repulsive Coulombic forces due to reduced screening at low ionic strength.

Both the DLVO and the Bratko model capture the correct trends, i. e. with increasing ionic strength the critical temperature rises and the solubility decreases. Including an osmotic potential as described in Sec. 4.5 has little effect on the B_2 value but shifts the critical temperature T_{crit} to even lower temperatures.

The B_2 provides a measure for the strength of intermolecular forces. Positive values of B_2 indicate net repulsive interactions while negative values reflect net attraction. Therefore, it appears self-evident to connect the B_2 value to the solubility of the protein. Investigating the crystallization behavior of several proteins at different solution conditions George and Wilson¹²⁴ found out that crystallization predominantly occurs in a narrow B_2 slot at negative values. For positive B_2 the net repulsion inhibits the formation of crystal seeds. Solution conditions resulting in a too negative B_2 , i. e. provoking strong intermolecular

[‡]DLVO and Bratko model yield almost indistinguishable results when the dipole moment is set to lower values, e. g. 180 Debye.

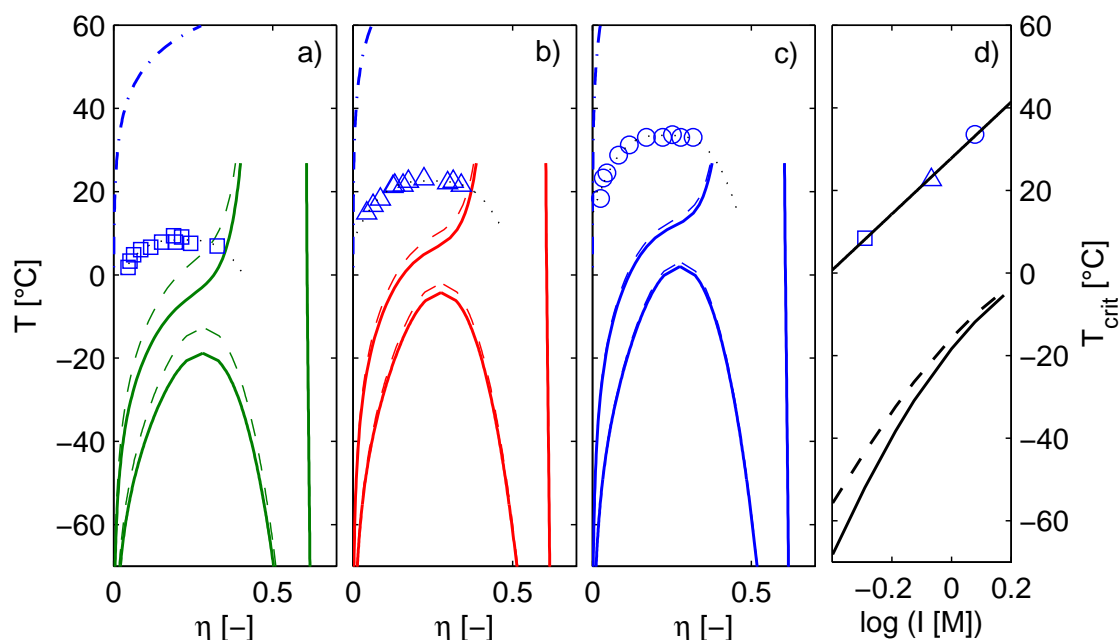


Fig. 7.6: Liquid-liquid and solid-liquid equilibrium of HEW lysozyme in NaCl solutions at pH 4.5 vs. reduced density at ionic strengths a) $I = 510$ mM (\square), b) $I = 860$ mM (\triangle), and c) $I = 1200$ mM (\circ). Experimental lysozyme solubilities for the tetragonal crystal form are regressed with the van't Hoff equation as described in Ref.¹¹⁰ (---). Experimental data for the LLE are taken from Ref.¹¹⁰ The dotted lines are to guide the reader's eye. d) Critical temperature T_{crit} vs. logarithm of ionic strength. Calculations with the DLVO model (continuous lines), Bratko model (dashed lines).

attraction, lead to amorphous agglomerates which may also remain insoluble. Quantitative relationships between B_2 and the solubility have been given e. g. by Haas et al.¹²⁵ or by Curtis et al.¹²⁶ Both groups propose a physically sound model based on statistical mechanics.

Chapter 8

Summary and Outlook

The main focus of this thesis lay in modeling thermodynamic properties of aqueous electrolyte solutions, aqueous amino acid or peptide solutions, and their combination, i. e. aqueous electrolyte/amino acid solutions. Therefore, as a first step, a thermodynamic model, the original PC-SAFT equation of state – developed for modeling non-polar, non-associating compounds – was enhanced by an electrostatic term in order to account for interactions emanating from the charged salt-ions. No additional parameters other than those already needed for the PC-SAFT model were introduced for the extension. Ion parameters fitted to experimental data show reasonable trends demonstrating the sound physical basis of the model. Solution densities, vapor pressures, and (mean ionic) activity coefficients (MIAC) in 25 electrolyte solutions calculated with the electrolyte PC-SAFT (ePC-SAFT) match experimental data very well as can be shown by overall low mean AARD values for each data set: 0.94%, 4.96%, and 10.81%, respectively. However, the performance of the model for some electrolyte systems (e. g. sulfates) still demands improvement. Therefore, effects like ion pairing and chemical equilibria between undissociated salt and respective ions have to be accounted for in the equation of state. By this it should be possible to model weak electrolytes such as acetates. Till now, the systems have been limited to the solvent water and mostly only one salt. Consequently, solvent mixtures as well as more mixed-salt solutions are predestined for future work. In addition to the already investigated properties density, vapor pressure, and MIAC solution enthalpies and the temperature-dependence of the activity coefficients should be addressed in order to check the limits of the ePC-SAFT model.

In a second step, thermodynamic properties of aqueous solutions of 14 amino acids and 5 peptides were modeled and compared to experimental data. Densities, vapor pressures, activity coefficients, and solubilities could be described with only one parameter set for each component obtaining excellent results. However, the temperature dependence of the activity coefficients is not captured quantitatively by the ePC-SAFT model. The overall good performance of the model encourages to extend the parameter estimation to more amino acids and peptides as well as to model mixed-solvent and mixed-solute systems.

It can be shown that for homo-oligopeptides most model parameters can be inherited from the monomeric unit, the respective amino acid. Only segment number and binary interac-

tion parameter have to be refitted in order to reproduce densities and activity coefficients. This approach is surely limited to small peptides. For longer chain lengths structure effects like chain folding, forming of intramolecular bonds, etc. will render modeling with an equation of state very difficult.

For ternary electrolyte/amino acid systems the influence of the amino acid on the ratio of MIAC can be described quantitatively by the model if a binary interaction parameter is introduced between amino acid and salt ions. This k_{ij} depends on salt molality. Unfortunately, with the same approach solubilities of amino acids and peptides in electrolyte solutions cannot even be described qualitatively for the investigated systems. Perhaps consideration of the zwitterionic form of the biomolecules may lead to better results in this case. Therefore, dipole-dipole and dipole-charge interactions have to be implemented in the ePC-SAFT model. In order to obtain a consistent description of the water/electrolyte/amino acid systems, water and amino acids have to be regarded as dipolar and all parameters have then to be refitted.

The ePC-SAFT approach was tested for its applicability to aqueous protein solutions. Here the model failed in the description of phase equilibria. Numerical investigation revealed that no physically meaningful pure-component parameters can be found in order to match experimental LLE data of aqueous protein solutions containing electrolytes. A chain model like the PC-SAFT approach appears to be unsuitable for proteins. Although they consist of long amino acid chains, the physical effects emanating from the tertiary structure cannot be captured properly. For example, some amino acid groups are buried inside the protein sphere and cannot interact with the solvent. This is difficult to consider in the equation of state.

For modeling protein systems, the best approach turned out to be one based on the potential of mean force (PMF). Protein parameters were adjusted to experimental second osmotic virial coefficients for two PMF models. Although varying in complexity the DLVO and the Bratko model gave very similar results. The influence of ionic strength on liquidus line and meta-stable LLE could be described qualitatively. However, due to the simplifying assumptions made in the PMF framework it cannot be expected to obtain quantitative agreement between experimental and modeled phase equilibria.

Bibliography

- [1] A. Kleemann, W. Leuchtenberger, B. Hoppe, and H. Tanner. *Ullmann's Encyclopedia of Industrial Chemistry, Vol. A2*, chapter Amino Acids, pages 57–97. VCH, 1985.
- [2] J. Groß and G. Sadowski. Perturbed-Chain SAFT: An equation of state based on a perturbation theory for chain molecules. *Ind. Eng. Chem. Res.*, 40:1244–1260, 2001.
- [3] G. Sadowski. *Thermodynamik der Polymerlösungen*. Shaker Verlag, Berlin, 2000.
- [4] M. P. Breil. *Thermodynamics, Experimental, and Modelling of Aqueous Electrolyte and Amino Acid Solutions*. PhD thesis, DTU, Lyngby, Denmark, 2001.
- [5] A. M. Soto-Campos, M. K. Khoskbarchi, and J. H. Vera. Activity coefficients of the electrolyte and the amino acid in water + NaNO₃ + glycine and water + NaCl + DL-methionine systems at 298.15. *Biophys. Chem.*, 67:97–105, 1997.
- [6] A. M. Soto-Campos, M. K. Khoshkbarchi, and J. H. Vera. Effect of the anion and the cation of an electrolyte on the activity coefficient of DL-alanine in aqueous solutions. *Fluid Phase Equilib.*, 142:193–204, 1998.
- [7] J. A. Barker and D. Henderson. Monte Carlo values for the radial distribution function of a system of fluid hard spheres. *Molec. Phys.*, 21(1):187–191, 1971.
- [8] J. K. Percus and G. J. Yevick. Analysis of classical statistical mechanics by means of collective coordinates. *Phys. Rev.*, 110(1):1–13, 1958.
- [9] R. W. Zwanzig. High-temperature equation of state by a perturbation method. I. Nonpolar gases. *J. Chem. Phys.*, 22(8):1420–1426, 1954.
- [10] R. W. Zwanzig. High-temperature equation of state by a perturbation method. II. Polar gases. *J. Chem. Phys.*, 23(10):1915–1922, 1955.
- [11] D. A. McQuarrie. *Statistical Mechanics*. University Science Books, Sausalito (CA), 2000.
- [12] J. A. Barker and D. Henderson. Perturbation theory and equation of state for fluids. I. The square-well potential. *J. Chem. Phys.*, 47(11):2856–2861, 1967.
- [13] J. A. Barker and D. Henderson. Perturbation theory and equation of state for fluids. II. A successful theory of liquids. *J. Chem. Phys.*, 47(11):4714–4721, 1967.

-
- [14] J. D. Weeks, D. Chandler, and H. C. Andersen. Role of repulsive forces in determining the equilibrium structure of simple liquids. *J. Chem. Phys.*, 54(12):5237–5247, 1971.
- [15] B. J. Alder, D. A. Young, and M. A. Mark. Studies in molecular dynamics. X. corrections to the augmented van der waals theory for the square well fluid. *J. Chem. Phys.*, 56:3013–3029, 1972.
- [16] S. S. Chen and A. Kreglewski. Applications of the augmented van der Waals theory of fluids. I. Pure fluids. *Ber. Bunsen. Ges.*, 81:1048–1052, 1977.
- [17] W. G. Chapman, G. Jackson, and K. E. Gubbins. Phase equilibria of associating fluids. Spherical molecules with multiple bonding sites. *Mol. Phys.*, 65(5):1057–1079, 1988.
- [18] G. Jackson, W. G. Chapman, and K. E. Gubbins. Phase equilibria of associating fluids. Spherical molecules with multiple bonding sites. *Mol. Phys.*, 65(1):1–31, 1988.
- [19] S. H. Huang and M. Radosz. Equation of state for small, large, polydisperse, and associating molecules. *Ind. Eng. Chem. Res.*, 29:2284–2294, 1990.
- [20] S. H. Huang and M. Radosz. Equation of state for small, large, polydisperse, and associating molecules: Extension to fluid mixtures. *Ind. Eng. Chem. Res.*, 30:1994–2005, 1991.
- [21] M. S. Wertheim. Fluids with highly directional attractive forces. I. Statistical thermodynamics. *J. Stat. Phys.*, 35:19–34, 1984.
- [22] M. S. Wertheim. Fluids with highly directional attractive forces. II. Thermodynamic perturbation theory and integral equations. *J. Stat. Phys.*, 35:35–47, 1984.
- [23] M. S. Wertheim. Fluids of dimerizing hard spheres, and fluid mixtures of hard spheres and dispheres. *J. Chem. Phys.*, 85(5):2929–2936, 1986.
- [24] M. S. Wertheim. Fluids with highly directional attractive forces. III. Multiple attraction sites. *J. Stat. Phys.*, 42:459–476, 1986.
- [25] M. S. Wertheim. Fluids with highly directional attractive forces. IV. Equilibrium polymerization. *J. Stat. Phys.*, 42:477–492, 1986.
- [26] M. S. Wertheim. Thermodynamic perturbation theory of polymerization. *J. Chem. Phys.*, 87(12):7323–7331, 1987.
- [27] J. Groß and G. Sadowski. Modeling polymer systems using the perturbed-chain statistical associating fluid theory equation of state. *Ind. Eng. Chem. Res.*, 41:1084–1093, 2002.
- [28] J. Groß and G. Sadowski. Application of the Perturbed-Chain SAFT equation of state to associating systems. *Ind. Eng. Chem. Res.*, 41:5510–5515, 2002.

- [29] T. Boublik. Hard-sphere equation of state. *J. Chem. Phys.*, 53:471–472, 1970.
- [30] G. A. Mansoori, N. F. Carnahan, K. E. Starling, and T. W. Leland Jr. . Equilibrium thermodynamic properties of the mixture of hard spheres. *J. Chem. Phys.*, 54(4):1523–1525, 1971.
- [31] J. Groß. *Entwicklung einer Zustandsgleichung für einfache, assoziierende und makromolekulare Stoffe*. VDI Verlag, Düsseldorf, 2001.
- [32] J. Gross, O. Spuhl, F. Tumakaka, and G. Sadowski. Modeling copolymer systems using the Perturbed-Chain SAFT equation of state. *Ind. Eng. Chem. Res.*, 42:1266–1274, 2003.
- [33] G. Navascúes, E. Velasco, and L. Mederos. Theories of phase behavior of colloidal suspensions. *Int. J. Modern Phys. B*, 18(2):143–169, 2004.
- [34] N. Asherie. Protein crystallization and phase diagrams. *Methods*, 34:266–272, 2004.
- [35] A. Jayaraman, R. C. Newton, and J. M. McDonough. Phase relations, resistivity, and electronic structure of cesium at high pressures. *Phys. Rev.*, 159(3):527–533, 1967.
- [36] W. G. McMillan and J. E. Mayer. The statistical thermodynamics of multicomponent systems. *J. Chem. Phys.*, 13(7):276–305, 1945.
- [37] T. L. Hill. Theory of Solutions. I. *J. Am. Chem. Soc.*, 79:4885–5890, 1957.
- [38] T. L. Hill. Theory of solutions. II. Osmotic pressure virial expansion and light scattering in two component solutions. *J. Chem. Phys.*, 30(1):93–97, 1959.
- [39] B. V. Derjaguin and L. D. Landau. *Acta Phys. Chim. USSR*, 14:633, 1941.
- [40] E. J. W. Verwey and J. T. G. Overbeek. *Theory of the Stability of Lyophobic Colloids*. Elsevier, New York, 1948.
- [41] D. E. Kühner, H. W. Blanch, and J. M. Prausnitz. Salt-induced protein precipitation: Phase equilibria from an equation of state. *Fluid Phase Equilib.*, 116:140–147, 1996.
- [42] J. N. Israelachvili. *Intermolecular and Surface Forces*. Academic Press Inc., London, 1994.
- [43] C. A. Haynes, K. Tamura, H. R. Körfer, H. W. Blanch, and J. M. Prausnitz. Thermodynamic properties of aqueous α -chymotrypsin solutions from membrane osmometry measurements. *J. Phys. Chem.*, 96(2):905–912, 1992.
- [44] M. Muschol and F. Rosenberger. Interactions in undersaturated and supersaturated lysozyme solutions: Static and dynamic light scattering results. *J. Chem. Phys.*, 103(24):10424–10432, 1995.

- [45] C. J. Coen, H. W. Blanch, and J. M. Prausnitz. Salting out of aqueous proteins: Phase equilibria and intermolecular potentials. *AIChE J.*, 41(4):996–1004, 1995.
- [46] S. Nir. Van der Waals interactions between surfaces of biological interest. *Prog. Surf. Sci.*, 8:1–58, 1977.
- [47] M. Farnum and C. Zukoski. Effect of glycerol on the interactions and solubility of bovine pancreatic trypsin inhibitor. *Biophys. J.*, 76:2716–2726, 1999.
- [48] I. Sogami and N. Ise. On the electrostatic interaction in macroionic solutions. *J. Chem. Phys.*, 81(12):6320–6332, 1984.
- [49] J. Wu, D. Bratko, and J. M. Prausnitz. Interaction between like-charged colloidal spheres in electrolyte solutions. *PNAS*, 95:15169–15172, 1998.
- [50] A. Striolo, D. Bratko, J. Z. Wu, N. Elvassore, H. W. Blanch, and J. M. Prausnitz. Forces between aqueous nonuniformly charged colloids from molecular simulation. *J. Chem. Phys.*, 116(17):7733–7743, 2002.
- [51] V. L. Vilker, C. K. Colton, and K. A. Smith. The osmotic pressure of concentrated protein solutions: Effect of concentration and pH in saline solutions of bovine serum albumin. *J. Col. Int. Sci.*, 79(2):548–566, 1981.
- [52] G. D. Phillies. Excess chemical potential of dilute solutions of spherical polyelectrolytes. *J. Chem. Phys.*, 60(7):2721–2731, 1974.
- [53] D. Bratko, A. Striolo, J. Z. Wu, H. W. Blanch, and J. M. Prausnitz. Orientation-averaged pair potentials between dipolar proteins or colloids. *J. Chem. Phys. B*, 106:2714–2720, 2002.
- [54] S. Asakura and F. Oosawa. Interaction between particles suspended in solutions of macromolecules. *Journal of Polymer Science*, 33:183–192, 1958.
- [55] R. A. Curtis, J. M. Prausnitz, and H. W. Blanch. Protein-protein and protein-salt interactions in aqueous protein solutions containing concentrated electrolytes. *Biotech. Bioeng.*, 57(1):11–21, 1998.
- [56] F. W. Tavares and J. M. Prausnitz. Analytic calculation of phase diagrams for solutions containing colloids or globular proteins. *Colloid Polym. Sci.*, 282:620–632, 2004.
- [57] N. F. Carnahan and K. E. Starling. Equation of state for nonattracting rigid spheres. *J. Chem. Phys.*, 51(2):635–636, 1969.
- [58] J. Chang and S. I. Sandler. A real function for the structure of the hard-sphere fluid. *Mol. Phys.*, 81(3):735–744, 1994.
- [59] E. Velasco, L. Mederos, and G. Navascués. Phase diagram of colloid systems. *Langmuir*, 14:5652–5655, 1998.

- [60] J. M. Kincaid and J.-J. Weis. Radial distribution function of a hard-sphere solid. *Molec. Phys.*, 34(4):931–938, 1977.
- [61] P. Debye and E. Hückel. Zur Theorie der Elektrolyte. *Phys. Z.*, 9:185–206, 1923.
- [62] C.-C. Chen, H. I. Britt, J. F. Boston, and L. B. Evans. Local composition model for excess gibbs energy of electrolyte systems. *AIChE J.*, 28:588–596, 1982.
- [63] C.-C. Chen and L. B. Evans. A local composition model for excess gibbs energy of aqueous electrolyte systems. *AIChE J.*, 32(3):444–454, 1986.
- [64] B. Mock, C.-C. Chen, and L. B. Evans. Thermodynamic representation of phase equilibria and mixed-solvent electrolyte systems. *AIChE J.*, 32:1655–1664, 1986.
- [65] C.-C. Chen, P. M. Mathias, and H. Orbey. Use of hydration and dissociation chemistries with the electrolyte-NRTL model. *AIChE J.*, 45(7):1576–1586, 1999.
- [66] F. Pérez-Villaseñor, G. Iglesias-Silva, and K. R. Hall. Prediction of osmotic and activity coefficients using a modified pitzer equation for multicomponent strong electrolyte systems at 298 K. *Ind. Eng. Chem. Res.*, 42:1087–1092, 2003.
- [67] X. Xu and E. A. Macedo. New modified wilson model for electrolyte solutions. *Ind. Eng. Chem. Res.*, 42:5702–5707, 2003.
- [68] W. Fürst and H. Renon. Representation of excess properties of electrolyte solutions using a new equation of state. *AIChE J.*, 39(2):335–343, 1993.
- [69] J. Wu and J. M. Prausnitz. Phase equilibria for systems containing hydrocarbons, water, and salt: An extended peng-robinson equation of state. *Ind. Eng. Chem. Res.*, 37(5):1634–1643, 1998.
- [70] J. A. Myers, S. I. Sandler, and R. H. Wood. An equation of state for electrolyte solutions covering wide ranges of temperature, pressure, and composition. *Ind. Eng. Chem. Res.*, 41:3282–3297, 2002.
- [71] A. Galindo, A. Gil-Villegas, G. Jackson, and A. N. Burgess. SAFT-VRE: Phase behaviour of electrolyte solutions with the statistical associating fluid theory for potentials of variable range. *J. Phys. Chem. B*, 103:10272–10281, 1999.
- [72] A. Gil-Villegas, A. Galindo, and G. Jackson. A statistical associating fluid theory for electrolyte solutions (SAFT-VRE). *Mol. Phys.*, 99(6):531–546, 2001.
- [73] A. Gil-Villegas, A. Galindo, P. J. Whitehead, S. J. Mills, G. Jackson, and A. N. Burgess. Statistical associating fluid theory for chain molecules with attractive potentials of variable range. *J. Chem. Phys.*, 106:4168–4186, 1997.
- [74] X. Ji, S. Tan, H. Adidharma, and M. Radosz. Statistical associating fluid theory coupled with restricted primitive model to represent aqueous strong electrolytes: Multiple-salt solutions. *Ind. Eng. Chem. Res.*, 44:7784–7590, 2005.

- [75] L. L. Lee. *Molecular Thermodynamics of Nonideal Fluids*. Butterworth Publishers, Stoneham (MA), USA, 1988.
- [76] Y. Qin and J. M. Prausnitz. Phase behavior and critical properties of size-asymmetric, primitive-model electrolytes. *J. Chem. Phys.*, 121(7):3181–3183, 2004.
- [77] C. Held. Thermodynamic modeling of aqueous solutions. Master’s thesis, University of Dortmund, Dortmund (Germany). Dept. of Biochemical and Chemical Engineering. Chair of Thermodynamics, 2007.
- [78] N. Seyfkar, C. Ghotbi, V. Taghikhani, and G. Azimi. Application of the non-primitive MSA-based models in predicting the activity and the osmotic coefficients of aqueous electrolyte solutions. *Fluid Phase Equilib.*, 221:189–196, 2004.
- [79] H. Zhao, M. C. dos Ramos, and C. McCabe. Development of an equation of state for electrolyte solutions by combining the statistical associating fluid theory and the mean spherical approximation for the nonprimitive model. *J. Chem. Phys.*, 126:244503, 2007.
- [80] M. K. Khoshkbarchi and J. H. Vera. A simplified perturbed hard-sphere model for the activity coefficients of amino acids and peptides in aqueous solutions. *Ind. Eng. Chem. Res.*, 35 (11):4319–4327, 1996.
- [81] H. Kuramochi, H. Noritomi, D. Hoshino, and K. Nagahama. Representation of activity coefficients of fundamental biochemicals in water by the UNIFAC model. *Fluid Phase Equilib.*, 130:117–132, 1997.
- [82] K. K. Nass. Representation of the solubility behavior of amino acids in water. *AIChE J.*, 34:1257–1266, 1988.
- [83] M. K. Khoshkbarchi and J. H. Vera. ERRATUM: A simplified perturbed hard-sphere model for the activity coefficients of amino acids and peptides in aqueous solutions. *Ind. Eng. Chem. Res.*, 41:6636, 1996.
- [84] M. K. Khoshkbarchi and J. H. Vera. A theoretically improved perturbation model for activity coefficients of amino acids and peptides in aqueous solutions. *Ind. Eng. Chem. Res.*, 37:3052–3057, 1998.
- [85] J.-C. Liu, J.-F. Lu, and Y.-G. Li. Study on the activity coefficients and the solubilities of amino acids in water by the perturbation theory. *Fluid Phase Equilib.*, 142:67–82, 1998.
- [86] D. Fuchs, J. Fischer, F. Tumakaka, and G. Sadowski. Solubility of amino acids: Influence of the pH-value and addition of alcoholic cosolvents on aqueous solubility. *Ind. Eng. Chem. Res.*, 45:6578–6584, 2006.
- [87] The Mathworks. *Optimization Toolbox-For Use with MATLAB*. The MathWorks Inc., Natick (MA), USA, 2004.

- [88] *VDI-Wärmeatlas*. VDI-Gesellschaft Verfahrenstechnik und Chemieingenieurwesen (GVC), Düsseldorf, Germany, 1994.
- [89] C. J. Parisod and E. Plattner. Vapor-liquid equilibria of the $\text{NaCl-H}_2\text{O}$ system in the temperature range 300–440 °C. *J. Chem. Eng. Data*, 26:16–20, 1981.
- [90] W. B. Floriano and M. A. C. Nascimento. Dielectric constant and density of water as a function of pressure at constant temperature. *Braz. J. Phys.*, 34(1):38–41, 2004.
- [91] L. F. Cameretti, G. Sadowski, and J. M. Mollerup. Modeling of aqueous electrolyte solutions with perturbed-chain statistical associated fluid theory. *Ind. Eng. Chem. Res.*, 44:3355–3362, 2005.
- [92] L. F. Cameretti, G. Sadowski, and J. M. Mollerup. ERRATUM: Modeling of aqueous electrolyte solutions with perturbed-chain statistical associated fluid theory. *Ind. Eng. Chem. Res.*, 44:8944, 2005.
- [93] R. A. Robinson and H. S. Harned. Some aspects of the thermodynamics of strong electrolytes from electromotive force and vapor pressure measurements. *Chem. Rev.*, 28(3):419–476, 1941.
- [94] A. L. Horvath. *Handbook of Aqueous Electrolyte Solutions*. Ellis Horwood, Chichester, England, 1985.
- [95] Y. Marcus. *Ion Properties*. Marcel Dekker Inc., New York, 1997.
- [96] R. A. Robinson and R. H. Stokes. *Electrolyte Solutions: Second Revised Edition*. Dover Publications Inc., 2002.
- [97] R. Buchner, G. T. Hefter, and J. Barthel. Dielectric relaxation of aqueous NaF and KF solutions. *J. Chem. Soc. Faraday Trans.*, 90(17):2475–2479, 1994.
- [98] H. Hsu, Y. Wu, and L. Lee. Vapor pressures of aqueous solutions with mixed salts of NaCl-KBr and NaBr-kl. *J. Chem. Eng. Data*, 48:514–518, 2003.
- [99] H. J. Svec and D. D. Clyde. Vapor pressures of some α -amino acids. *J. Chem. Eng. Data*, 10(2):151–152, 1965.
- [100] L. F. Cameretti and G. Sadowski. Modeling of aqueous amino acid and polypeptide solutions with PC-SAFT. *Chem. Eng. Process.*, in press (available online), 2007.
- [101] M. J. Locke and R. T. McIver, Jr. Effect of solvation on the Acid/Base properties of glycine. *J. Am. Chem. Soc.*, 105:4226–4232, 1982.
- [102] C. M. Romero and M. E. González. Osmotic and activity coefficients of glycine, DL- α -alanine and DL- α -aminobutyric acid in aqueous solutions at temperatures between 288.15 and 303.15 K. *Fluid Phase Equilib.*, 250:99–104, 2006.

- [103] R. A. Robinson. The vapor pressure of aqueous solutions of alanine. *J. Biol. Chem.*, 199:71–73, 1952.
- [104] A. Khavaninzadeh, H. Modarress, V. Taghikhani, and M. K. Khoshkbarchi. Activity coefficients of electrolyte and amino acid in the systems (water + potassium chloride + DL-valine) at $T = 298.15$ K and (water + sodium chloride + L-valine) at $T = 308.15$ K. *J. Chem. Thermodynamics*, 34:1297–1309, 2002.
- [105] M. K. Khoshkbarchi and J. H. Vera. Measurement of activity coefficients of amino acids in aqueous electrolyte solutions: Experimental data for the systems $H_2O + NaCl + glycine$ and $H_2O + NaCl + DL\text{-alanine}$ at $25^\circ C$. *Ind. Eng. Chem. Res.*, 35(11):4755–4766, 1996.
- [106] M. K. Khoshkbarchi and J. H. Vera. A perturbed hard-sphere model with mean spherical approximation for the activity coefficients of amino acids in aqueous electrolyte solutions. *Ind. Eng. Chem. Res.*, 35(12):4755–4766, 1996.
- [107] C. Gao. Activity coefficients of glycine, DL-serine and DL-valine in aqueous solutions containing nitrates at 298.15 K. Master’s thesis, Dept. Chem. Eng., McGill University, Montreal, Canada, 2000.
- [108] S. Shimizu and W. McLaren. The Hofmeister series and protein-salt interactions. *J. Chem. Phys.*, 124:234905, 2006.
- [109] A. A. Pradhan and J. H. Vera. Effect of anions on the solubility of zwitterionic amino acids. *J. Chem. Eng. Data*, 45:140–143, 2002.
- [110] M. Muschol and F. Rosenberger. Liquid-liquid phase separation in supersaturated lysozyme solutions and associated precipitate formation/crystallization. *J. Chem. Phys.*, 107(6):1953–1962, 1997.
- [111] D. E. Kuehner, J. Engmann, F. Fergg, M. Wernick, H. W. Blanch, and J. M. Prausnitz. Lysozyme net charge and ion binding in concentrated aqueous electrolyte solutions. *J. Phys. Chem. B*, 103(8):1368–1374, 1999.
- [112] R. A. Curtis, C. Steinbrecher, M. Heinemann, H. W. Blanch, and J. M. Prausnitz. Hydrophobic forces between protein molecules in aqueous solutions of concentrated electrolyte. *Biophys. Chem.*, 98:249–265, 2002.
- [113] R. A. Curtis, J. Ulrich, A. Montaser, J. M. Prausnitz, and H. W. Blanch. Hofmeister-series effects protein-protein interactions in concentrated electrolyte solutions. *Biotech. Bioeng.*, 79(4):367–380, 2002.
- [114] Y. U. Moon, C. O. Anderson And. H. W. Blanch, and J. M. Prausnitz. Osmotic pressures and second virial coefficients for aqueous saline solutions of lysozyme. *Fluid Phase Equilib.*, 168:229–239, 2000.

- [115] J. Wu and J. M. Prausnitz. Osmotic pressures of aqueous bovine serum albumin solutions at high ionic strength. *Fluid Phase Equilib.*, 155:139–154, 1999.
- [116] D. F. Rosenbaum, A. Kulkarni, S. Ramakrishnan, and C. F. Zukoski. Protein interactions and phase behavior: Sensitivity to the form of the pair potential. *J. Chem. Phys.*, 111(21):9882–9890, 1999.
- [117] F. W. Tavares, D. Bratko, H. W. Blanch, and J. M. Prausnitz. Ion-specific effects in the colloid-colloid or protein-protein potential of mean force: Role of salt-macroion van der waals interactions. *J. Phys. Chem. B*, 108:9228–9235, 2004.
- [118] M. Boström, F. W. Tavares, B. W. Ninham, and J. M. Prausnitz. Effect of salt identity on the phase diagram for a globular protein in aqueous electrolyte solution. *J. Phys. Chem. B*, 110:24757–24760, 2006.
- [119] J. Antosiewicz. Computation of the dipole moments of proteins. *Biophys. J.*, 69:1344–1354, 1995.
- [120] S. Takashima. Electric dipole moments of globular proteins: Measurement and calculation with NMR and x-ray databases. *J. Non-Cryst. Solids*, 305:303–310, 2002.
- [121] M. L. Grant. Nonuniform charge effects in protein-protein interactions. *J. Phys. Chem. B*, 105:2858–2863, 2001.
- [122] M. Lund, T. Åkenson, and B. Jönsson. Enhanced protein adsorption due to charge regulation. *Langmuir*, 21:8385–8388, 2005.
- [123] B. W. Ninham and V. Yaminsky. Ion binding and ion specificity: The Hofmeister effect and onsager and lifshitz theories. *Langmuir*, 13:2097–2108, 1997.
- [124] A. George and W. W. Wilson. Predicting protein crystallization from a dilute solution property. *Acta Cryst.*, D50:361–365, 1994.
- [125] C. Haas, J. Drenth, and W. W. Wilson. Relation between the solubility of proteins in aqueous solutions and the second virial coefficient of the solution. *J. Phys. Chem. B*, 103(14):2808–2811, 1999.
- [126] R. A. Curtis, H. W. Blanch, and J. M. Prausnitz. Calculation of phase diagrams for aqueous protein solutions. *J. Phys. Chem. B*, 105(12):2445–2452, 2001.
- [127] Landolt-Börnstein. *Numerical Data and Functional Relationships in Science and Technology, New Series, Group IV, Volume 1b*. Springer-Verlag, Berlin, 1977.
- [128] V. M. M. Lobo and J. L. Quaresma. *Handbook of Electrolyte Solutions, Parts A and B*. Elsevier, Amsterdam, 1989.
- [129] K. R. Patil, A. D. Tripathi, G. Pathak, and S. S. Katti. Thermodynamic properties of aqueous electrolyte solutions. 1. Vapor pressures of aqueous solutions of LiCl, LiBr, and LiI. *J. Chem. Eng. Data*, 35:166–168, 1990.

- [130] A. Apelblat and E. Korin. The vapor pressures of saturated aqueous solutions of sodium chloride, sodium bromide, sodium nitrate, sodium nitrite, potassium iodate, and rubidium chloride at temperatures from 227 K to 323 K. *J. Chem. Therm.*, 30:59–71, 1998.
- [131] K. R. Patil, A. D. Tripathi, G. Pathak, and S. S. Katti. Thermodynamic properties of aqueous electrolyte solutions. 2. Vapor pressures of aqueous solutions of NaBr, NaI, KCl, KBr, KI, RbCl, CsCl, CsBr, MgCl₂, CaCl₂, CaI₂, SrCl₂, SrBr₂, SrI₂, BaCl₂, and BaBr₂. *J. Chem. Eng. Data*, 36:225–230, 1991.
- [132] L. Ninni and A. J. A. Meirelles. Water activity, pH and density of aqueous amino acids solutions. *Biotechnol. Prog.*, 17:703–711, 2001.
- [133] H. Kuramochi, H. Noritomi, D. Hoshino, and K. Nagahama. Measurements of vapor pressures of aqueous amino acid solutions and determination of activity coefficients of amino acids. *J. Chem. Eng. Data*, 42:470–474, 1997.
- [134] G. C. Barrett and T. H. Lilley. *Chemistry and Biochemistry of the Amino Acids*, chapter Physical Properties of Amino Acid Solutions, pages 591–624. Chapman and Hall, 1985.
- [135] H.A. Sober. *Handbook of Biochemistry: Selected Data for Molecular Biology*. CRC Press, Cleveland, Ohio, 1973.
- [136] J. B. Dalton and C. Schmidt. The solubilities of certain amino acids in water, the densities of their solutions at twenty-five degrees, and the calculated heats of solutions and partial molal volumes. *J. Biol. Chem.*, pages 549–578, 1933.
- [137] Z. Yan, J. Wang, W. Liu, and J. Lu. Apparent molar volumes and viscosity *b*-coefficients of some α -amino acids in aqueous solutions from 278.15 to 308.15 K. *Thermochim. Acta*, 334:17–27, 1999.
- [138] M. Kikuchi, M. Sakurai, and K. Nitta. Partial molar volumes and adiabatic compressibilities of amino acids in dilute aqueous solutions at 5, 15, 25, 35, and 45°C. *J. Chem. Eng. Data*, 40:935–942, 1995.
- [139] J. P. Amend and H. C. Helgeson. Solubilities of the common L- α -amino acids as a function of temperature and solution pH. *Pure & Appl. Chem.*, 69(5):935–942, 1997.
- [140] J.-L. Shen, Z.F. Li, B.H. Wang, and Y.-M. Zhang. Partial molar volumes of some amino acids and a peptide in water, DMSO, NaCl and DMSO/NaCl aqueous solutions. *J. Chem. Thermodynamics*, 32:805–819, 2000.
- [141] D. Sapoundjiev, H. Lorenz, and A. Seidel-Morgenstern. Solubility of chiral threonine species in water/ethanol mixtures. *J. Chem. Eng. Data*, 51(5):1562–1566, 2006.

- [142] C. Jolicoeur, B. Riedl, D. Desrochers, L. L. Lemelin, R. Zamojska, and O. Enea. Solvation of amino acid residues in water and urea-water mixtures: Volumes and heat capacities of 20 amino acids in water and in 8 molar urea at 25 °C. *J. Sol. Chem.*, 15(2):109–128, 1986.
- [143] O. D. Bonner. Osmotic and activity coefficients of some amino acids and their hydrochloride salts at 298.15 K. *J. Chem. Eng. Data*, 27:422–423, 1982.
- [144] E. N. Tsurko, R. Neueder, and W. Kunz. Water activity and osmotic coefficients in solutions of glycine, glutamic acid, histidine and their salts at 298.15 K and 310.15 K. *J. Sol. Chem.*, 36:651–672, 2007.
- [145] L. S. Mason. The solubilities of four amino butyric acids and the densities of aqueous solutions of the acids at 25°. *J. Am. Chem. Soc.*, 69(12):3000–3002, 1947.
- [146] E. R. B. Smith and P. K. Smith. Thermodynamic properties of solutions of amino acids and related substances IV. The effect of increasing dipolar distance on the activities of aliphatic amino acids in aqueous solution at twenty-five degrees. *J. Biol. Chem.*, 132:47–56, 1940.
- [147] A. K. Mishra and J. C. Ahluwalia. Apparent molal volumes of amino acids, n-acetylamino acids, and peptides in aqueous solutions. *J. Phys. Chem.*, 88:86–92, 1984.
- [148] E. J. Cohn and J. T. Edsall. *Proteins, Amino Acids and Peptides as Ions and Dipolar Ions*. Reinhold Publ. Corp., New York, 1943.
- [149] A. Bonincontro, C. Cametti, and B. Sesta. Density, viscosity and dielectric constant of aqueous solutions of triglycine and tetraglycine. *Z. Naturforsch.*, 33a:462–467, 1978.
- [150] S. H. Dyke, G. R. Hedwig, and I. D. Watson. Relative partial molar enthalpies and apparent molar volumes of dipeptides in aqueous solution. *J. Sol. Chem.*, 10(5):321–331, 1981.
- [151] A. W. Hakin, H. Hoiland, and G. R. Hedwig. Volumetric properties of some oligopeptides in aqueous solution: Partial molar expansibilities and isothermal compressibilities at 298.15 K for the peptides of sequence ala(gly)_n, n = 1–4. *Phys. Chem. Chem. Phys.*, 2:4850–4857, 2000.
- [152] M. K. Khoskbarchi and J. H. Vera. Effect of NaCl and KCl on the solubility of amino acids in aqueous solutions at 298.2 K: Measurements and modeling. *Ind. Eng. Chem. Res.*, 36(6):2445–2451, 1997.
- [153] M. Kamali-Ardakani, A. Modarress, V. Taghikhani, and M. Khoskbarchi. Activity coefficients of glycine in aqueous electrolyte solutions: Experimental data for (H₂O + KCl + glycine) at t=298.15 K and (H₂O+NaCl+Glycine) at T=308.15 K. *J. Chem. Therm.*, 33:821–836, 2001.

- [154] A. Khavaninzadeh, H. Modarress, V. Taghikhani, and M. Khoshkbarchi. Measurement of activity coefficients of amino acids in aqueous electrolyte solutions: Experimental data for the systems ($\text{H}_2\text{O} + \text{NaBr} + \text{glycine}$) and ($\text{H}_2\text{O} + \text{NaBr} + \text{L-valine}$) at $T = 298.15$ K. *J. Chem. Therm.*, 35:1553–1565, 2003.
- [155] Y. Chung and J. Vera. Activity coefficients of the peptide and the electrolyte in ternary system water + glycylglycine + NaCl, + NaBr, + KCl, and + KBr at 298.2 K. *Biophysical Chemistry*, 92:77–88, 2001.

Appendix

Appendix A

Symbols and Abbreviations

Latin Symbols

symbol	unit	meaning
A	[J]	Helmholtz free energy
a	[–]	dimensionless Helmholtz energy
a_i	[–]	activity of component i
B_2	[$10^{-4}mL/molg^2$]	second osmotic virial coefficient
B_2^*	[–]	second virial coefficient
$c(r)$	[–]	direct correlation function
c_i	[$1/m^3$]	number concentration of i
d_i	[m]	temperature dependent segment diameter
$f(r)$	[–]	Mayer f -function
f_i	[Pa]	fugacity of component i
G	[J]	Gibbs free enthalpy
$g(r)$	[–]	radial distribution function
g_{ij}^{hs}	[–]	hard-sphere radial distribution function between i and j
H	[J]	enthalpy
$h(r)$	[–]	correlation function
Ha	[J]	Hamaker constant
I	[mol/L]	ionic strength
k	[$1/m$]	screening length of Yukawa potential
k_{ij}	[–]	binary (dispersion) interaction parameter between i and j
$m_{seg,i}$	[–]	segment number
\bar{m}_{seg}	[–]	mean segment number of mixture
m_i	[mol/kg]	molality (mol solute i / kg solvent)
M_i	[g/mol]	molecular weight
N	[–]	total particle number

symbol	unit	meaning
N	[-]	total number of association sites
N^{A_i}	[-]	number of sites of type A on i
n_i	[-]	number of particles of type i
P	[Pa]	pressure
Poy	[-]	Poynting factor
Q	[-]	partition function
q	[C]	charge
r	[-]	interparticle distance
S	[J/K]	entropy
T	[K]	temperature
$t_{1..4}$	[$\text{\AA}, 1/K$]	parameters for the temperature-dependent segment diameter of water
U	[J]	internal energy
$u(r)$	[J]	intermolecular potential between two particles at distance r
V	[m^3]	volume
v	[m^3]	specific volume (based on particle number)
$w(r)$	[J]	potential of mean force between two particles at distance r
X^{A_i}	[-]	fraction of molecules i not bonded at site A
x_i	[-]	mole fraction of component i
$y(r)$	[-]	distribution function, see Sec. 3.1
Z	[-]	compressibility factor
z	[-]	charge number

Greek Symbols

symbol	unit	meaning
β	[$1/J$]	$\beta = 1/k_B T$
χ_k	[-]	abbreviation for the Debye-Hückel term
δ	[\AA]	Stern-layer thickness
ε	[J]	dispersion energy
ε	[C/Vm]	$\varepsilon = \varepsilon_0 \cdot \varepsilon_r$
ε	[J]	potential depth of the Yukawa potential
$\varepsilon^{A_i B_j}$	[J]	association energy between site A on i and site B on j
ε_r	[-]	relative permittivity
η	[-]	reduced density
γ	[-]	activity coefficient ([kg/mol] molality scale)

symbol	unit	meaning
κ	[1/m]	inverse Debye length
$\kappa^{A_i B_j}$	[-]	dimensionless association volume between site A on i and site B on j
Λ	[m]	de Broglie wavelength
μ	[J]	chemical potential
μ	[Cm]	dipole moment
ν	[-]	stoichiometric coefficient
ω_1, ω_2	[J]	Barker-Henderson Theory integrals of 1 st and 2 nd order
φ	[-]	fugacity coefficient
Φ	[-]	configuration integral
Φ	[V]	electric potential
Π	[Pa]	osmotic pressure
ρ	[kg/m ³]	density
ρ_N	[1/m ³]	number density
σ	[m, Å]	diameter
σ^*	[m]	temperature-dependent segment diameter of water
σ_k	[-]	abbreviation for the Debye-Hückel term
σ_{ij}	[m]	arithmetic mean of segment diameters of i and j
$\xi(r)$	[-]	screening parameter
ζ_i	[m ⁱ]	moments of the segment diameter

Indices

index	meaning
∞	infinite dilution
μ - μ	dipole-dipole
\pm	mean ionic
\sim	unsymmetrical scaling of γ
' , "	phase ' , "
- , an	anion
+ , cat	cation
0i	pure component
A	amino acid, peptide
assoc	association
bin	binary system
CS	Carnahan-Starling
disp	dispersion

index	meaning
elec	electrostatic
fcc	face-centered-cubic lattice
hc	hard chain
hs	hard sphere
hydr	hydration
i,j,k	component in mixture
id	ideal
L	liquid phase
LJ	Lennard-Jones
LV	liquid-vapor transition
m	molality scale
osmo	osmotic
q- μ	charge-dipole
q-q	charge-charge
ref	reference
res	residual
S	solid phase, salt (m_S : salt molality)
seg	segment
SL	solid-liquid transition
ss	sticky sphere
sw	square-well
ter	ternary system
Tr	triple point
V	vapor phase
W	water
x	mole fraction scale
Yuk	Yukawa

Constants

constant	value	unit	meaning
ε_0	$8.854187817 \cdot 10^{-12}$	$[C/Vm]$	dielectric constant of vacuum
τ	$\pi\sqrt{2}/12$	$[-]$	packing fraction at closest packing
h	$6.6260755 \cdot 10^{-34}$	$[Js]$	Planck's constant
k_B	$1.380658 \cdot 10^{-23}$	$[J/K]$	Boltzmann factor
N_A	$6.0221367 \cdot 10^{23}$	$[1/mol]$	Avogadro number
R_G	$8.314(= k_B \cdot N_A)$	$[J/molK]$	ideal gas constant

Acronyms

acronym	meaning
AAD	absolute average deviation
AARD	absolute average relative deviation
ABA	aminobutyric acid
AVA	aminovaleric acid
DH	Debye-Hückel theory of electrolyte solutions
DLVO	Derjaguin-Landau-Vervey-Overbeek theory
EOS	equation of state
ePC-SAFT	Electrolyte Perturbed-Chain Statistical Association Theory
HEW	hen-egg white (lysozyme)
MIAC	mean ionic activity coefficient γ_{\pm}
MSA	mean spherical approximation
PC-SAFT	Perturbed-Chain Statistical Association Theory
PM	primitive model
PMF	potential of mean force
PREOS	Peng-Robinson equation of state
RPM	restricted primitive model
SI	Sogami-Ise theory
TPT1	Thermodynamic Perturbation Theory, 1 st order

Appendix B

Electrolytes

Tab. B.1: ePC-SAFT ion parameters. The segment number is set to unity.

ion	molar mass M [g/mol]	diameter σ_j [Å]	disp. energy ϵ_j [1/K]	valence z_j [-]
Li ⁺	6.94	1.8177	2697.280	+1
Na ⁺	22.99	2.4122	646.050	+1
K ⁺	39.10	2.9698	271.052	+1
NH ₄ ⁺	18.04	3.6824	176.393	+1
Mg ²⁺	24.30	2.3229	8145.330	+2
Ca ²⁺	40.08	2.8889	2146.979	+2
F ⁻	19.00	1.6132	648.313	-1
Cl ⁻	35.45	3.0575	47.288	-1
Br ⁻	79.90	3.4573	60.222	-1
I ⁻	126.90	3.9319	80.435	-1
OH ⁻	17.01	1.6401	2444.756	-1
NO ₃ ⁻	62.00	3.2284	0.000	-1
SO ₄ ²⁻	96.06	2.5465	0.000	-2

Absolute Average Deviation (AAD) and Absolute Average Relative Deviation (AARD) are calculated as follows:

$$AAD = \frac{1}{N} \sum_{k=1}^N \left| y_k^{\text{calc}} - y_k^{\text{exp}} \right| \quad AARD = \frac{100}{N} \sum_{k=1}^N \left| 1 - \frac{y_k^{\text{calc}}}{y_k^{\text{exp}}} \right|$$

Tab. B.2: Absolute and relative average deviations for densities, vapor pressures and MIAC of electrolytes.

electrolyte	density			vapor pressure			MIAC			
	N	m_{max} [mol/kg]	AARD [%]	N	m_{max} [mol/kg]	AARD [%]	N	m_{max} [mol/kg]	AARD [%]	AAD [-]
LiCl	18	15.73	1.83	13	12.69	5.87	14	5.00	9.49	0.13
NaCl	18	5.82	0.74	6	6.22	0.77	18	3.50	8.05	0.05
KCl	17	3.93	0.49	8	4.29	1.13	14	5.00	14.82	0.08
MgCl ₂	18	5.66	1.69	40	4.80	1.90	20	4.50	11.08	0.19
CaCl ₂	19	7.37	2.79	40	7.89	12.52	7	0.08	5.78	0.04
NH ₄ Cl	9	6.23	0.97	14	5.32	0.62	22	7.00	0.95	0.01
LiBr	18	7.68	0.86	45	15.97	30.27	20	4.50	3.52	0.04
NaBr	18	6.48	1.03	14	7.98	1.38	12	4.00	6.65	0.05
KBr	18	5.60	0.56	35	4.35	0.68	7	1.10	2.03	0.01
MgBr ₂	20	4.44	0.89	11.60	4.60	6.25	20	4.50	13.43	0.35
CaBr ₂	22	5.00	2.06	28.62	4.60	6.25	22	3.50	18.31	0.24
NaI	18	4.45	0.52	6.55	8.40	2.90	19	4.50	1.37	0.01
KI	18	4.02	0.16	1.94	5.65	1.26	20	4.50	1.44	0.01
MgI ₂	18	2.40	0.76	9.96	2.92	3.66	20	4.50	47.18	3.29
CaI ₂	18	2.27	1.36	17.73	2.92	3.66	15	2.00	10.15	0.09
NaF	18	0.93	0.24	2.44	2.90	3.66	17	1.00	2.38	0.02
KF	18	8.59	0.43	4.83	2.90	3.66	17	5.00	3.26	0.02
LiF	15	0.04	0.01	0.06	2.90	3.66	17	1.00	3.76	0.02
LiOH	15	3.79	0.20	2.17	4.77	0.91	4	1.20	15.36	0.11
NaOH	15	10.88	0.44	5.07	8.42	10.37	22	17.00	15.33	1.25
KOH	15	15.51	0.70	9.44	8.42	10.37	7	4.00	5.87	0.06
Li ₂ SO ₄	6	3.03	2.23	26.26	2.99	2.70	20	3.17	20.29	0.06
Na ₂ SO ₄	6	2.35	0.41	4.86	3.18	3.12	23	4.25	32.63	0.05
K ₂ SO ₄	5	0.64	0.08	0.86	0.97	0.39	13	0.69	1.61	0.01
(NH ₄) ₂ SO ₄	19	7.57	2.16	26.59	6.01	2.49	17	1.10	15.59	0.04
average			0.94	11.65		4.69		0.43	10.81	0.25

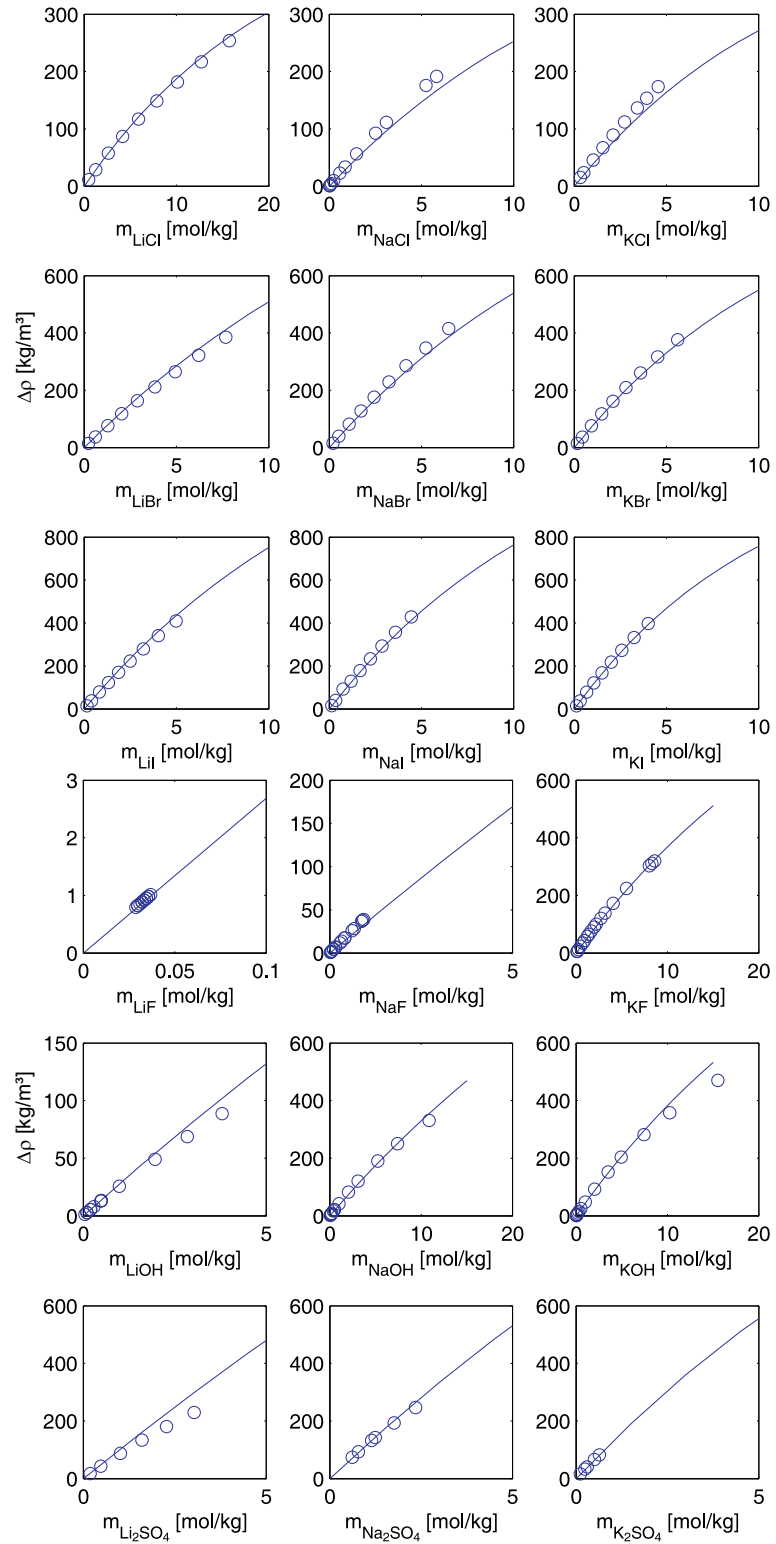


Fig. B.1: Densities ($\Delta\rho = \rho_{\text{solution}} - \rho_{\text{water}}$) of 18 alkali salt solutions at 293.15 K (298.15 K for the fluorides). Experimental data taken from Refs.^{127,128} Lines are calculated with the ePC-SAFT model.

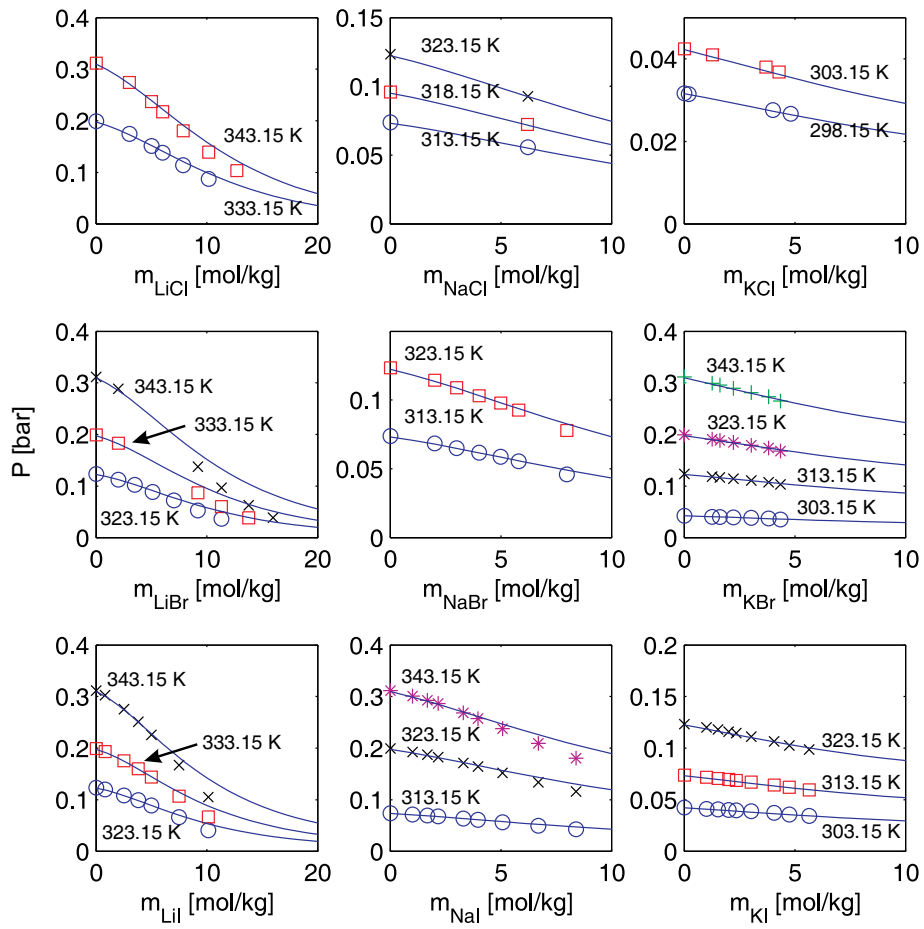


Fig. B.2: Vapor pressures of 9 alkali halide solutions at different temperatures (298.15-343.15 K). Experimental data taken from Refs. ¹²⁹⁻¹³¹ Lines are calculated with the ePC-SAFT model.

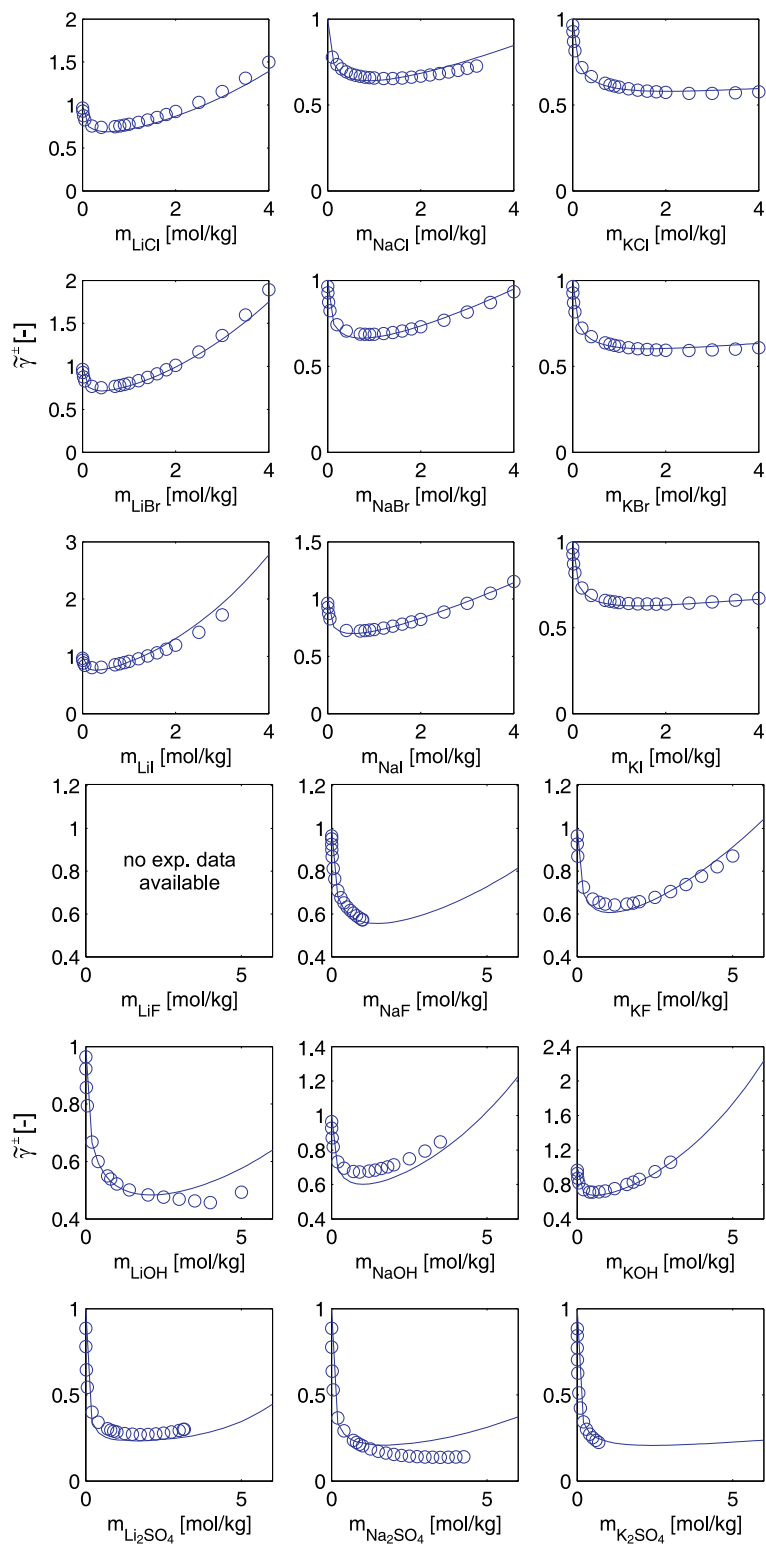


Fig. B.3: MIAC of 18 alkali salt solutions at 298.15 K. Experimental data taken from Ref. ¹²⁸ Lines are calculated with the ePC-SAFT model.

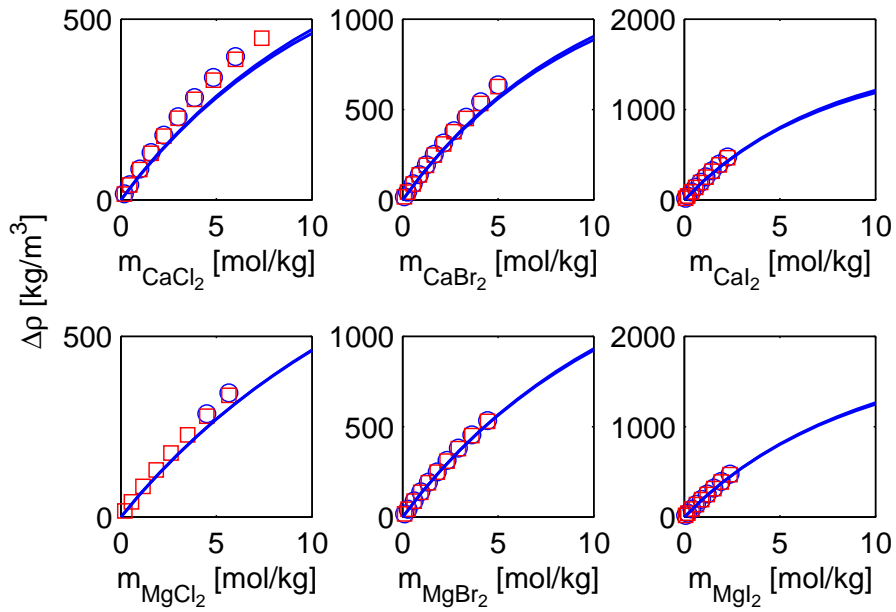


Fig. B.4: Densities of 6 earth alkali halide solutions at 293.15 K (o) and 313.15 K (□). Experimental data taken from Ref. ¹²⁷ Lines are calculated with the ePC-SAFT model.

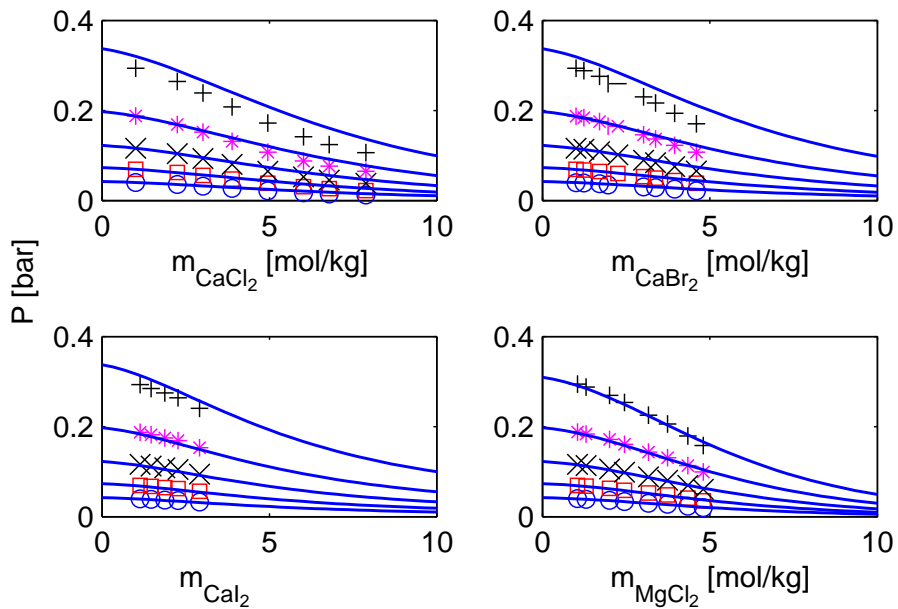


Fig. B.5: Vapor pressures of 4 earth alkali halide solutions at different temperatures (from bottom to top: 303.15, 313.15, 323.15, 333.15, 343.15 K). Experimental data taken from Ref. ¹³¹ Lines are calculated with the ePC-SAFT model.

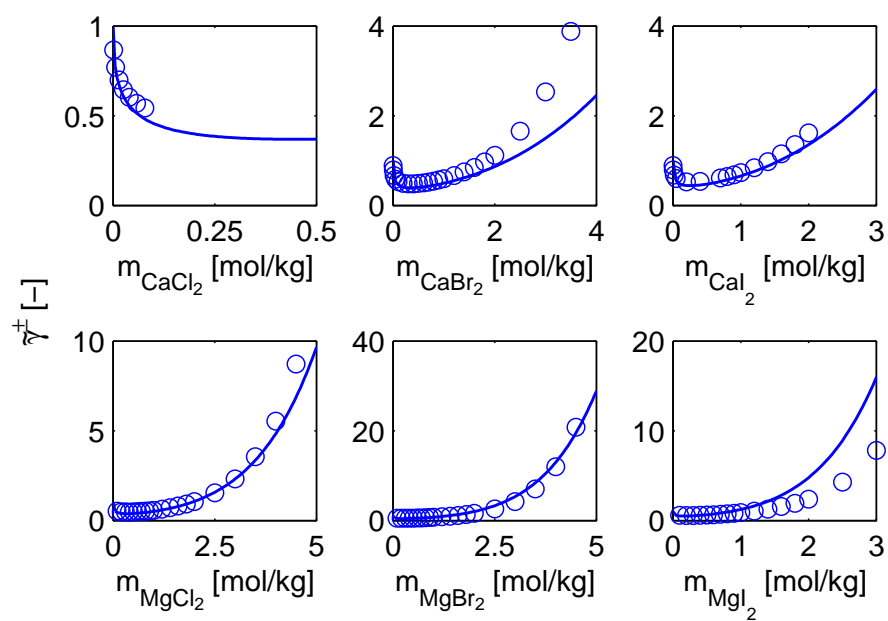


Fig. B.6: MIAC of 6 earth alkali halide solutions at 298.15 K. Experimental data taken from Ref.¹²⁸ Lines are calculated with the ePC-SAFT model.

Appendix C

Amino Acids and Peptides

Tab. C.1: Amino acids considered in this thesis, their chiral type, and references for experimental data. *Densities calculated from apparent partial molal volumes. ^[pc] Personal communication with Ms. Elena Tsurko from University of Regensburg.

amino acid	ρ	ΔP	$\tilde{\gamma}_A$	m_S
glycine	132	133	134	135
alanine	DL ¹³²	L ¹³³	DL ¹⁰³	DL ¹³⁶
serine	L ¹³⁷	L ¹³³	L ¹³³	DL,L ¹³⁵
proline	L ¹³⁸	L ¹³²	DL ¹³⁴	L ¹³⁵
valine	L ¹³⁸	L ¹³³	L ¹³³	L ¹³⁹
threonine	DL ¹⁴⁰	-	DL ¹³⁴	DL ¹⁴¹ , L ¹³⁹
lysine	L ¹⁴²	L ¹⁴³	L ¹⁴³	L ¹³⁹
histidine	DL ¹⁴⁰	L ^[pc]	L ¹⁴⁴	L ¹³⁹
arginine	L ¹³²	L ¹⁴³	L ¹⁴³	L ¹³⁹
α -ABA	DL ¹⁴⁵	-	DL ^{102,134}	-
β -ABA	DL ¹⁴⁵	-	DL ¹³⁴	-
γ -ABA	DL ¹⁴⁵	-	DL ¹⁴⁶	-
α -AVA	DL ^{147*}	-	DL ¹³⁴	-
γ -AVA	DL ^{148*}	-	DL ¹³⁴	-
diglycine	140	-	134	own data
triglycine	149	-	134	-
dialanine	DL ¹⁵⁰	-	DL ¹³⁴	-
Gly-Ala	L ¹⁵⁰	-	DL ¹³⁴	-
Ala-Gly	DL ¹⁵¹	-	DL ¹³⁴	-

Experimental and modeled densities, vapor pressure depressions, activity coefficients, and solubilities of amino acids and peptides in aqueous solutions are presented on the following pages. All curves (except the solubility lines) are for 298.15 K.

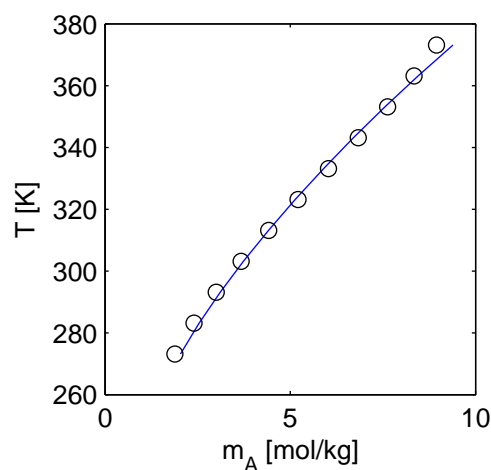
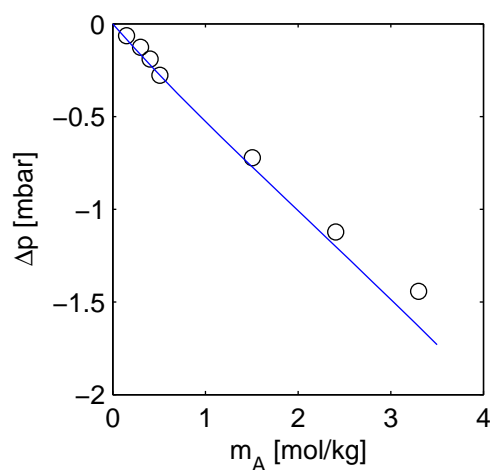
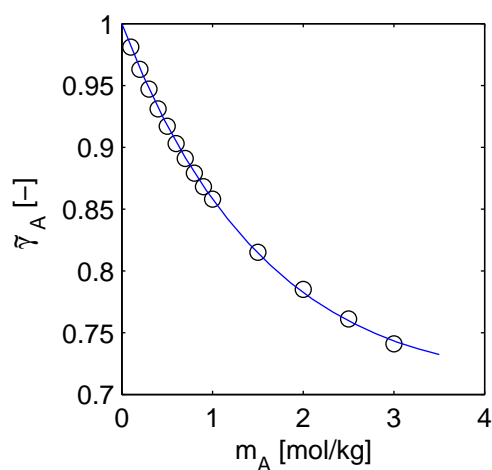
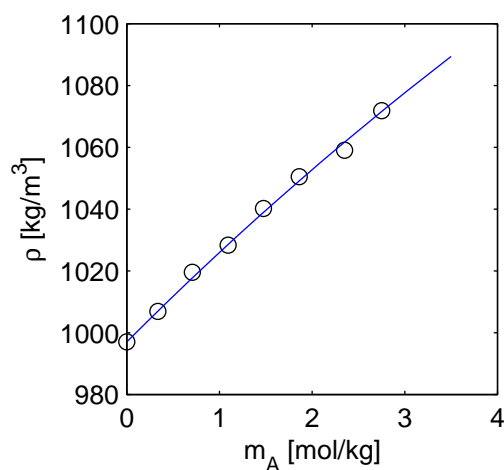
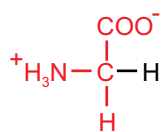
Tab. C.2: ePC-SAFT parameters of amino acids fitted to densities, activity coefficients and solubilities of aqueous solutions.

component	M_i [g/mol]	$(m_{\text{seg}}/M)_i$ [mol/g]	σ_i [Å]	ε_i [K]	$N^{\text{assoc}, a}$ [-]	$\varepsilon^{A_i B_j}/k_B$ [K]	$\kappa^{A_i B_j}$ [-]	T_{0v}^{SL} [K]	$\Delta h_{0v}^{SL}/R_G$ [K]	k_{ij}^b [-]
glycine	75.07	0.0646	2.3270	216.960	(1,1)	2598.0609	0.03931	714.25	2109.29	-0.0612
alanine	89.09	0.0613	2.5222	287.593	(1,1)	3176.5956	0.08192	3454.84	1579.12	-0.0612
L-serine	105.09	0.0668	2.2840	236.924	(2,1)	2671.9306	0.03850	496.84	3264.58	-0.0257
DL-serine	105.09	0.0668	2.2840	236.924	(2,1)	2671.9306	0.03850	824.80	2764.13	-0.0257
proline	115.13	0.0606	2.5481	289.716	(1,1)	5527.7546	0.03617	562.55	1600.33	-0.0699
valine	117.15	0.0558	2.7211	397.073	(1,1)	3332.4949	0.03857	4000.00	2100.00	-0.0614
L-threonine	119.12	0.0531	2.6055	325.375	(2,1)	2519.4077	0.03891	5886.08	1577.06	-0.0278
DL-threonine	119.12	0.0531	2.6055	325.375	(2,1)	2519.4077	0.03891	5167.74	1360.00	-0.0278
lysine	146.19	0.0798	2.3775	301.214	(1,2)	3787.3109	0.03295	595.50	5800.00	-0.0707
histidine	155.16	0.0391	2.8529	316.147	(2,1)	1316.9730	0.00925	2500.00	1120.00	-0.0195
arginine	174.20	0.0569	2.6572	349.706	(1,3)	2555.4454	0.03926	647.86	2232.60	-0.0145
α -ABA	103.12	0.0713	2.4873	355.362	(1,1)	3481.9875	0.02490			-0.0711
β -ABA	103.12	0.0686	2.4873	268.008	(1,1)	3481.9875	0.02490			-0.0744
γ -ABA	103.12	0.0659	2.4873	262.375	(1,1)	3481.9875	0.02490			-0.0729
α -AVA	117.15	0.0755	2.5984	339.171	(1,1)	3481.9875	0.02490			-0.0599
γ -AVA	117.15	0.0726	2.5984	262.375	(1,1)	3481.9875	0.02490			-0.0733
diglycine	132.12	0.0555	2.3270	216.960	(1,1)	2598.0609	0.03931	2000.00	2108.00	-0.0800
triglycine	189.18	0.0467	2.3270	216.960	(1,1)	2598.0609	0.03931			-0.0700
dialanine	160.16	0.0639	2.5222	287.593	(1,1)	3176.5956	0.08192			-0.0735
Ala-Gly, Gly-Ala	146.15	0.0630	2.4108	279.316	(1,1)	2912.2134	0.03923			-0.0750

^a $N^{\text{assoc}} = (2,1)$ means: 2 association sites of type 1 (proton donator), 1 association site of type 2 (proton acceptor).

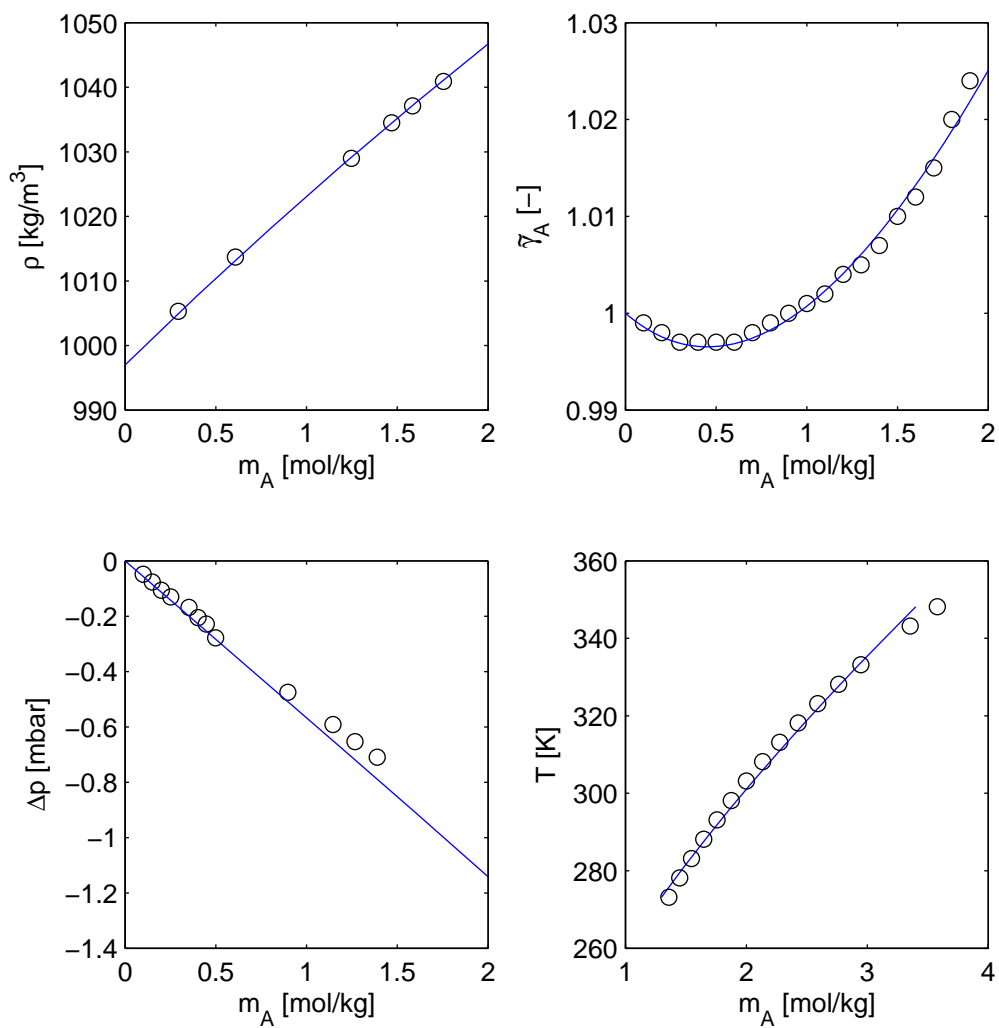
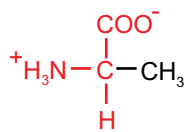
^b k_{ij} between water and component.

Glycine, Gly



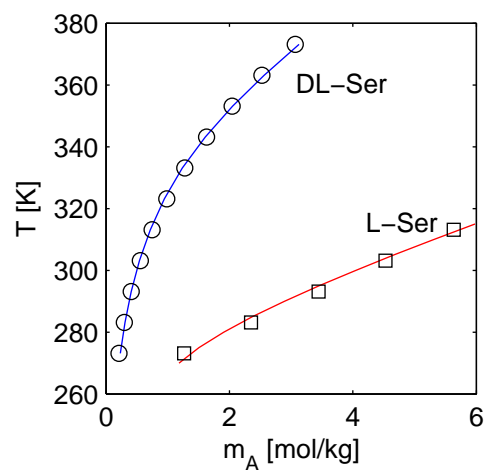
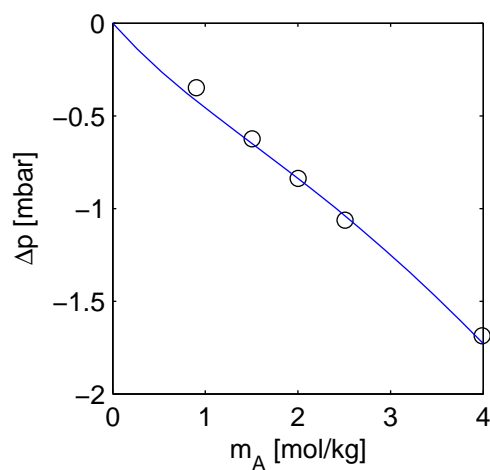
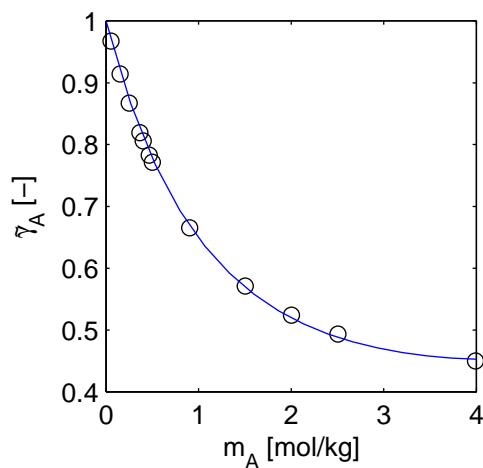
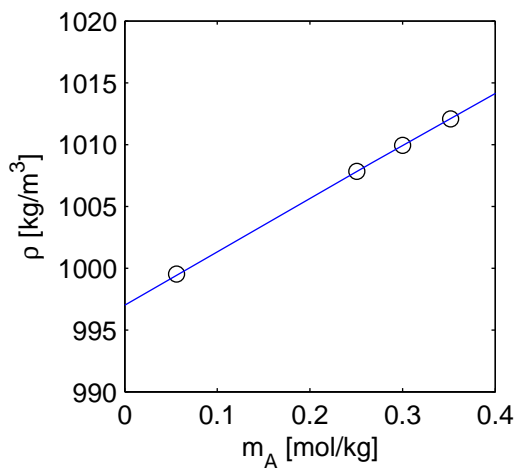
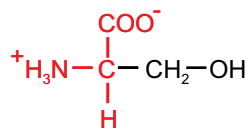
glycine	N	AARD		AAD	
ρ	8	0.09	[%]	0.96	[kg/m ³]
P	7	2.68	[%]	0.84	[mbar]
$\tilde{\gamma}_A$	14	0.11	[%]	$0.09 \cdot 10^{-2}$	[-]
m_S	9	4.34	[%]	0.14	[mol/kg]

Alanine, Ala



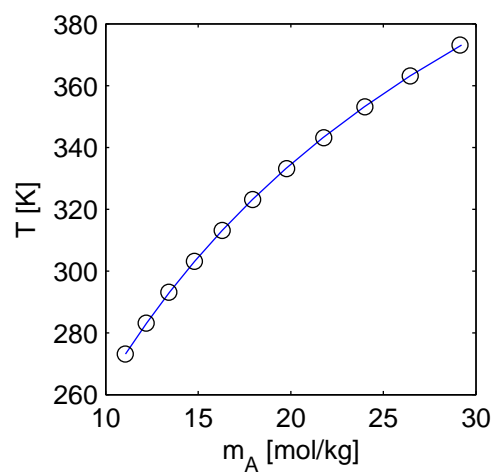
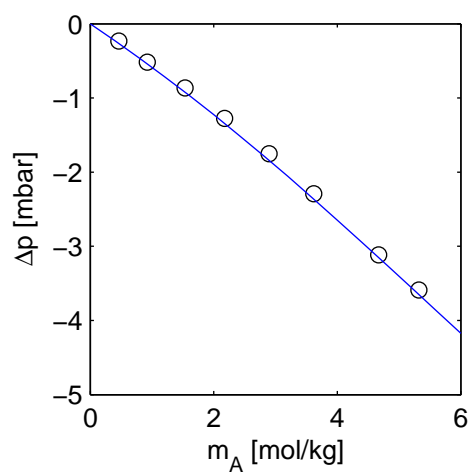
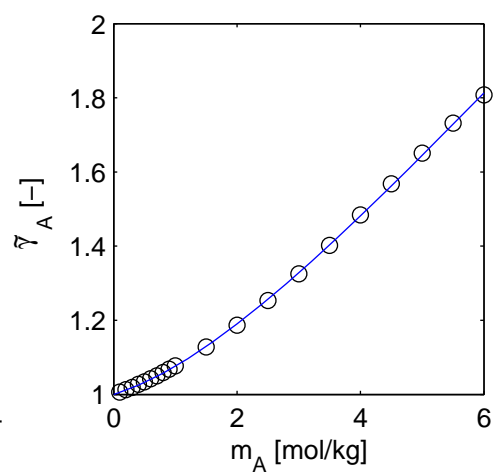
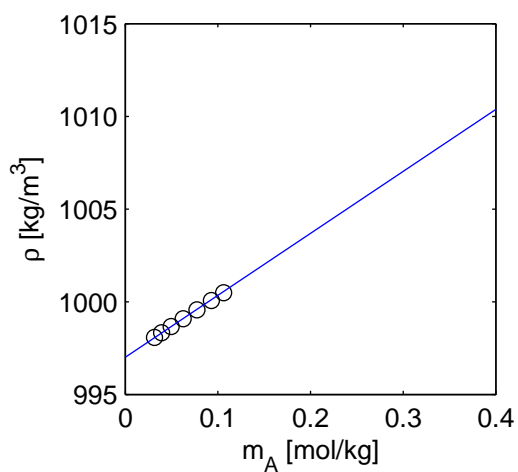
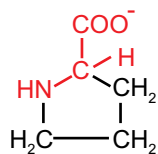
alanine	N	AARD	AAD
ρ	6	0.02 [%]	0.23 [kg/m ³]
P	12	0.68 [%]	0.21 [mbar]
$\tilde{\gamma}_A$	19	0.07 [%]	$0.07 \cdot 10^{-2}$ [-]
m_S	15	2.24 [%]	0.05 [mol/kg]

Serine, Ser



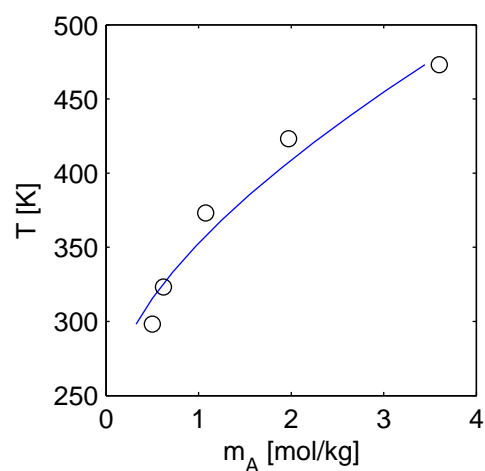
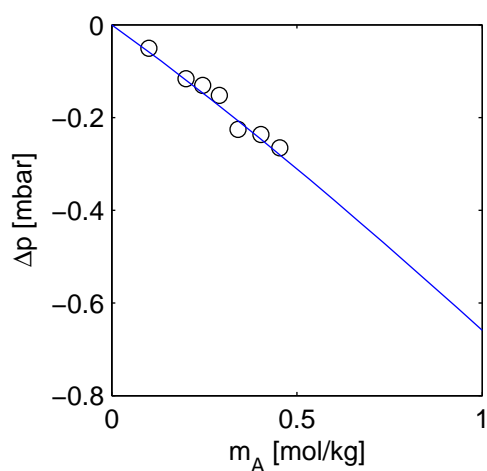
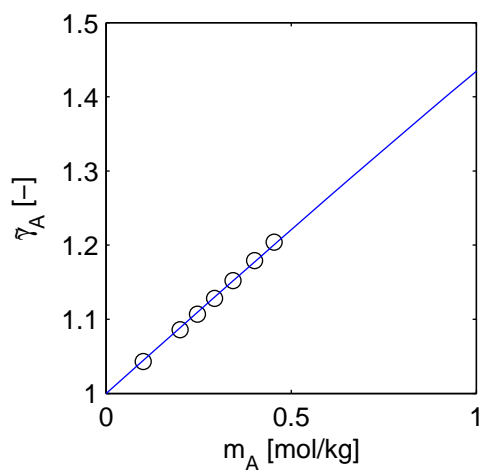
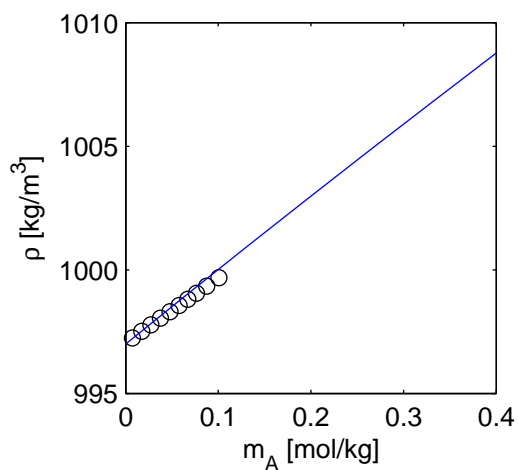
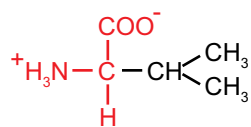
serine	N	AARD	AAD
ρ	5	0.01 [%]	0.09 [kg/m ³]
P	5	2.63 [%]	0.8 [mbar]
$\tilde{\gamma}_A$	12	0.66 [%]	$0.46 \cdot 10^{-2}$ [-]
(DL) m_S	11	3.05 [%]	0.03 [mol/kg]
(L) m_S	5	5.09 [%]	0.13 [mol/kg]

Proline, Pro



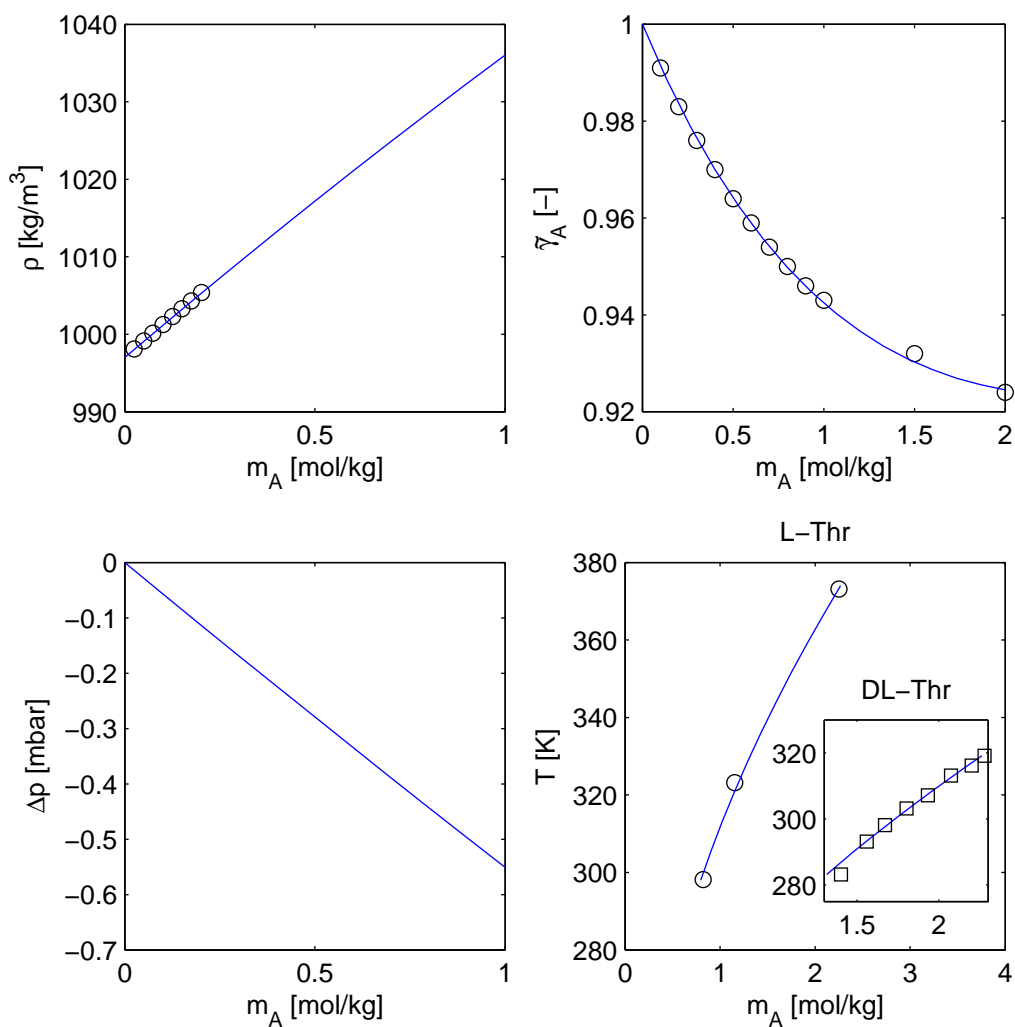
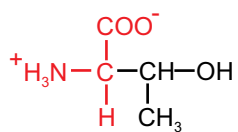
proline	N	AARD	AAD
ρ	7	0.01 [%]	0.06 [kg/m ³]
P	8	3.34 [%]	0.98 [mbar]
$\tilde{\gamma}_A$	20	0.19 [%]	$0.25 \cdot 10^{-2}$ [-]
m_S	11	0.14 [%]	0.03 [mol/kg]

Valine, Val



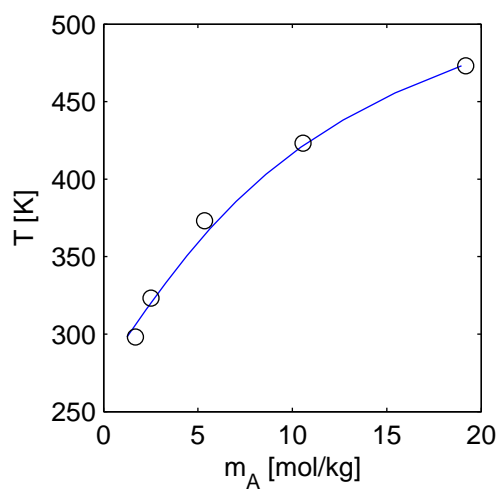
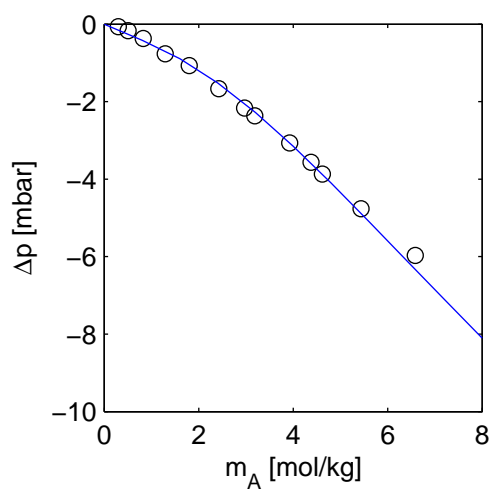
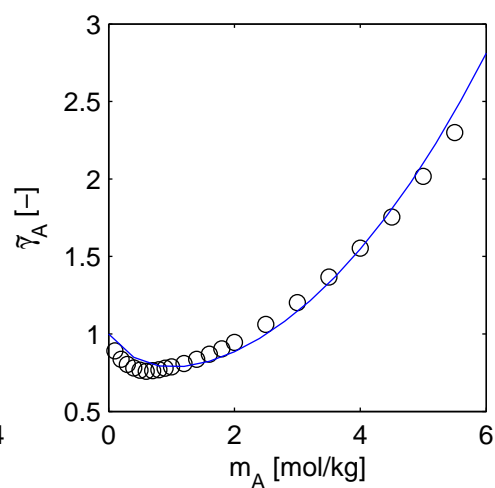
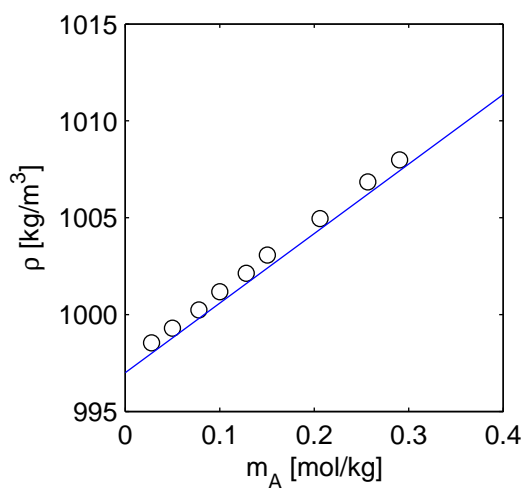
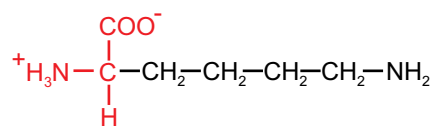
valine	N	AARD		AAD	
ρ	10	0.02	[%]	0.17	[kg/m ³]
P	7	3.87	[%]	1.22	[mbar]
$\tilde{\gamma}_A$	7	0.18	[%]	$0.2 \cdot 10^{-2}$	[-]
m_S	5	16.83	[%]	0.19	[mol/kg]

Threonine, Thr



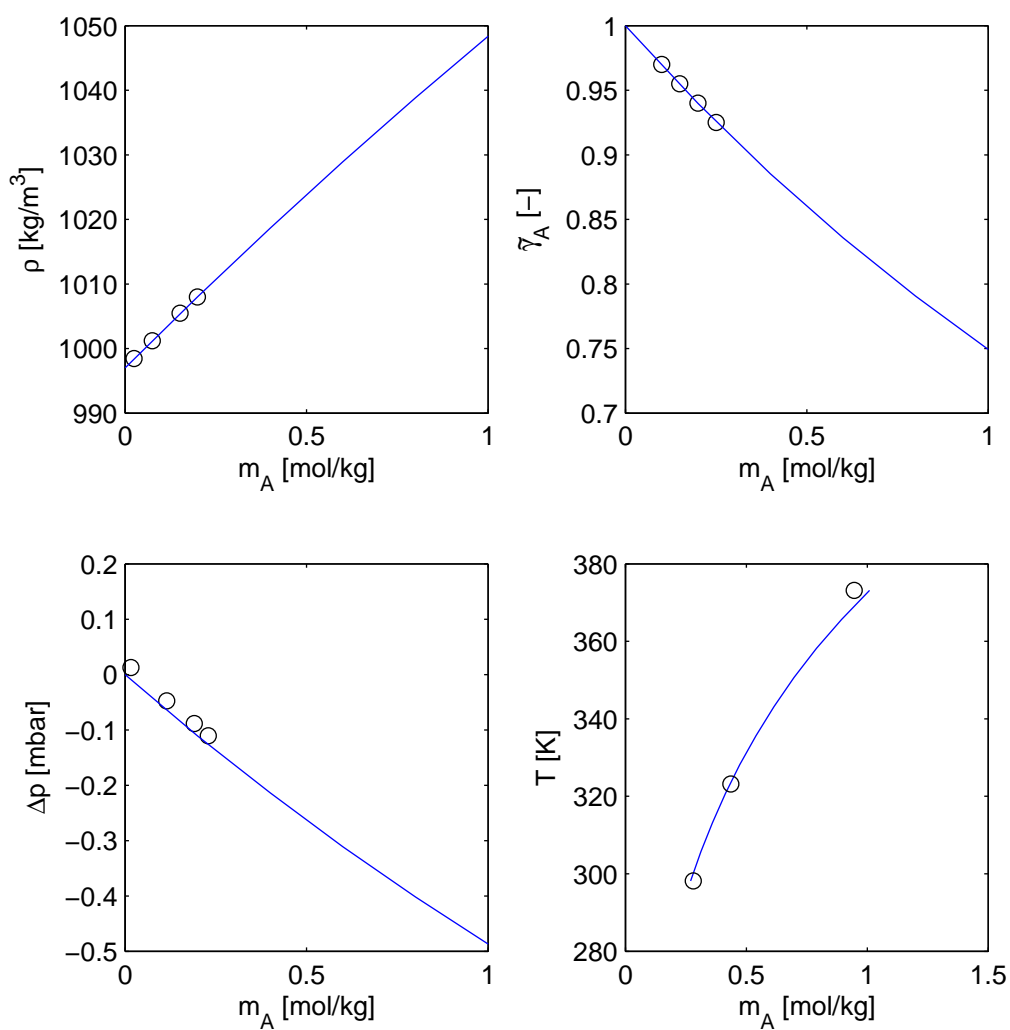
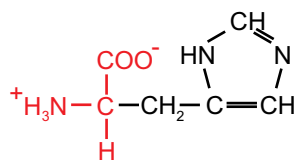
threonine	N	AARD		AAD	
ρ	8	0.01	[%]	0.07	[kg/m ³]
$\tilde{\gamma}_A$	12	0.04	[%]	$0.04 \cdot 10^{-2}$	[-]
(DL-) m_S	8	1.38	[%]	0.02	[mol/kg]
(L-) m_S	3	2.16	[%]	0.02	[mol/kg]

Lysine, Lys



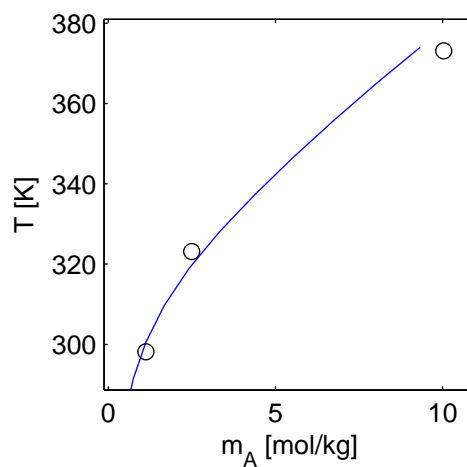
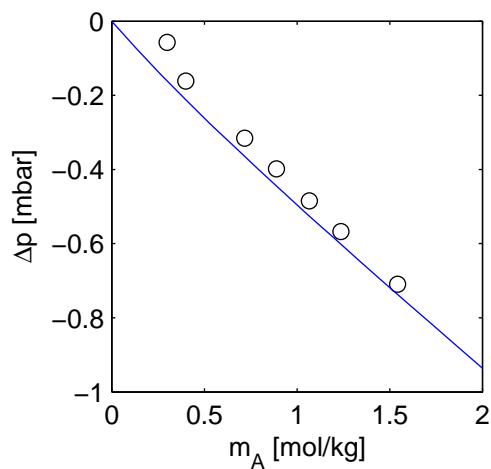
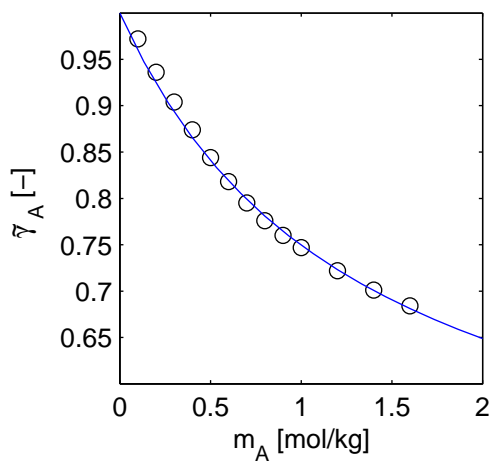
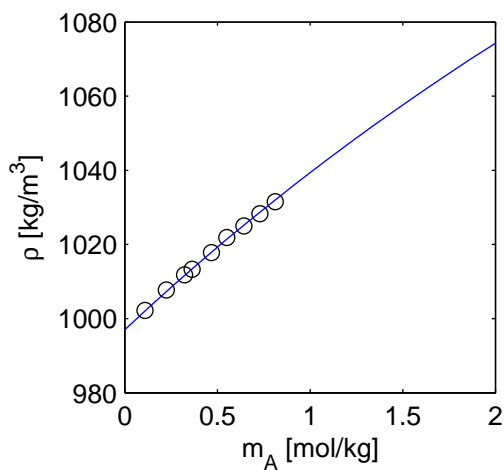
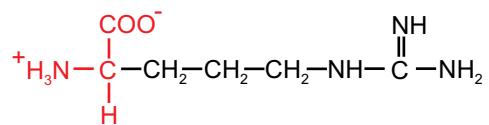
lysine	N	AARD		AAD	
ρ	9	0.03	[%]	0.33	[kg/m ³]
P	13	5.71	[%]	1.6	[mbar]
$\tilde{\gamma}_A$	22	4.93	[%]	$5.03 \cdot 10^{-2}$	[-]
m_S	5	9.81	[%]	0.34	[mol/kg]

Histidine, His

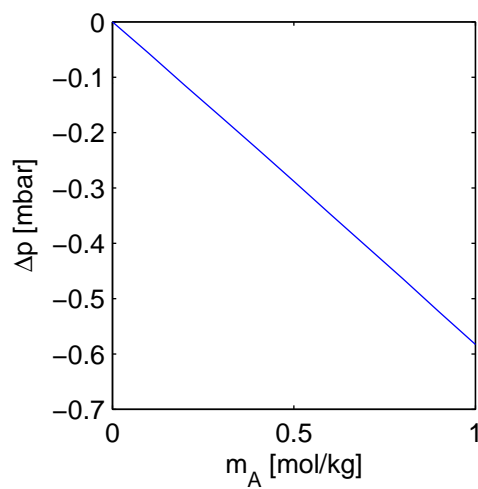
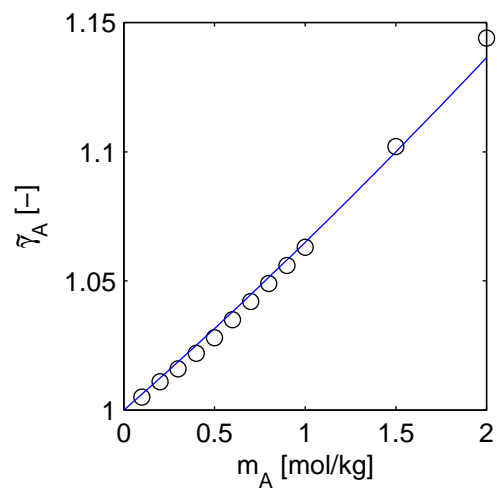
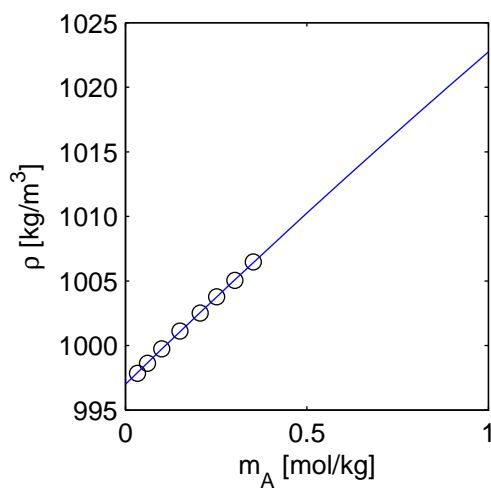
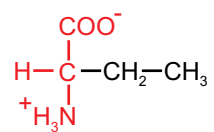


histidine	N	AARD		AAD	
ρ	4	<0.01	[%]	0.04	[kg/m ³]
P	4	0.16	[%]	0.05	[mbar]
$\tilde{\gamma}_A$	4	0.06	[%]	$0.06 \cdot 10^{-2}$	[-]
m_S	3	3.84	[%]	0.03	[mol/kg]

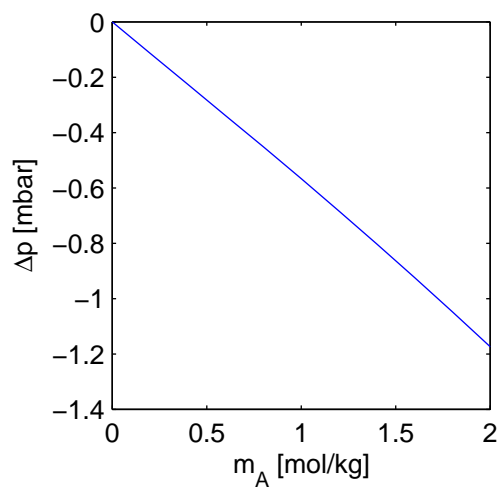
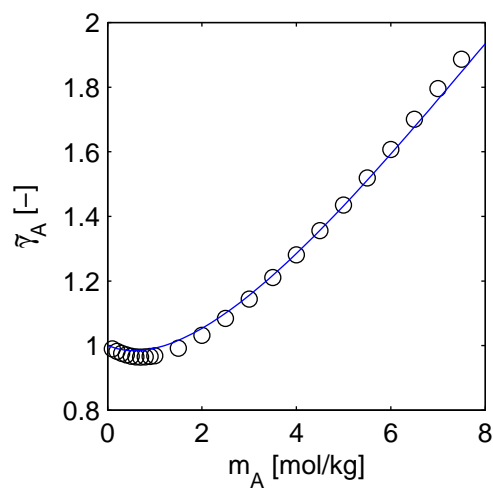
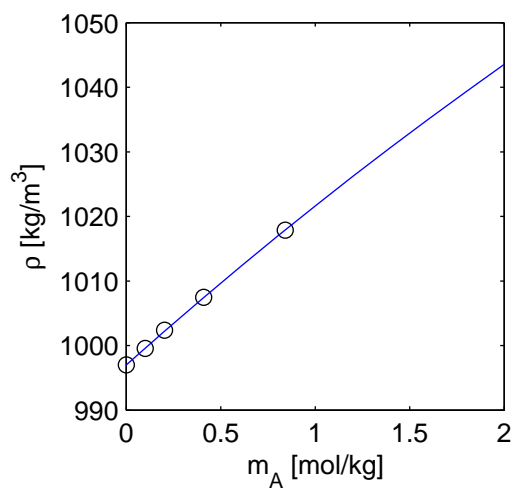
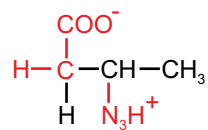
Arginine, Arg



arginine	N	AARD		AAD	
ρ	9	0.03	[%]	0.29	[kg/m ³]
P	7	3.2	[%]	1	[mbar]
$\tilde{\gamma}_A$	13	0.6	[%]	$0.52 \cdot 10^{-2}$	[-]
m_S	3	10.4	[%]	0.42	[mol/kg]

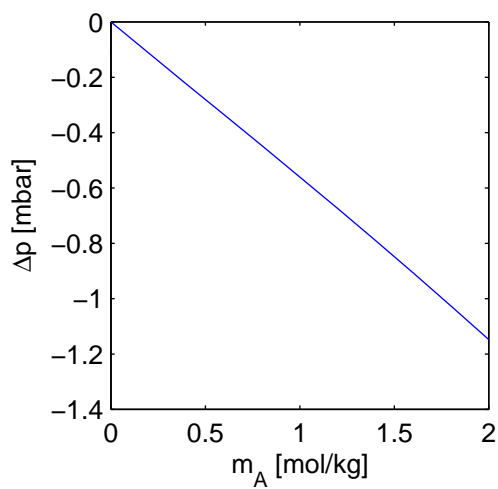
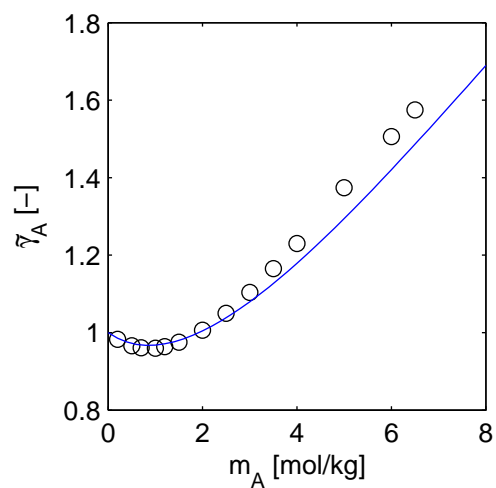
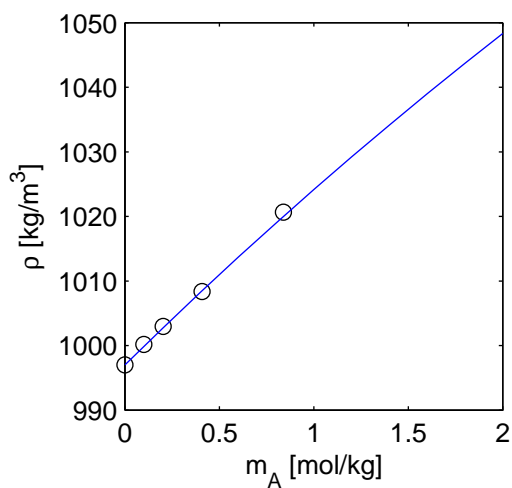
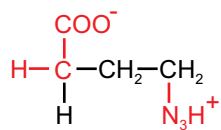
α -Aminobutyric Acid, α -ABA

α -ABA	N	AARD	AAD
ρ	8	0 [%]	0.04 [kg/m ³]
$\tilde{\gamma}_A$	12	0.27 [%]	$0.28 \cdot 10^{-2}$ [-]

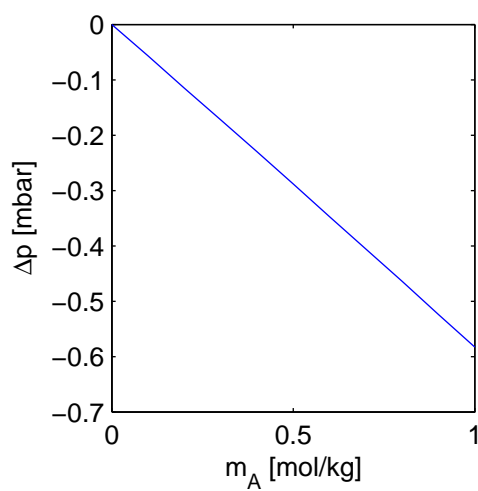
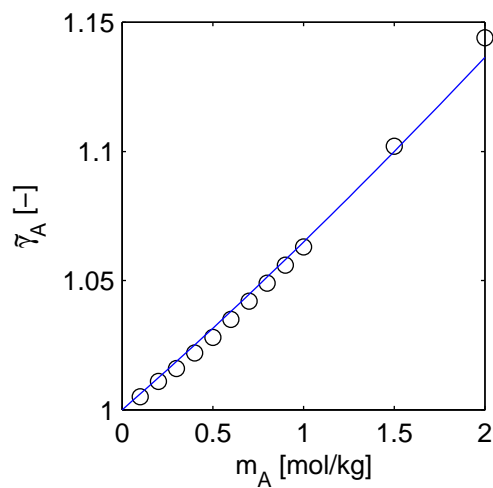
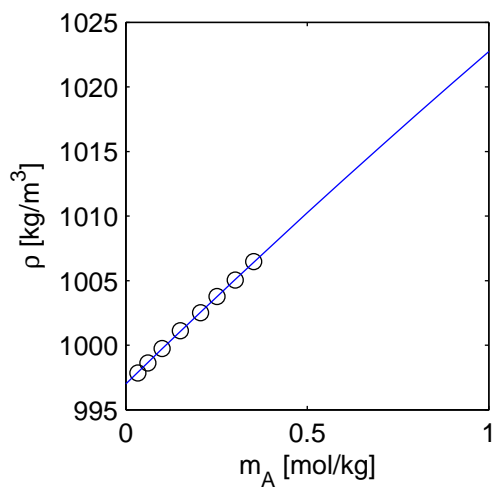
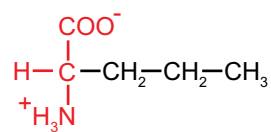
β -Aminobutyric Acid, β -ABA

β -ABA	N	AARD		AAD	
ρ	5	0.01	[%]	0.05	[kg/m ³]
$\tilde{\gamma}_A$	23	1.36	[%]	$1.59 \cdot 10^{-2}$	[-]

γ -Aminobutyric Acid, γ -ABA

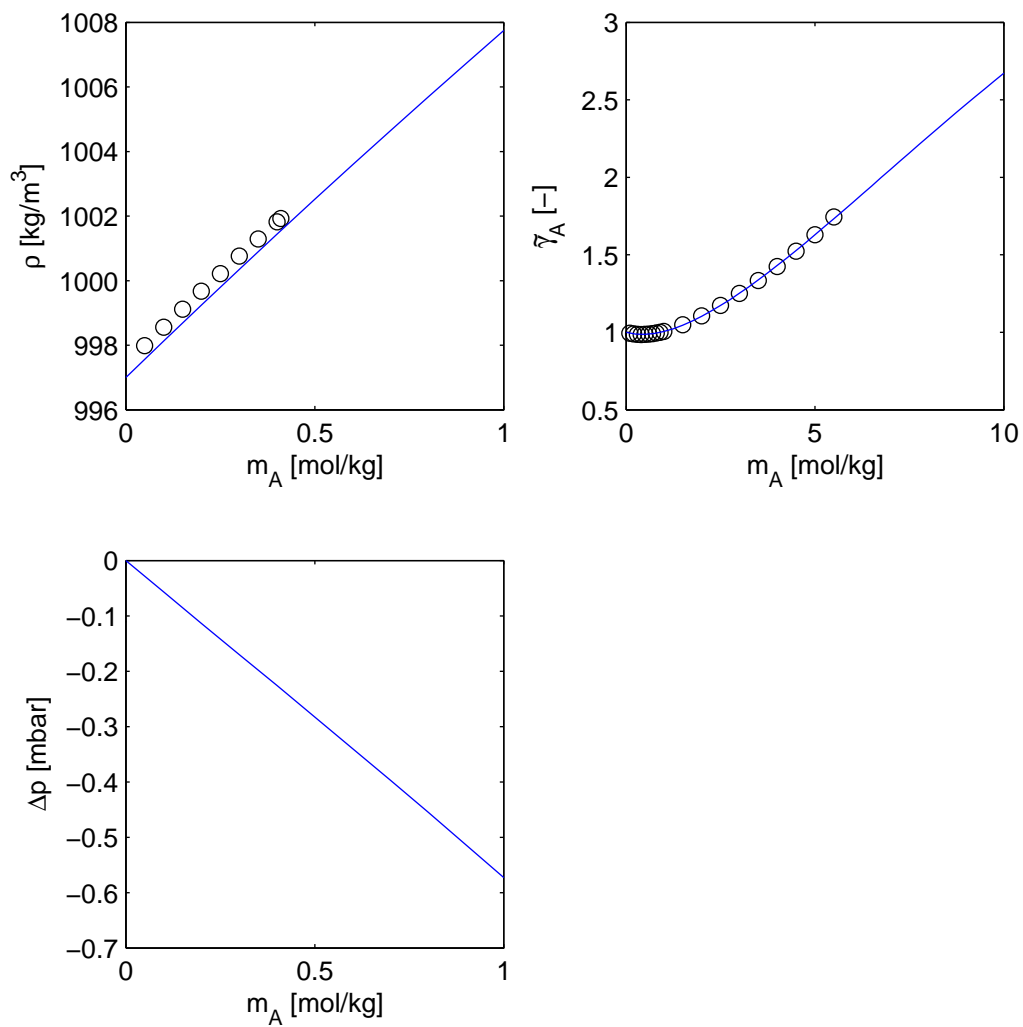
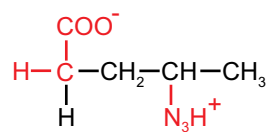


γ -ABA	N	AARD	AAD
ρ	5	0.02 [%]	0.25 [kg/m ³]
$\tilde{\gamma}_A$	14	2.26 [%]	$2.97 \cdot 10^{-2}$ [-]

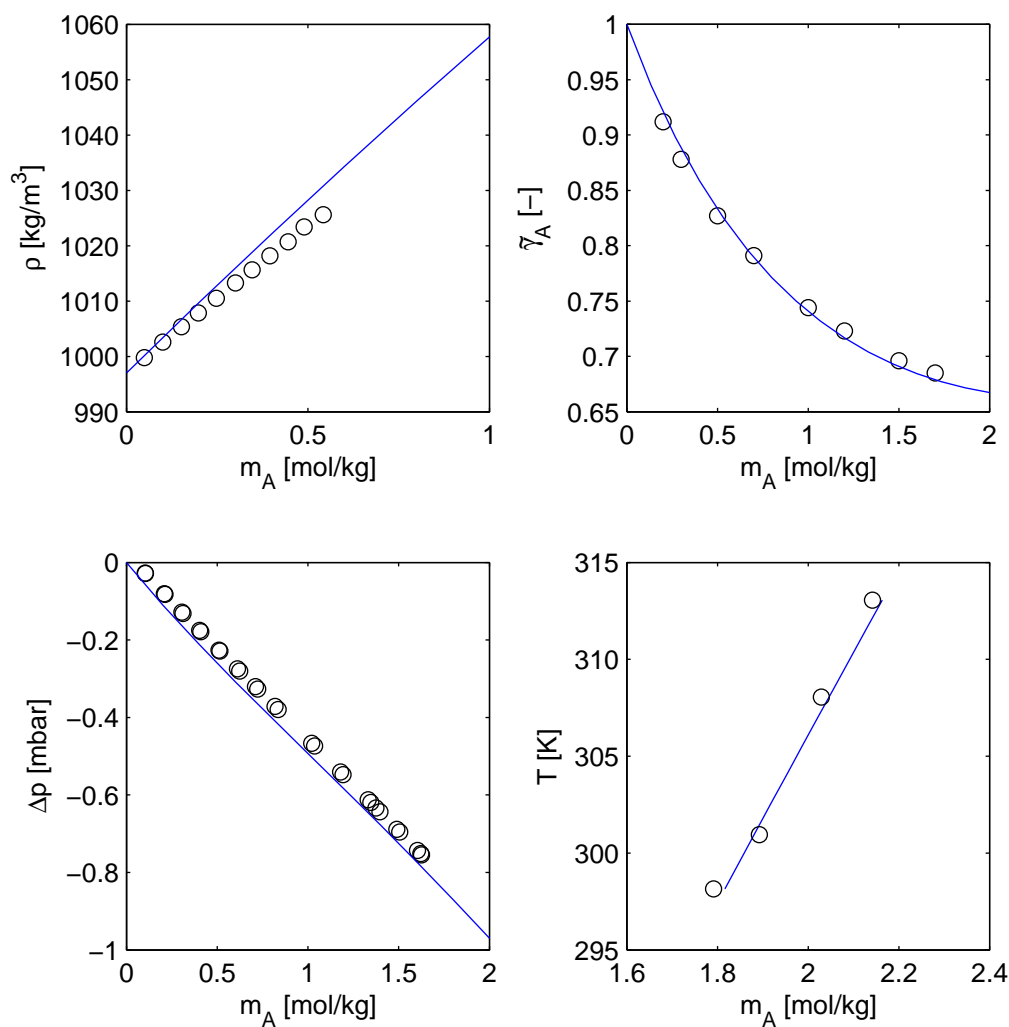
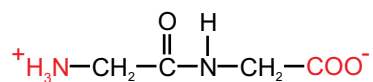
α -Aminovaleric Acid, α -AVA

α -AVA	N	AARD		AAD	
ρ	9	0.04	[%]	0.41	[kg/m ³]
$\tilde{\gamma}_A$	7	0.02	[%]	$0.02 \cdot 10^{-2}$	[-]

γ -Aminovaleric Acid, γ -AVA

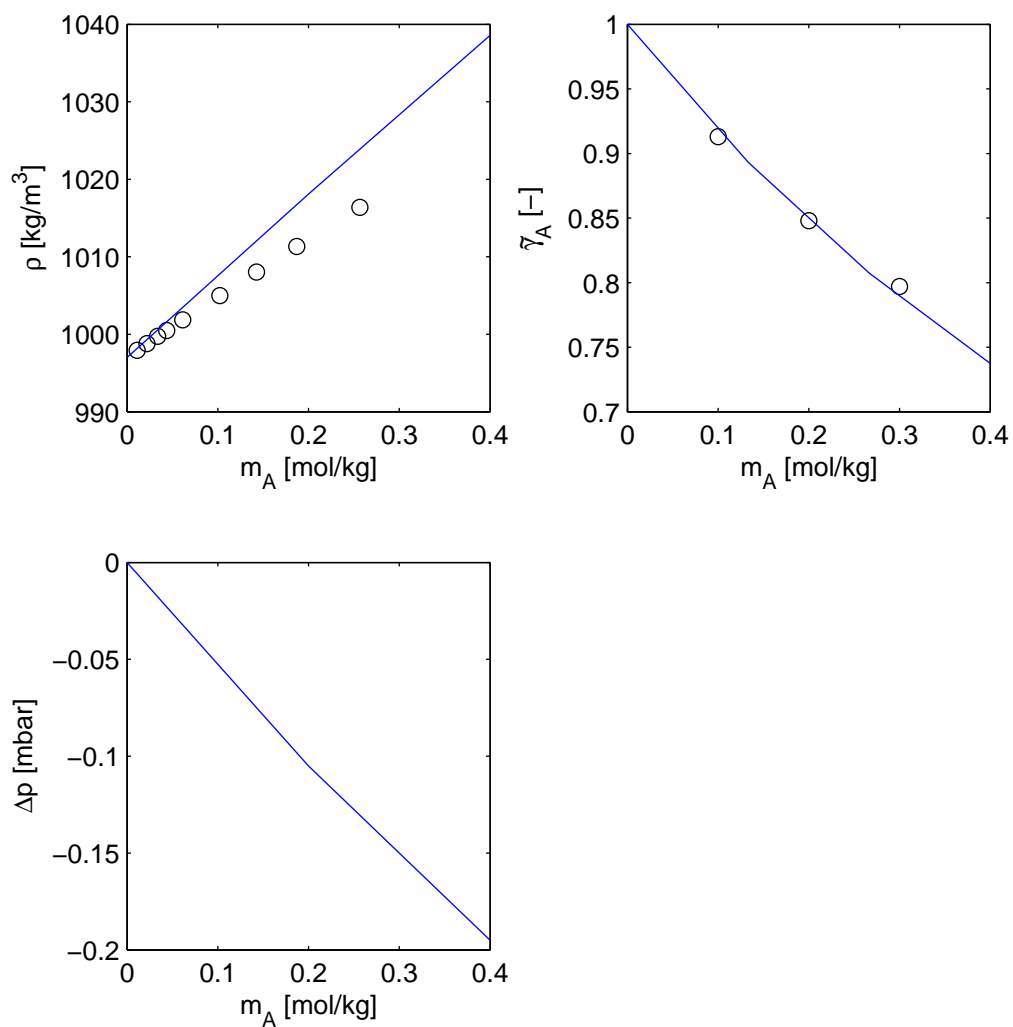
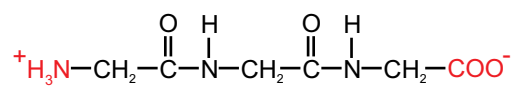


γ -AVA	N	AARD		AAD	
ρ	9	0.04	[%]	0.41	[kg/m ³]
$\tilde{\gamma}_A$	19	0.14	[%]	$0.2 \cdot 10^{-2}$	[-]

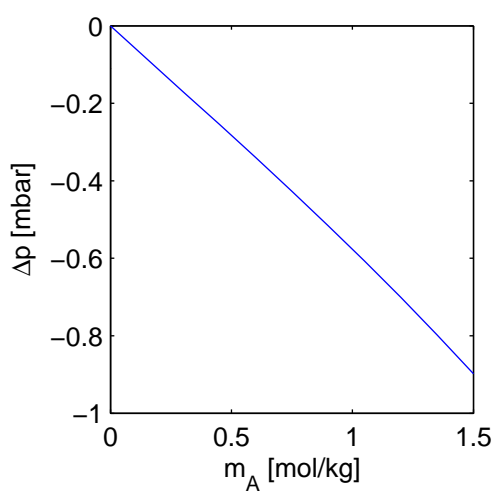
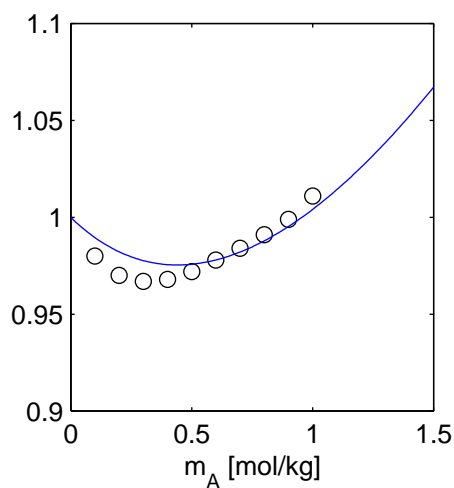
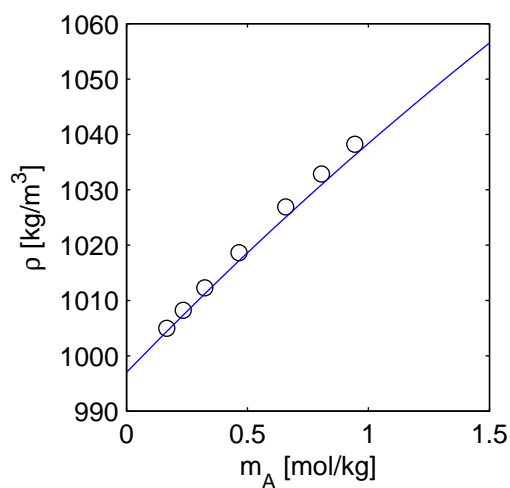
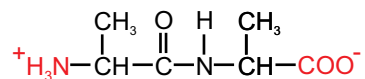
Glycylglycine, Diglycine, Gly₂

diglycine	N	AARD	AAD
ρ	11	0.27 [%]	2.7 [kg/m ³]
P	29	0.96 [%]	0.3 [mbar]
$\tilde{\gamma}_A$	8	0.75 [%]	$0.59 \cdot 10^{-2}$ [-]
m_S	14	5.45 [%]	0.11 [mol/kg]

Triglycine, Gly₃

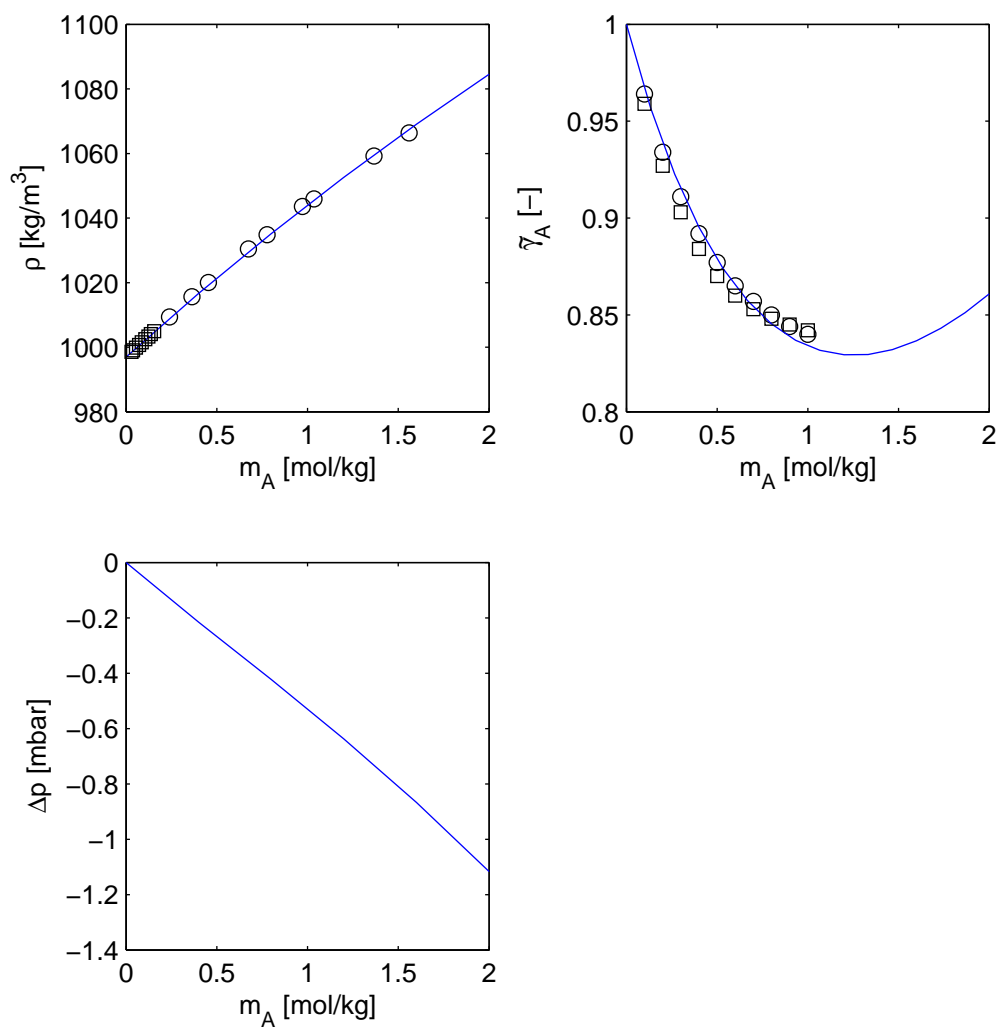
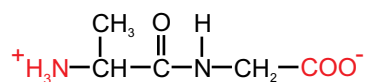
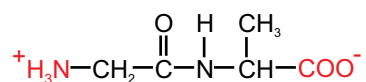


triglycine	N	AARD	AAD
ρ	9	0.27 [%]	2.73 [kg/m ³]
$\tilde{\gamma}_A$	3	0.53 [%]	$0.44 \cdot 10^{-2}$ [-]

Alanylalanine, Dialanine, Ala₂

dialanine	N	AARD	AAD
ρ	7	0.13 [%]	1.38 [kg/m ³]
$\tilde{\gamma}_A$	10	0.61 [%]	$0.6 \cdot 10^{-2}$ [-]

Glycylalanine, GlyAla & Alanylglycine, AlaGly



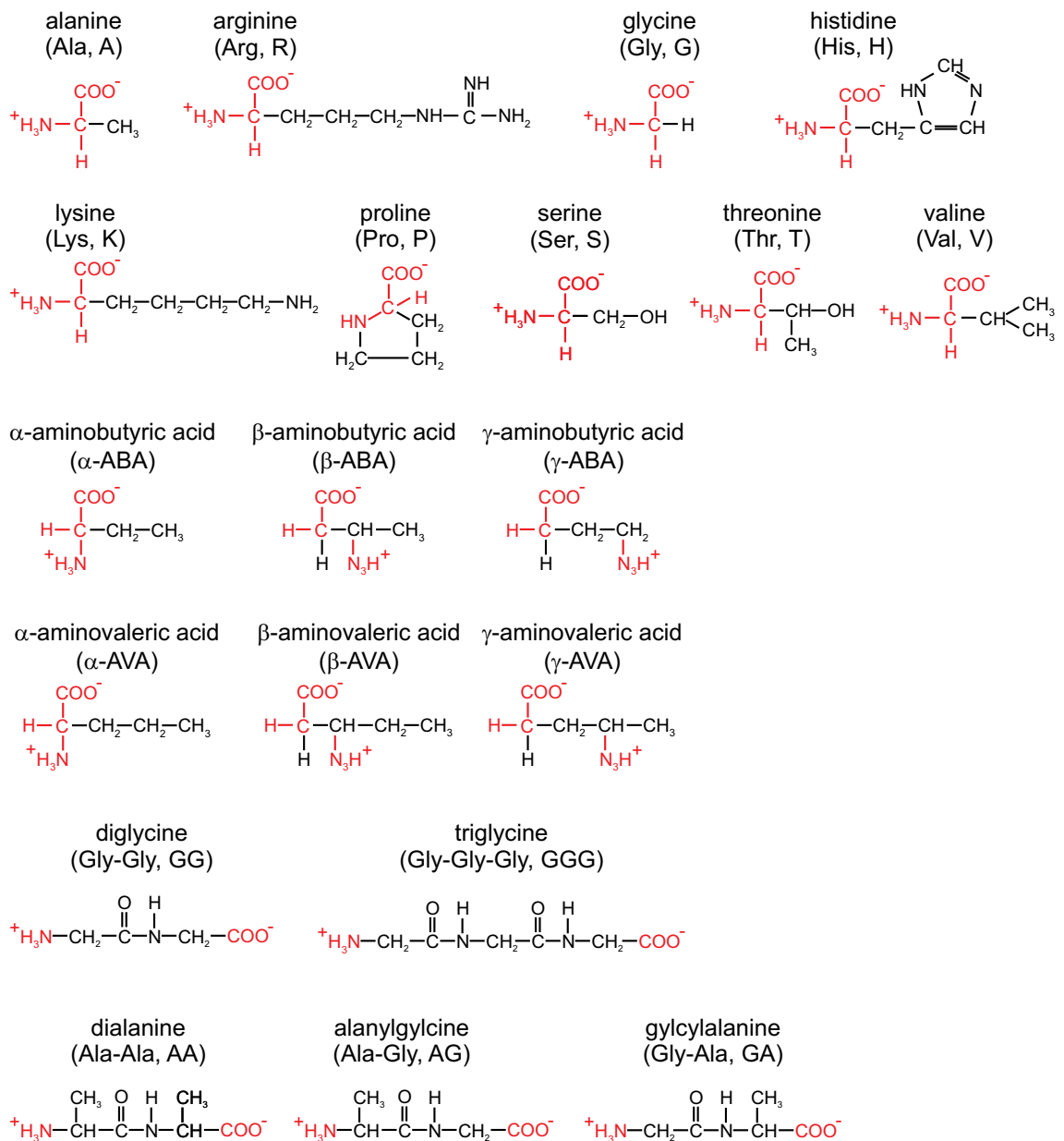
Gly-Ala (\square)		N	AARD		AAD	
ρ	9	0.06	[%]	0.66	[kg/m ³]	
$\tilde{\gamma}_A$	10	0.41	[%]	$0.36 \cdot 10^{-2}$	[-]	
Ala-Gly (\circ)		N	AARD		AAD	
ρ	9	0.01	[%]	0.12	[kg/m ³]	
$\tilde{\gamma}_A$	10	0.85	[%]	$0.75 \cdot 10^{-2}$	[-]	

Tab. C.3: Absolute Average Deviation (AAD) and Absolute Average Relative Deviation (AARD) for solution properties of aqueous amino acid and peptide solutions. N is the number of experimental data points.

amino acid	N	ρ		P			$\tilde{\gamma}_A$			m_S		
		AARD [%]	AAD [kg/m ³]	AARD [%]	AAD [mbar]	N	AARD [%]	AAD [$\cdot 10^{-2}$ -]	N	AARD [%]	AAD [mol/kg]	
glycine	8	0.09	0.96	7	0.54	0.17	24	1.64	1.44	11	2.88	0.13
alanine	6	0.02	0.23	12	0.45	0.14	19	0.07	0.07	15	2.24	0.05
L-serine	5	0.01	0.09	5	0.43	0.13	12	0.66	0.46	5	5.09	0.13
DL-serine										11	3.05	0.03
proline	7	0.01	0.06	8	0.55	0.17	20	0.19	0.25	11	0.14	0.03
valine	10	0.02	0.17	7	0.37	0.12	7	0.18	0.20	5	16.83	0.19
arginine	9	0.03	0.29	7	0.51	0.16	13	0.60	0.52	3	10.42	0.42
lysine	9	0.03	0.33	13	0.49	0.14	22	4.93	5.03	5	9.81	0.34
L-threonine	8	0.01	0.07				12	0.04	0.04	3	2.16	0.02
DL-threonine										8	1.38	0.02
α -ABA	8	<0.01	0.04	12	0.26		12	0.26	0.28			
β -ABA	5	0.01	0.05	23	1.36		23	1.36	1.59			
γ -ABA	5	0.02	0.25	14	2.26		14	2.26	2.97			
α -AVA	9	0.04	0.41	7	0.02		7	0.02	0.02			
γ -AVA	9	0.04	0.41	19	0.14		19	0.14	0.20			
diglycine	11	0.27	2.70	29	0.46	0.14	8	0.75	0.59	15	5.18	0.10
triglycine	9	0.27	2.73				3	0.53	0.44			
dialanine	7	0.13	1.38				10	0.61	0.60			
Gly-Ala	9	0.06	0.66				10	0.41	0.36			
Ala-Gly	9	0.01	0.12				10	0.85	0.75			
average		0.06	0.61		0.48	0.15		0.86	0.88		5.38	0.25

Appendix D

Chemical Structures



Appendix E

Conversion of the Activity Coefficients

In this Appendix the conversion of the mean ionic activity coefficient from mole fraction scale to molality scale (Eq. 2.48) is derived. Starting point is the equality of the chemical potential, i. e.

$$\mu_{\pm}^m = \mu_{\pm}^x \quad (\text{E.1})$$

$$\mu_{0\pm}^m + RT \ln a_{\pm}^m = \mu_{0\pm}^x + RT \ln a_{\pm}^x \quad (\text{E.2})$$

The activity of the electrolyte can be expressed as $a_s^m = (m_s \gamma_{\pm}^m)^\nu$ or $a_s^x = (x_s \gamma_{\pm}^x)^\nu$, respectively. Hence

$$\mu_{0\pm}^m + \nu RT \ln m_s + \nu RT \ln \gamma_{\pm}^m = \mu_{0\pm}^x + \nu RT \ln x_s + \nu RT \ln \gamma_{\pm}^x \quad (\text{E.3})$$

Rearrangement yields

$$\ln \gamma_{\pm}^m = \frac{\mu_{0\pm}^m - \mu_{0\pm}^x}{\nu RT} + \ln \frac{x_s}{m_s} + \ln \gamma_{\pm}^x \quad (\text{E.4})$$

To obtain the difference between the reference chemical potentials Eq. E.4 is evaluated at infinite dilution:

$$\lim_{x_s \rightarrow 0} \gamma_{\pm}^x = 1; \quad \lim_{m_s \rightarrow 0} \gamma_{\pm}^m = 1; \quad \lim_{x_s \rightarrow 0} \frac{x_s}{m_s} = \nu M_w$$

Therefore,

$$\frac{\mu_{0\pm}^m - \mu_{0\pm}^x}{\nu RT} = -\ln(\nu M_w) \quad (\text{E.5})$$

and Eq. E.4 becomes

$$\ln \gamma_{\pm}^m = -\ln(\nu M_w) + \ln \frac{x_s}{m_s} + \ln \gamma_{\pm}^x \quad (\text{E.4})$$

With the conversion formula from mole fraction to molality

$$x_s = \frac{\nu m_s}{\nu m_s + \frac{1000}{M_w}} \quad (\text{E.6})$$

we finally obtain

$$\tilde{\gamma}_{\pm}^m = \frac{\tilde{\gamma}_{\pm}^x}{1 + \frac{M_W}{1000} \cdot \nu \cdot m_S} \quad (2.48)$$

Appendix F

The Cross-Differential Equation

In this appendix the cross-differential equation as used in Sec. 2.3.3 (p. 15) is derived first for mixtures of uncharged components and then for the special case of one solvent, one uncharged solute, and one electrolyte.

Starting point is the excess Gibbs free energy

$$G^E = \sum_i^N n_i \mu_i^E \quad (\text{F.1})$$

The first derivative of G^E with respect to n_i is equivalent to the excess chemical potential

$$\mu_i^E = \frac{\partial G^E}{\partial n_i} \quad (\text{F.2})$$

Taking the derivative of μ_i^E with respect to n_j yields

$$\frac{\partial^2 G^E}{\partial n_i \partial n_j} = \frac{\partial \mu_i^E}{\partial n_j} \quad (\text{F.3})$$

Combining Eq. F.3 with

$$\mu_i^E = RT \ln \gamma_i \quad (\text{F.4})$$

directly leads to

$$\frac{\partial^2 G^E}{\partial n_i \partial n_j} = RT \frac{\partial \ln \gamma_i}{\partial n_j} \quad (\text{F.5})$$

Since G^E is a homogeneous function the Maxwell criterion holds true and the order of differentiation is irrelevant. Therefore,

$$\begin{aligned} \frac{\partial^2 G^E}{\partial n_i \partial n_j} &= \frac{\partial^2 G^E}{\partial n_j \partial n_i} \\ \frac{\partial \ln \gamma_i}{\partial n_j} &= \frac{\partial \ln \gamma_j}{\partial n_i} \end{aligned} \quad (\text{F.6})$$

Eq. F.6 represents the interlink of the activity coefficients of components in a mixture.

For electrolytes the derivation is analogous. Without loss of generality mole numbers can be replaced by molalities and the activity coefficients are based on molality instead of mole fractions. First the chemical potential of the salt has to be derived

$$\begin{aligned}\mu_{\pm} &= \nu_+ \mu_+ + \nu_- \mu_- \\ &= \mu_{0\pm} + \nu_+ RT \ln(m_+ \gamma_+) + \nu_- RT \ln(m_- \gamma_-) \\ &= \mu_{0\pm} + RT \ln(m_+^{\nu_+} m_-^{\nu_-}) + RT \ln(\gamma_+^{\nu_+} \gamma_-^{\nu_-})\end{aligned}\quad (\text{F.7})$$

Applying Eq. 2.47 and Eq. 2.49 one obtains

$$\mu_{\pm} = \mu_{0\pm} + \nu RT \ln m_{\pm} + \nu RT \ln \gamma_{\pm} \quad (\text{F.8})$$

$\mu_{0\pm}$ is the chemical potential of the reference state and a function of T and P only. The last term corresponds to the excess chemical potential μ_{\pm}^E . For the special case of a water/electrolyte/amino acid system Eq. F.1 is rewritten as

$$G^E = m_W \mu_W^E + m_A \mu_A^E + m_{\pm} \mu_{\pm}^E \quad (\text{F.9})$$

Application of the Maxwell criterion leads in a straightforward way to

$$\begin{aligned}\frac{\partial^2 G^E}{\partial m_{\pm} \partial m_A} &= \frac{\partial^2 G^E}{\partial m_A \partial m_{\pm}} \\ \nu \frac{\partial \ln \gamma_{\pm}}{\partial m_A} &= \frac{\partial \ln \gamma_A}{\partial m_{\pm}}\end{aligned}\quad (\text{F.10})$$

After integration of Eq. F.10 one gets the cross-differential equation on molal basis

$$\nu \int_{m_{\pm}=0}^{m_{\pm}} \left(\frac{\partial \ln \gamma_{\pm}^{ter}}{\partial m_A} \right)_{m_{\pm}} dm_{\pm} = \ln \left(\frac{\gamma_A^{ter}}{\gamma_A^{bin}} \right)_{m_{\pm}} \quad (\text{F.11})$$

Note that here the activity coefficients are normalized with respect to the pure component and not as usual for electrolytes and solute systems to the infinite dilution. Further, when evaluating the integral one must keep in mind that m_{\pm} is not equivalent to m_S (except for 1:1, 2:2, 3:3 electrolytes).

The question arises how to calculate γ_{\pm}^{ter} (symmetric convention!) with the help of an equation of state such as the ePCSAFT EOS. One may write

$$\gamma_{\pm}^{ter} = (\gamma_+^{\nu_+} \gamma_-^{\nu_-})^{\frac{1}{\nu}} = \left(\left(\frac{\varphi_+}{\varphi_{0+}} \right)^{\nu_+} \left(\frac{\varphi_-}{\varphi_{0-}} \right)^{\nu_-} \right)^{\frac{1}{\nu}} \quad (\text{F.12})$$

where φ_{0+} and φ_{0-} are the fugacity coefficients of the pure cation ($x_+ \rightarrow 1$) and anion ($x_- \rightarrow 1$), respectively. But which meaning do these values have? Cations and anions do not exist as pure components. Is it thus thermodynamically consistent to set, for example, $x_+ = 1$ while all other mole fractions (and also x_-) are zero in order to calculate φ_{0+} ? This would violate the electroneutrality condition. The reference state 'pure component' appears to be inapplicable. However, the cross-differential equation as given above is clearly

defined for this reference state.

Appendix G

Activity Coefficients in Ternary Solutions

In the following, the applicability of the cross-differential equation (see p. 14) for the calculation of activity coefficients of amino acids in amino acid/electrolyte solutions is investigated using the pathological example of aqueous alanine/NaNO₃ solutions.

In order to obtain $\gamma_A^{ter}/\gamma_A^{bin*}$ the MIAC of the electrolyte is measured by the electrochemical method at various salt and amino acid molalities, m_{\pm} and m_A , respectively. The experimental data is fitted to a parameterized equation of arbitrary form. Two types of fitting equation are found in the literature (KV by Khoshkbarchi et al.¹⁰⁵ and BR by Breil⁴):

$$KV : \quad \nu \ln \frac{\gamma_{\pm}^{ter}}{\gamma_{\pm}^{bin}} = C_1 m_A + C_2 m_A m_{\pm} + C_3 m_A^2 + C_4 m_A m_{\pm}^2 + C_5 m_A^3 + C_6 m_A^2 m_{\pm} \quad (G.1)$$

$$BR : \quad \ln \frac{\gamma_{\pm}^{ter}}{\gamma_{\pm}^{bin}} = \frac{A_1 m_A}{(1 + A_2 m_A)(1 + A_3 m_{\pm})} + (A_4 + A_5 m_{\pm}) m_A + A_6 m_A^2 \quad (G.2)$$

As shown in Fig. G.1, both variants yield almost equivalent results[†] for the aqueous system alanine/NaNO₃.

Applying the cross-differential equation

$$\nu \int_{m_{\pm}=0}^{m_{\pm}} \left(\frac{\partial \ln \gamma_{\pm}^{ter}}{\partial m_A} \right)_{m_{\pm}} dm_{\pm} = \ln \left(\frac{\gamma_A^{ter}}{\gamma_A^{bin}} \right)_{m_{\pm}} \quad (2.50)$$

*Remember that in this case the activity coefficients are the symmetric ones.

[†]The parameters $C_{1..6}$ and $A_{1..6}$ were adjusted to experimental data using a least squares non-linear fitting routine. $C_{1..6} = [-0.1875, 0.3059, -0.0486, -0.1402, 0.0256, -0.0199]$; $A_{1..6} = [-0.1954, 0.0454, 1.2785, 0.0847, -0.0275, -0.0063]$.

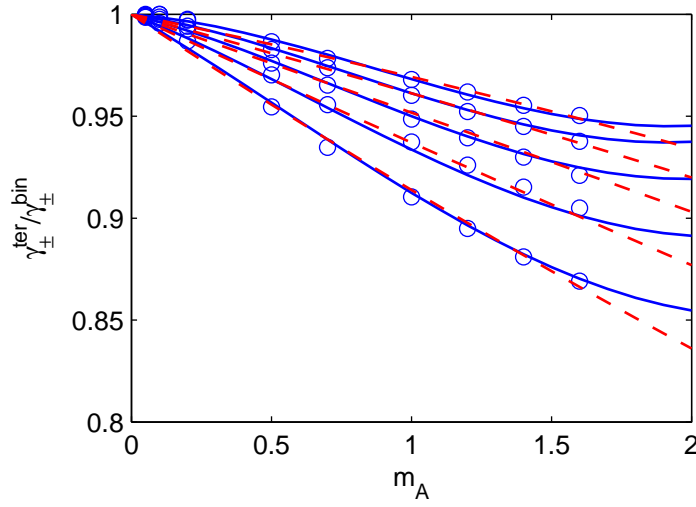


Fig. G.1: Ratio of the MIAC of NaNO_3 in the ternary aqueous solution to the binary solution without alanine for varying salt molalities (from top to bottom: 0.1, 0.3, 0.5, 0.7, and 1.0 mol/kg). Experimental data taken from Ref. ⁶ Lines are calculated with the KV Eq. G.1 (—) and the BR Eq. G.2 (---).

one obtains

$$\begin{aligned}
 KV: \quad \ln \frac{\gamma_A^{ter}}{\gamma_A^{bin}} &= C_1 m_{\pm} + \frac{1}{2} C_2 m_{\pm}^2 + 2C_3 m_A m_{\pm} \\
 &+ \frac{1}{3} C_4 m_{\pm}^3 + 3C_5 m_A^2 m_{\pm} + C_6 m_A m_{\pm}^2 \quad (G.3)
 \end{aligned}$$

$$\begin{aligned}
 BR: \quad \frac{1}{\nu} \ln \frac{\gamma_A^{ter}}{\gamma_A^{bin}} &= \frac{C_1/C_3}{(1 + C_2 m_A)^2} \ln(1 + C_3 m_{\pm}) \\
 &+ C_4 m_{\pm} + \frac{1}{2} C_5 m_{\pm}^2 + 2C_6 m_A m_{\pm} \quad (G.4)
 \end{aligned}$$

Fig. G.2 shows that the ratio of the activity coefficients of alanine in the ternary aqueous solution to the one in the binary solution without salt ($\gamma_A^{ter}/\gamma_A^{bin}$) strongly depends on the equation type used for the regression of $\gamma_{\pm}^{ter}/\gamma_{\pm}^{bin}$. The KV equations yield $\gamma_A^{ter}/\gamma_A^{bin}$ which first decrease and then increase with amino acid molality, whereas the BR ansatz reveals a monotonic decrease of the ratio with increasing amino acid molality.

This example demonstrates that the conversion of $\gamma_{\pm}^{ter}/\gamma_{\pm}^{bin}$ to $\gamma_A^{ter}/\gamma_A^{bin}$ is dependent on the type of regression equation. Hence, conclusions drawn from plots of $\gamma_A^{ter}/\gamma_A^{bin}$ are questionable.

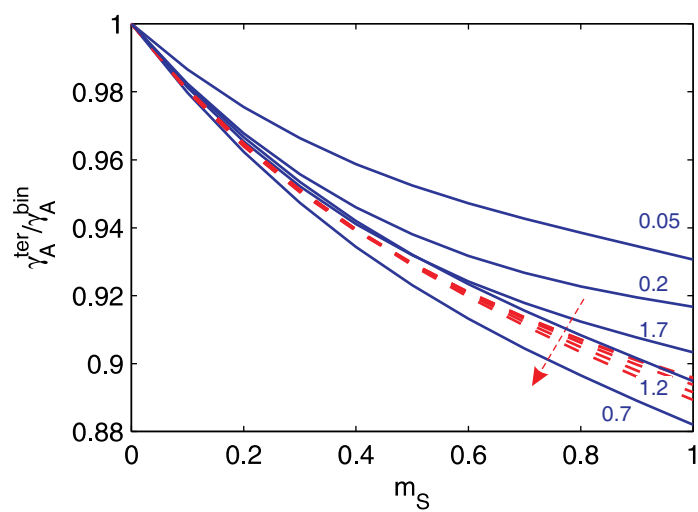


Fig. G.2: Ratio of the activity coefficient of alanine in the ternary aqueous solution to the binary solution without NaNO_3 for varying alanine molalities. Lines are calculated with KV Eq. G.3 (—) and BR Eq. G.4 (---). The arrow indicates the order of increasing alanine molalities for the BR equation.

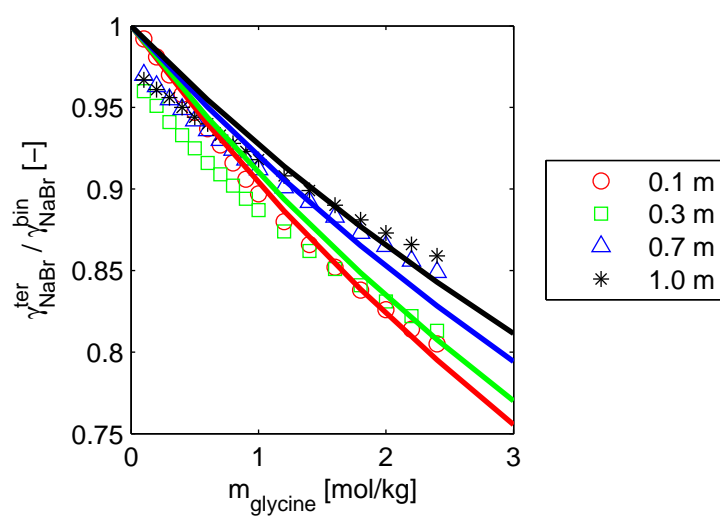
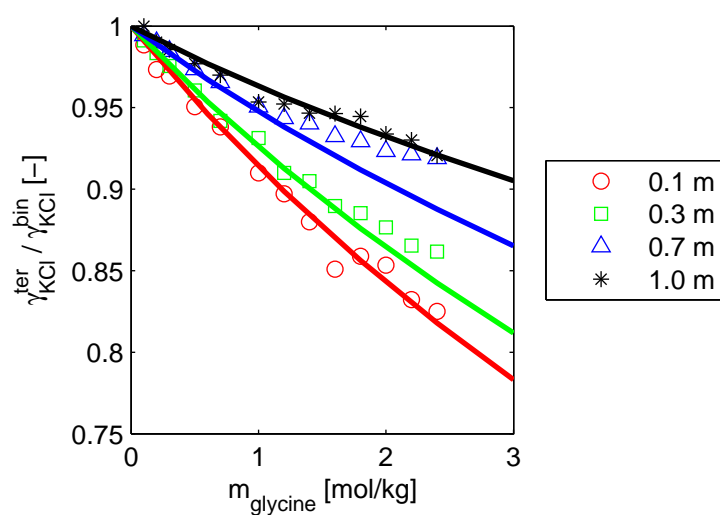
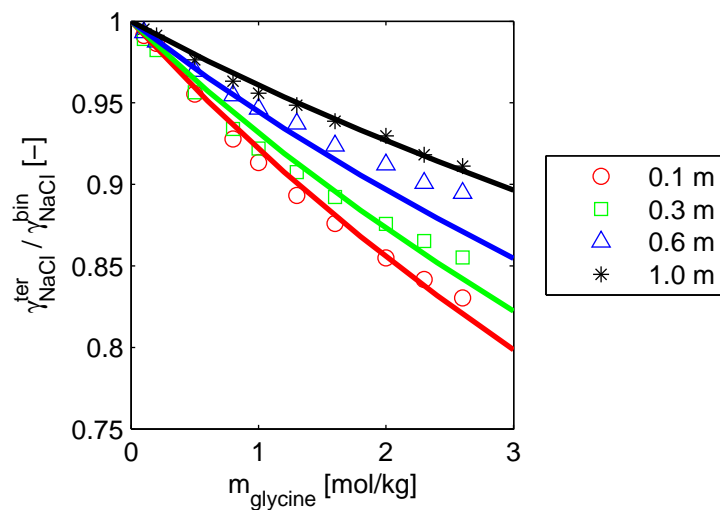
Appendix H

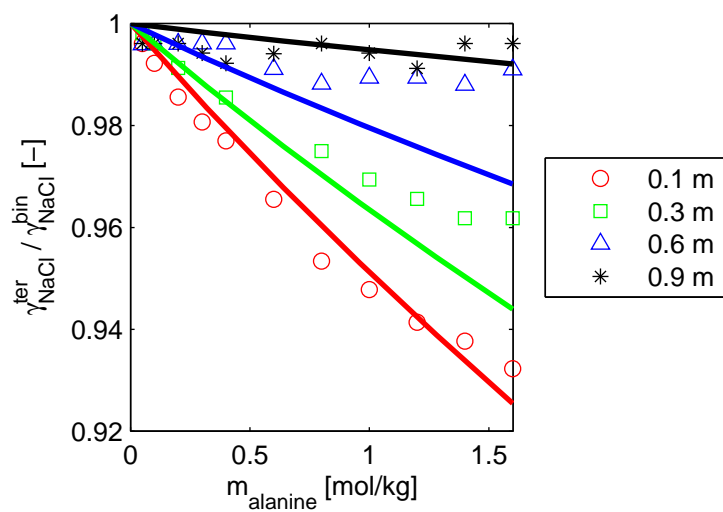
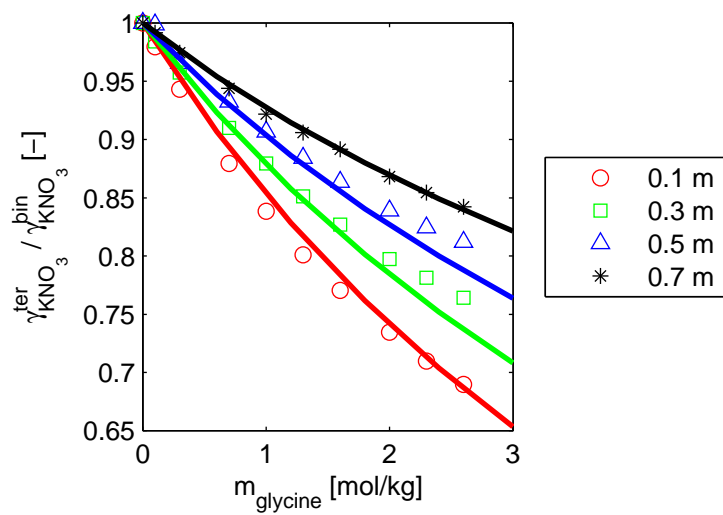
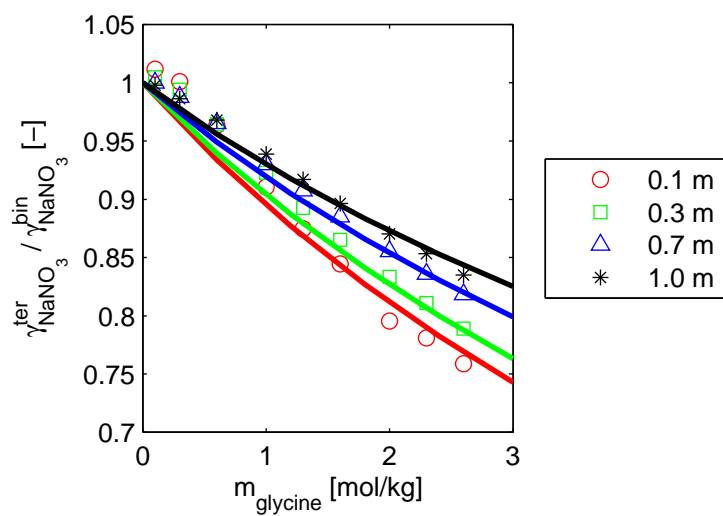
Electrolyte/Amino Acid Solutions

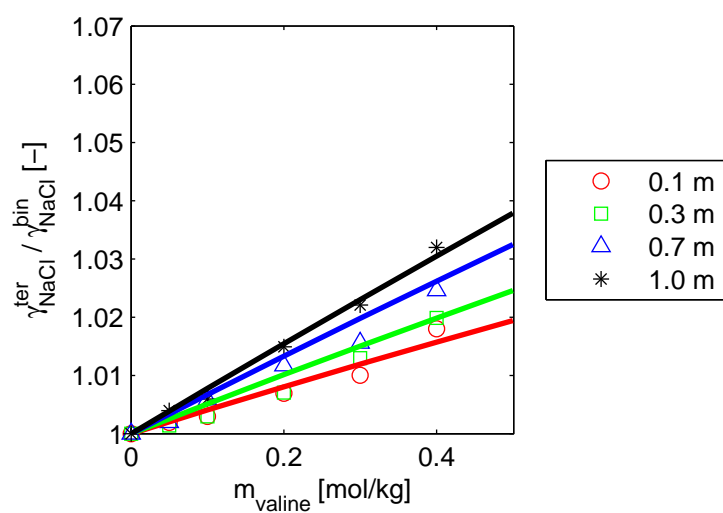
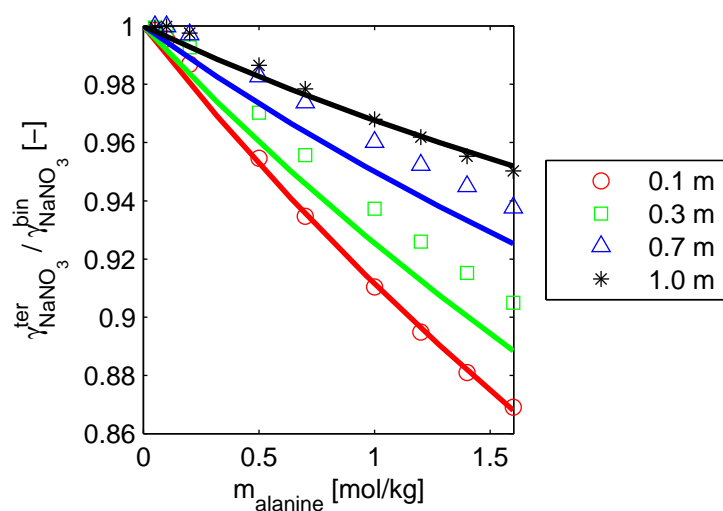
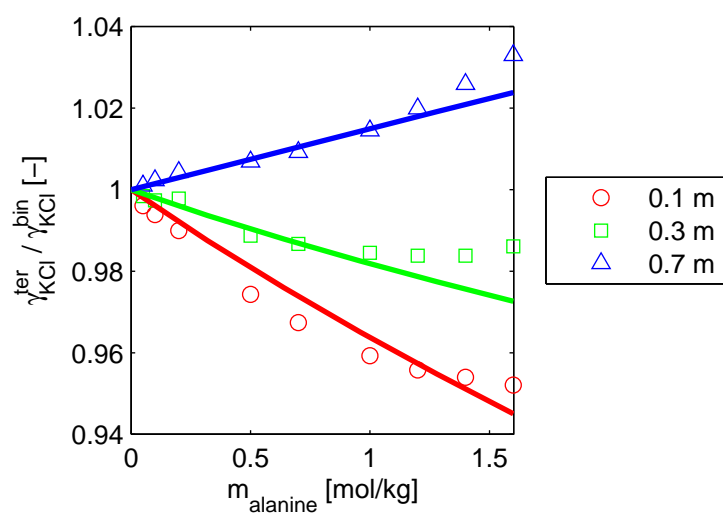
In this appendix the ratios of the MIAC for several systems are summarized. The quality of the measured data found in the literature is sometimes questionable. For example, the ratios for NaBr in glycine solutions do not start at 1 for $m_{glycine} = 0$. The data appears to be shifted to lower ratios which is physically not correct. The concentration dependent k_{ij} was fitted manually to the ratios of MIAC in ternary solutions at the highest and the lowest salt content, respectively. The coefficients k_{ij}^0 and k_{ij}^1 were then determined by linear regression. Solubilities of glycine and DL-serine in salt solutions are given below. Here, the model fails independently from the application of a binary interaction parameter.

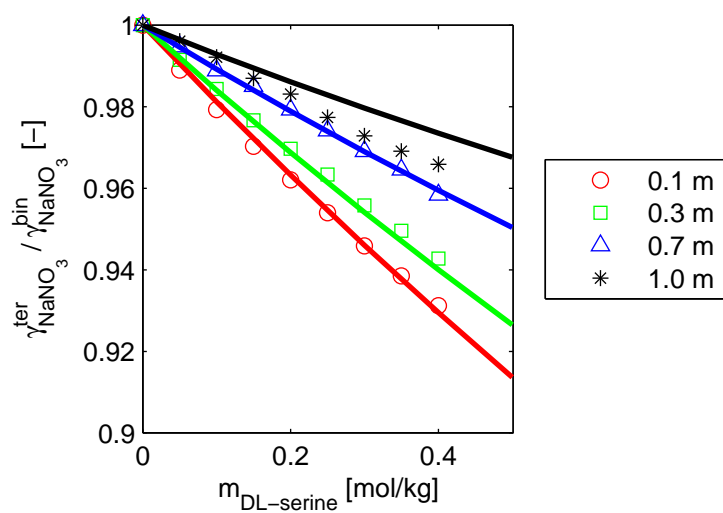
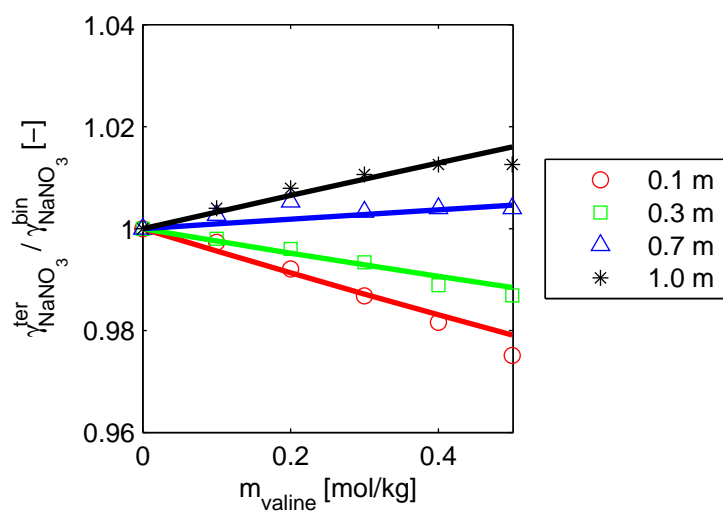
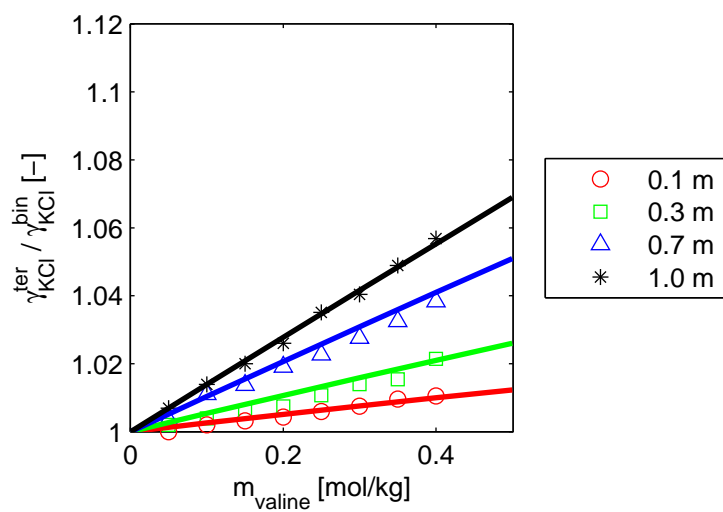
Tab. H.1: Ternary systems consisting of water, electrolyte and amino acid. Binary interaction parameters $k_{ij} = k_{ij}^0 + m_{salt} \cdot k_{ij}^1$.

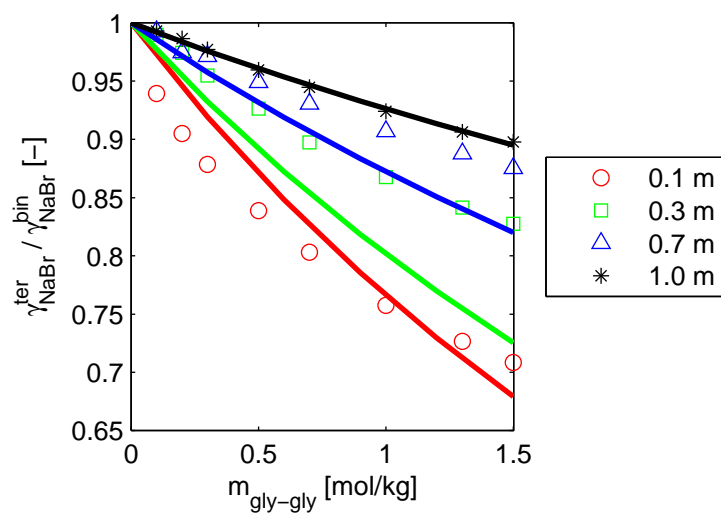
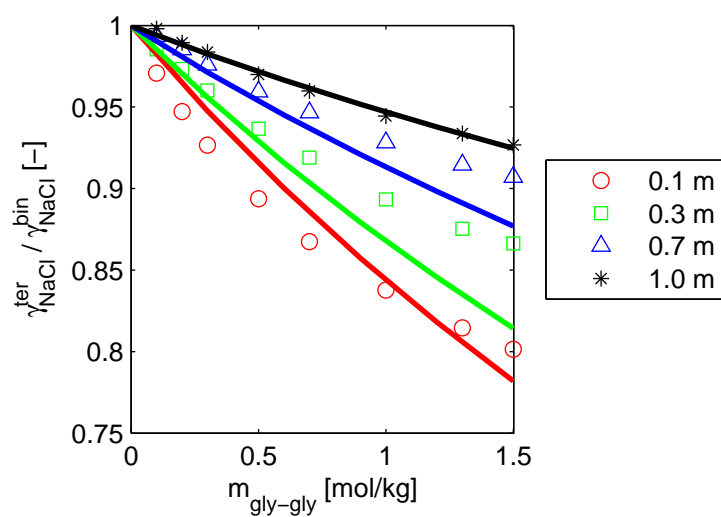
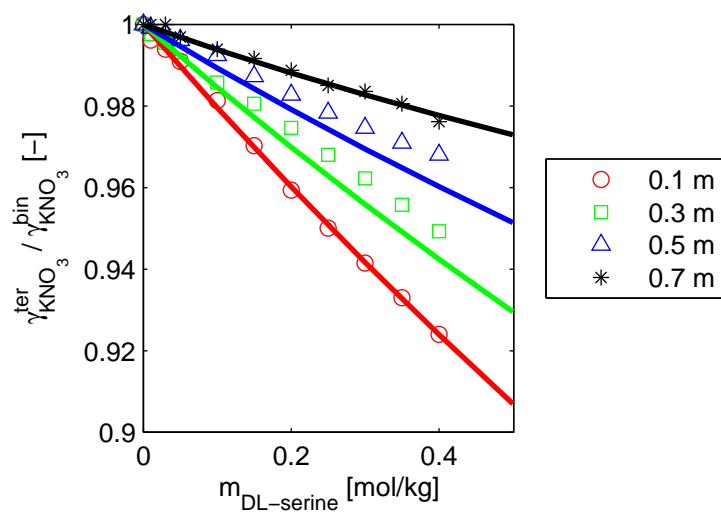
amino acid	electrolyte	k_{ij}^0	k_{ij}^1	Exp. data from Ref.	
				$\gamma_{\pm}^{ter} / \gamma_{\pm}^{bin}$	SLE
glycine	NaCl	-0.1982	0.1158	105	152
glycine	KCl	-0.2039	0.1491	153	-
glycine	NaBr	-0.2115	0.0699	154	-
glycine	NaNO ₃	-0.2707	0.1200	152	109
glycine	KNO ₃	-0.4485	0.4343	107	-
alanine	NaCl	-0.0868	0.1010	105	-
alanine	KCl	-0.0766	0.1563	105	-
alanine	NaNO ₃	-0.1730	0.1362	6	-
valine	NaCl	0.0332	0.0559	80	-
valine	KCl	-0.0288	0.1448	104	-
valine	NaNO ₃	-0.0965	0.1071	107	-
DL-serine	NaNO ₃	-0.3234	0.2526	107	109
DL-serine	KNO ₃	-0.3940	0.5033	107	109
diglycine	NaCl	-0.3000	0.2030	155	-
diglycine	NaBr	-0.4101	0.2939	155	-
diglycine	KCl	-0.2041	0.1467	155	-
diglycine	KBr	-0.6744	0.5406	155	-

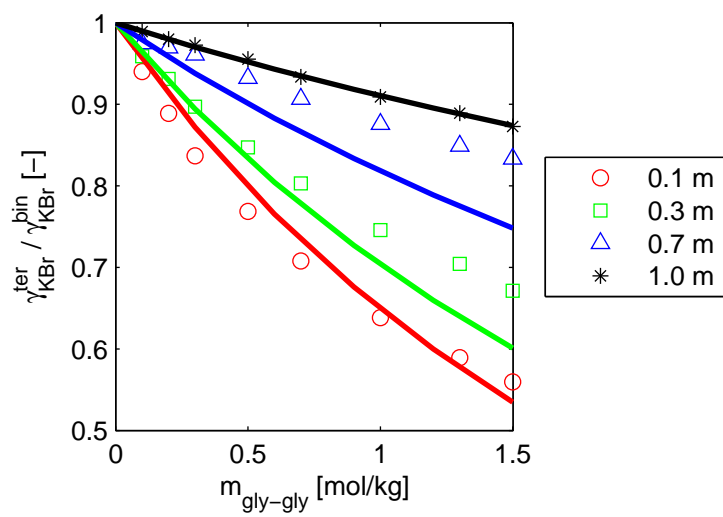
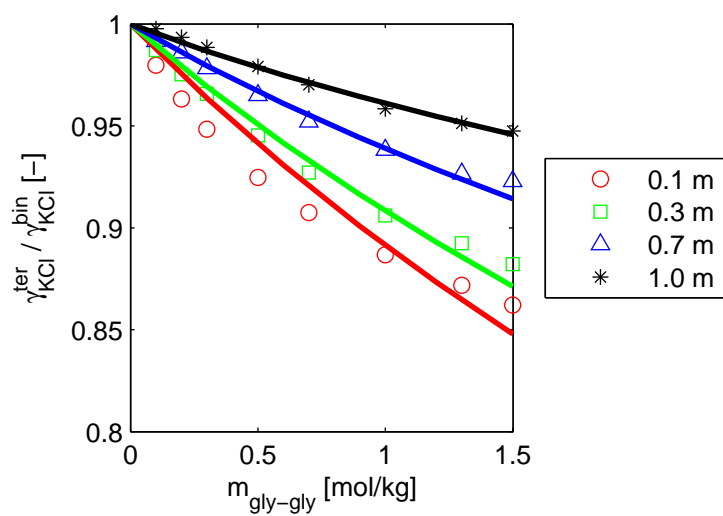
Ratios of MIAC $\gamma_{\pm}^{ter} / \gamma_{\pm}^{bin}$ 





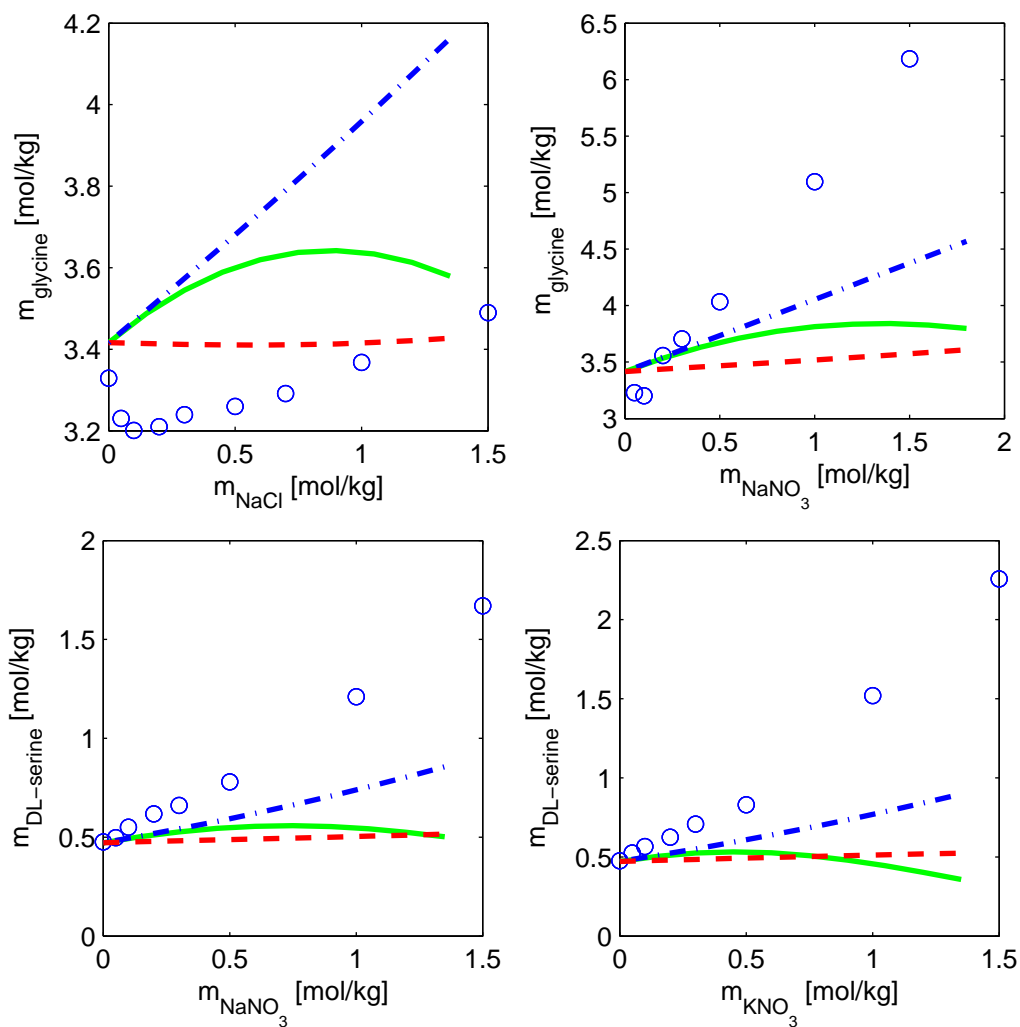






Solubilities

The red dashed line shows the SLE calculations with ePC-SAFT without binary interaction parameter k_{ij} between amino acid and ions. The blue dashed-dotted line represents calculations with a constant $k_{ij} = k_{ij}^0$. The green line gives the results for $k_{ij} = k_{ij}^0 + m_{salt} \cdot k_{ij}^1$.



CURRICULUM VITAE

Name Luca Fabiano Cameretti
Born September 15th, 1978 in Iserlohn (Germany)
Nationality Italian

EDUCATION

10/2003 – 12/2007 PhD Thesis, "Modeling of Thermodynamic Properties in Biological Solutions",
Laboratory of Thermodynamics, TU Dortmund (Germany)
01/2003 – 07/2003 Research and Diploma Thesis, "Self-Interaction of Lysozyme and α -Lactalbumin in Denaturing Solutions",
University of California, Berkeley in association with
Prof. John M. Prausnitz
10/1997 – 08/2003 Degree course "Chemietechnik" (Chemical Process Engineering),
TU Dortmund (Germany)
1988 – 1997 High School "Friedrich-Leopold-Woeste Gymnasium", Hemer

PUBLICATIONS

- L. Cameretti, G. Sadowski; Modeling of aqueous amino acid and polypeptide solutions with PC-SAFT; Chem. Eng. Proc. (2007); online
- L. Cameretti, G. Sadowski, J. Mollerup; Modeling of Aqueous Electrolyte Solutions with Perturbed-Chain Statistical Association Fluid Theory; Ind. Eng. Chem. Res. 44 (2005); 3355-3362; *ibid*; 8944-8944
- L. Cameretti, C. Held, A. Azkan, G. Sadowski; Thermodynamische Modellierung wässriger Aminosäure/Elektrolyt-Lösungen (Talk); VDI-Thermodynamik-Kolloquium Rostock, 08.10.-10.10.2007
- L. Cameretti, G. Sadowski; Modeling of Aqueous Amino Acid and Polypeptide Solutions with PC-SAFT (Poster); AIChE Annual Meeting, San Francisco, USA, 12.11.-17.11.2006
- F. Tumakaka, L. Cameretti, D. Fuchs, G. Sadowski; Thermodynamische Eigenschaften von Aminosäure-Lösungen (Talk); Dechema/GVC-Jahrestagungen 2006, Wiesbaden, 26.09.- 28.09.2006
- F. Tumakaka, L. Cameretti, D. Fuchs, G. Sadowski; Thermodynamic Modeling of Amino Acids and Polypeptides in Aqueous Solutions (Talk); 1st International Symposium on Biothermodynamics, Frankfurt a. M., 16.02.-17.02.2006
- L. Cameretti, G. Sadowski; Modelling of Aqueous Electrolyte Solutions with PC-SAFT (Talk); VDI-Thermodynamik-Kolloquium Frankfurt a.M., 06.10.-07.10.2005
- L. Cameretti, G. Sadowski; Modelling of Aqueous Electrolyte Solutions with PC-SAFT (Talk); Thermodynamics 2005, Sesimbra, Portugal, 06.04.-08.04.2005

